

POLITECNICO DI TORINO

Master's Degree in Aerospace Engineering

Academic year 2021/2022

Master's Degree Thesis

Optimisation of Lunar descent trajectories with Direct Methods



**Politecnico
di Torino**

Supervisors:

Prof. Lorenzo Casalino
Eng. Andrea D'Ottavio
Dr. Giorgio Fasano

Candidate:

Davide Fabro s280351

July 2022

Summary

List of figures	3
List of tables.....	4
INTRODUCTION	5
STATE OF THE ART	6
2.1 Moon exploration	6
2.1.1 Moon curiosity build again	8
2.1.2 The Artemis program	9
OBJECTIVES AND METHODOLOGY	14
3.1 Optimization	14
3.1.1 General concept of optimization	14
3.1.2 Sequential Quadratic Programming	19
3.2 Model definition	19
3.2.1 Equations and reference frame	20
3.2.2 Control variables	22
3.2.3 Boundary conditions and constraints	23
3.2.4 Algorithm and tool architecture	24
RESULTS	27
4.1 Only thrust module control	27
4.1.1 Fixed altitude of 30000 meters	27
4.1.2 Variable altitude with fixed starting mass	39
4.2 Thrust module and pitch control	43
4.2.1 Architectures comparison	44
4.2.2 Comparison best cases	60
CONCLUSIONS	66
APPENDIX A1	67
APPENDIX A2	69
APPENDIX A3	73
BIBLIOGRAPHY	74
ACKNOWLEDGEMENTS	76

List of figures

Figure 1: John F. Kennedy famous speech in 1961.....	7
Figure 2: Apollo 11 mission	7
Figure 3: Artemis program milestones	9
Figure 4: Lunar Gateway.....	11
Figure 5: Artemis Base Camp with the LTV (bottom-right), the Habitable Mobility Platform (center) and the Foundation Surface Habitat (top-right).....	12
Figure 6: Genetic Algorithm functioning scheme.....	15
Figure 7: Discretization of u and x over the resulting grid	17
Figure 8: Polynomial approximation of the solution of the ODE	18
Figure 9: RTN reference system	20
Figure 10: Discretized Landing Trajectory	25
Figure 11: Local and Global minimum of a function	26
Figure 12: Altitude - Time for all feasible solutions.....	29
Figure 13: Altitude - Ground Track for all feasible solutions.....	29
Figure 14: Cross-track Angle - Time for all feasible solutions.....	30
Figure 15: Radial Velocity - Time for all feasible solutions.....	31
Figure 16: Tangential Velocity - Time for all feasible solutions.....	31
Figure 17: Pitch - Time for all feasible solutions.....	32
Figure 18: Landing masses - time for all feasible solutions	33
Figure 19: Mass evolution - Time for all feasible solutions	33
Figure 20: Thrust - time for all feasible solutions.....	34
Figure 21: Altitude - Time best case	35
Figure 22: Altitude - Ground track best case.....	35
Figure 23: Tangential and Vertical Velocities best case	36
Figure 24: Mass evolution - Time best case	36
Figure 25: Thrust and Pitch - Time best case.....	37
Figure 26: Pitch rate - Time best case.....	38
Figure 27: T_{dot} - time best case	38
Figure 28: Altitude - Time for different starting altitudes.....	39
Figure 29: Altitude - Ground Track for different starting altitudes.....	40
Figure 30: Final mass with descent time and starting altitude	41
Figure 31: Thrust trends - Time for different starting altitudes	42
Figure 32: Average thrust and descent time for different starting altitude.....	42
Figure 33: Altitude - Time for case 1.1	49
Figure 34: Altitude - Ground track for case 1.1	49
Figure 35: Altitude - Time for case 1.2	50
Figure 36: Altitude - Ground track for case 1.2	50
Figure 37: Altitude - Time for case 2.1	51
Figure 38: Altitude - Ground track for case 2.1	51
Figure 39: Altitude - Time for case 2.2	52
Figure 40: Altitude - Ground track for case 2.2	52
Figure 41: Pitch and Elevation angles for case 1.1	53
Figure 42: Pitch and Elevation angles for case 1.2	54
Figure 43: Pitch and Elevation angles for case 2.1	54
Figure 44: Pitch and Elevation angles for case 2.2	55

Figure 45: Pitch and Thrust module for case 1.1.....	56
Figure 46: Pitch rate and Thrust rate for case 1.1.....	56
Figure 47: Pitch and Thrust module for case 1.2.....	57
Figure 48: Pitch rate and Thrust rate for case 1.2.....	57
Figure 49: Pitch and Thrust module for case 2.1.....	58
Figure 50: Pitch rate and Thrust rate for case 2.1.....	58
Figure 51: Pitch and Thrust module for 2.2 case.....	59
Figure 52: Pitch rate and Thrust rate for case 2.2.....	59
Figure 53: Altitude - Time best cases comparison.....	61
Figure 54: Altitude - Ground track best cases comparison.....	62
Figure 55: 3D trajectory best cases comparison.....	62
Figure 56: zoomed 3D trajectory best cases comparison.....	63
Figure 57: Pitch and Elevation angles best cases comparison.....	63
Figure 58: Pitch and Thrust module best cases comparison.....	64
Figure 59: Pitch rate and Thrust rate best cases comparison.....	65
Figure 60: Vertical and Tangential velocity for case 1.1.....	67
Figure 61: Vertical and Tangential speed for case 1.2.....	67
Figure 62: Vertical and Tangential velocity for case 2.1.....	68
Figure 63: Vertical and Tangential speed for case 2.2.....	68
Figure 64: 3D trajectory for case 1.1.....	69
Figure 65: zoomed 3D trajectory for case 1.1.....	69
Figure 66: 3D trajectory for case 1.2.....	70
Figure 67: zoomed 3D trajectory for case 1.2.....	70
Figure 68: 3D trajectory for case 2.1.....	71
Figure 69: zoomed 3D trajectory for case 2.1.....	71
Figure 70: 3D trajectory for case 2.2.....	72
Figure 71: zoomed 3D trajectory for case 2.2.....	72
Figure 72: Vertical and Tangential velocity best cases comparison.....	73

List of tables

Table 1: Descent starting and final conditions.....	23
Table 2: Engine architecture.....	27
Table 3: Results fixed starting altitude.....	28
Table 4: Results for different starting altitudes.....	41
Table 5: Four Proto-1 engine architecture.....	43
Table 6: 5 Proto-1 engine architecture.....	43
Table 7: 3 Proto-2 engine architecture with $T_{\dot{}}= 2000$ N/s each.....	44
Table 8: 3 Proto-2 engine architecture with $T_{\dot{}} = 1000$ N/s each.....	44
Table 9: Results case 1.1.....	45
Table 10: results case 1.2.....	46
Table 11: results case 1.2.....	47
Table 12: results case 2.2.....	48
Table 13: best cases.....	60

INTRODUCTION

The renewed rising interest in Moon exploration is demanding for an improvement of many technologies in the space industry. New missions will require precise landing capabilities and robust pieces of software and hardware able to cope with the uncertainties and difficulties that landing on Earth's celestial satellite implies. While the Apollo program relied on the eyesight of the astronauts and their manual control, today everything must be autonomous.

New *Guidance, Navigation and Control systems (GNC)* must be developed, able to operate without human direct intervention, with soft-landing capabilities while satisfying plenty of restrictions required for safe operations. It's important to remember that the landing conditions may change in real time, and that's why new technologies must be able to detect these changes and adapt the trajectory consequently.

This will increase fuel consumption and therefore it becomes critical to have the optimal trajectory that guaranties the maximum possible landing mass as a guide for the GNC.

With this goal in mind in this thesis, developed at *Thales Alenia Space* in Turin, a direct optimization method is used to obtain the optimal descent trajectories that will lead to the highest value of landing mass.

In order to achieve this accomplishment a *Matlab* algorithm has been created relying in particular on two functions, *fmincon* and *multistart*.

Later a tradeoff between four different engine architectures has been made, in order to find the most suitable configuration for a real lunar mission today under development.

STATE OF THE ART

It was 1969 when Neil Armstrong touched the lunar soil uttering his famous phrase “One small step for a man, one giant leap for mankind”. A new era based upon the curiosity to discover the unknown started, with all the challenges and related goals that they are still trying to achieve today.

2.1 Moon exploration

Throughout the whole history of mankind, the Moon has always been source of fascination. Starting from bare-eye observations in ancient Greece until today’s most recent missions humans tried to discover our cosmic partner’s deepest secrets.

The early forays into lunar explorations arose from the ongoing Cold War when the U.S. government and the Soviet Union sent the first the first uncrewed spacecraft to the Moon.

The first point in this race was scored by the Soviets when *Luna 1* became the first spacecraft to escape Earth’s gravity flying at 6000 km from the Moon’s surface in January 1959. Later in the same year *Luna 2* became the first S/C to ‘touch’ the lunar surface, crashing in the *Mare Imbrium*, close to the *Aristides*, *Archimedes*, and *Autolycus* craters. Again in 1959 the third *Luna* mission captured the first pictures of the dark side of the Moon, showing the terrain differences from the light side of Earth’s satellite [1].

Then the U.S. sent nine *NANA Ranger* spacecrafts between 1961 and 1965, giving scientist proximity images of the Moon’s surface for the first time. These one-off missions had the objective of capturing as many images as possible before crashing onto the surface of the celestial body. Through those images Americans better understood Moon’s morphology and had a better understanding of the hardships of finding a smooth landing site for manned missions.

In 1966 Soviet *Luna 9* became the first spacecraft to land safely on the lunar surface, packed with communications devices and cameras to capture ground-level shots of the lunar landscape. In the same year the spacecraft *Luna 10* became the first orbiter of Earth’s satellite.

Year 1966 was also the one when NASA first *Surveyor* space probe landed on the lunar surface with the goal to explore the celestial body and analyze lunar soli. Then in 1967 and 1968 NASA launched five *Lunar Orbiter* missions designed to orbit the Moon while mapping its surface, photographing about 99 percent of its surface, revealing potential landing sites and establishing the necessary conditions for the next big step: landing the first man on the lunar surface.

Thanks to NASA’s effort to keep the promise made in 1961 by the President John F. Kennedy of landing a man on the Moon before a decade (Figure 1) the *Apollo* program was born. The program cost was about \$25.4 billion or around \$152 billion in today’s money proportionally to inflation, making it the most expensive space endeavor in history. The unbelievable effort of U.S. scientists and other companies such as *Pratt and Whitney*, *General Motors*, *Motorola* etc. led to this unimaginable milestone, beating the Soviet Union and ending the space race and making 24 astronauts orbit or land on the Moon.



Figure 1: John F. Kennedy famous speech in 1961

On July 20, 1969, *Apollo 11* (Figure 2) touched down in the *Sea of Tranquility* in the lunar lander *Eagle* while the astronaut Michael Collins orbited around the Moon inside the module *Columbia*. After all the routine checks the door of the module finally opened and Neil Armstrong and Edwin "Buzz" Aldrin got out. While pressing the first step on the Moon's surface Armstrong said the legendary words "*That's one small step for a man, one giant leap for mankind.*" The astronauts spent 21 hours and 36 minutes on the Moon's surface and performed EVA for about two and a half hours, taking notes and collecting samples, performing experiments, and taking pictures [2].

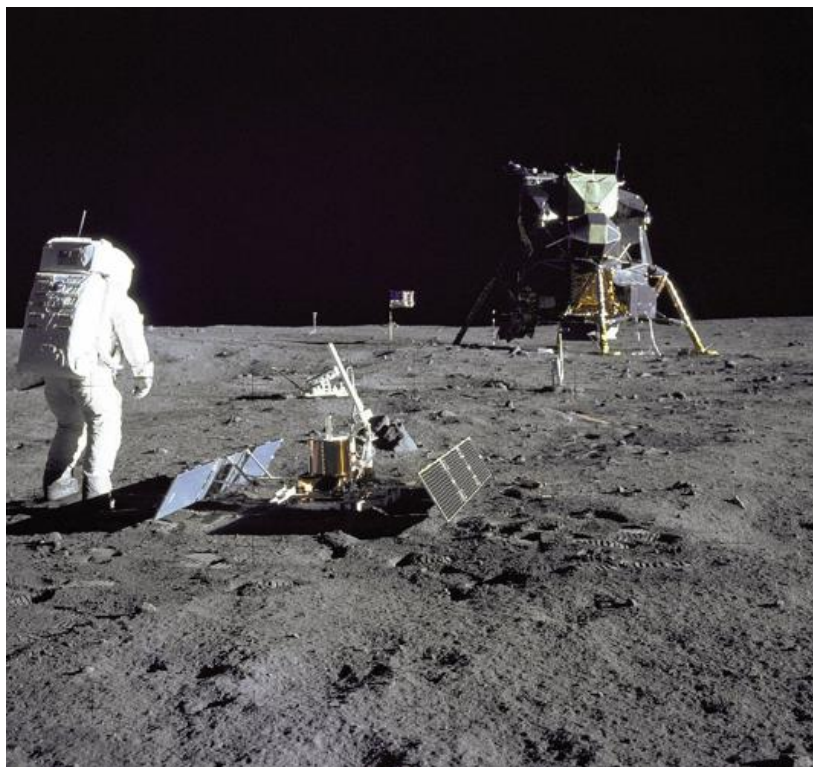


Figure 2: Apollo 11 mission

Just four months later *Apollo 12* touched down, followed by *Apollo 13* that nearly avoided a disaster when an Oxygen tank blow out and almost compromised the mission (luckily all three crew members safely came back to Earth).

In January 1971 was *Apollo 14* turn and commander Alan Shepard became famous for lobbing a golf ball in a crater with a makeshift 6-iron.

Five months later *Apollo 15* collected hundreds of pounds of Moon's samples and its astronauts travelled more than 27 km in the first piloted Moon buggy (actually, the first rover was the unmanned and remotely controlled *Lunokhod 1* of the Soviet Union).

In 1972 the two most recent and last crewed missions *Apollo 16* and *Apollo 17* reached the Moon, and Russia's *Luna-24* crewless spacecraft in 1976 was the last to land for the 20th century. All the samples collected during these final explorations gave scientist to a massive insight about lunar geology and soil formation.

After this thrilling race and sensational accomplishments governments and space agencies shifted their focus elsewhere and so far, only 12 humans have set foot on the Moon.

2.1.1 Moon curiosity build again

More than twenty years later, in 1994, the *Clementine* mission mapped the Moon's surface in different wavelengths, from ultraviolet to infrared spectrum, collecting more than 1.8 million photos giving the first hints of iced water in some creates of the lunar south pole.

Then, in 1999 the *Lunar Prospector* confirmed *Clementine's* discoveries, suggesting the possibility of creating a long-time base camp on the surface of the Moon. Unfortunately, *Prospector* dramatic mission ending, with the S/C that slammed into the Moon creating a cloud of dust, did not revealed any iced water.

Since 2009 *Lunar Reconnaissance Orbiter* has taken high-resolution maps of the Moon's surface and in 2011 NASA's *Grail* mission mapped Moon's gravitational field in detail.

In the last two decades, Moon exploration was not just an American affair, but it started to involve other countries and even private companies.

In 2007 JAXA, Japan's space agency, launched its first orbiter *SELENE* and in the same year China and India did the same. In 2013 China became the third country to land on the Moon's surface, even dropping a rover named *Yutu*. In 2019 *Yutu-2* became the first lander to explore the dark side of the Moon while India deployed to no avail its lander *Vikram* during the *Chandrayaan-2* mission. In the same year the first mission largely founded with private founds was launched by the Israeli government, named *Baresheet*. Unluckily, the spacecraft crashed on the lunar surface while trying to touch down, but this mission led to a new era of space exploration and to the rise of private companies in this sector.

Right now, NASA is partnering with private companies such as *SpaceX*, *Blue Origin* and *Astrobotic* to develop innovative manned and unmanned landers for Moon exploration. *Blue Origin* and Amazon CEO Jeff Bezos declared that they want to establish a permanent lunar settlement close to the south pole (where there is the highest concentration of iced water) of the celestial satellite where astronauts could stay steadily. Meanwhile *SpaceX* is developing *Starship*, a new spacecraft that would carry the astronauts to the Moon and even Mars, but also wants to bring tourists to the lunar orbit and has already ferried the astronauts Doug Hurley and Bob Behnken to the *International Space Station (ISS)* with the capsule *Crew Dragon*.

2.1.2 The Artemis program

Today NASA is shaping its new program *Artemis* (Figure 3), named after the sister of the god Apollo, aiming to ferry the first woman on the Moon by 2024. At the core of this ambitious program is NASA's new Orion capsule, albeit the agency is collaborating with private companies to fulfill its goal (Nasa, 2020).

If Artemis fulfills its premises, NASA and its commercial partners will even develop a space station in lunar orbit that could operate as a gateway to the Moon and beyond and a permanent outpost on the surface.

With *Artemis* missions, NASA will land the first woman and first person of color on the Moon, using innovative technologies to explore more of the lunar surface than ever before. Through a collaboration with private companies and international partners, NASA wants to establish the first long-term human-robotic presence on and around the Moon. Then, all the knowledge about our celestial satellite will be used for the next giant step: sending the first astronauts to Mars.

In fact, Moon's proximity to our home planet makes it relatively easier to address all concerns and develop the know-how necessary for the colonization of the Red Planet.

Moreover, the *Artemis* program aims to expand the knowledge about the origin and history Earth, the Moon, and our solar system while strengthening the partnership between NASA and their commercial partners.

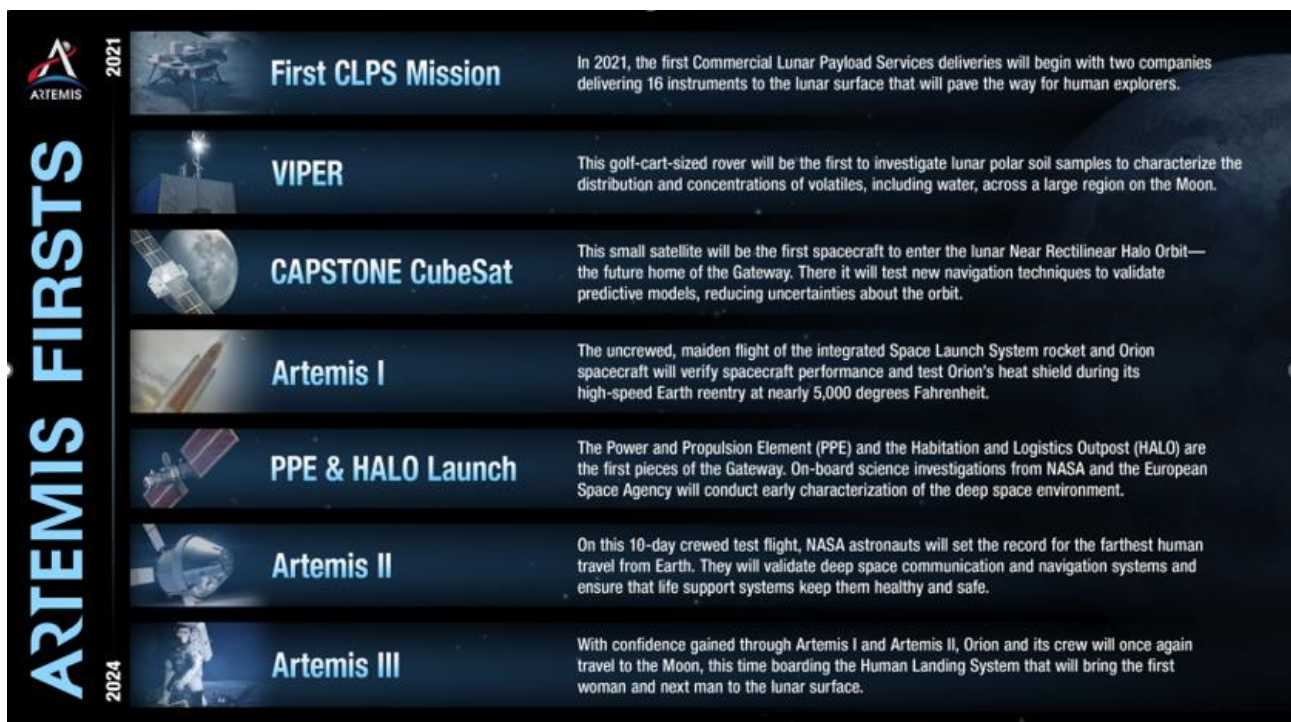


Figure 3: Artemis program milestones

The program officially started in 2021 with the first the *Commercial Lunar Payload Services (CLPS)* deliveries and through these payloads NASA is studying different regions that provide key desired traits:

- Access to enough sunlight, which will provide minimal temperature variations and will be the only available power source.
- Continuous line-of-sight to Earth for mission communications.
- Mild grading and surface debris for safe landing, walking and rover's mobility.
- Proximity regions which are believed to contain resources such as iced water.

Later, in 2023 NASA's *Volatiles Investigating Polar Exploration Rover (VIPER)* will gain even more surface data through science investigations and this will help support the identification of more areas of interest for human exploration. In particular, the rover *VIPER* will analyze lunar soil searching for water and other volatiles.

NASA will even launch *Cislunar Autonomous Positioning System Technology Operations and Navigation Experiment (CAPSTONE) CubeSat* to have a better grasp of the lunar *near-rectilinear halo orbit (NHRO)* and validate *Gateway's* operational models.

Later NASA will launch *Artemis I*, sending an uncrewed *Orion* module ferried by the *Space Launch System SLS* rocket on a lunar distant retrograde orbit. This mission will perform a fundamental flight test for both the capsule and the launcher, gathering data before *Orion* returns on a high speed to Earth, close to Mach 32 or 39500 km/h. In particular the high-speed reentry will be the top mission priority and a mandatory test of the heat shield's performance as it enters Earth's atmosphere, heating to nearly 2800 degrees Celsius before retrieval.

The program will continue with *Artemis II* and the first manned flight of *SLS* and *Orion*. The astronauts will reach the lunar environment for the first time in 50 years after committing two orbits around Earth. Initially the crew will reach the high-Earth orbit (HEO) and, after the separation of *SLS* and *Orion*, the astronauts will use the latter for a close proximity operations demonstration, piloting the capsule in manual mode. The crew will use on board cameras and *Orion's* windows to line up with the *ICPS* and this will provide data and operational experience that cannot be obtained on Earth in preparation for critical rendezvous.

Subsequently the crew will give back the lead to mission control, reach the Moon and then return back to Earth. In the meantime, they will remove the *Orion Crew Survival System* suit they wear for launch and spend the rest of the in-space mission in normal clothes. Meanwhile *Orion* will fly beyond the *Global Positioning System (GPS)* navigation system satellites and the *Tracking Data Relay Satellite System (TDRS)* communication satellites of NASA's Space Network and allow an early checkout of *Deep Space Network (DSN)* communication and navigation prowess.

During the 10 days of the mission the crew will set a new record for the farthest distance reached by humans beyond the far side of the Moon, paving the path for the most important part of the program, *Artemis III*.

This time *Orion* will travel to the Moon boarding the *Human Landing System (HLS)* that will finally bring the next man and the first woman to the lunar surface. For the development of the *HLS* NASA selected two private companies, *Blue Origin* and *SpaceX* which offered three distinct lander and mission designs. These had dissimilar redundancies, mounting a wide range of technology and offering different strategies and possibilities for lunar access. All three, however, provided the ability to dock with *Orion* and the *Lunar Gateway*, giving NASA good flexibility in mission planning.

The first mission will arrive directly to the Moon but later the American agency will make full use of the Gateway capabilities, such as refueling and reuse of all or parts of the lander to critical Mars mission simulations.

The exact landing site for *Artemis III* will depend on several factors, like the specific objectives and then the launch date, illumination conditions, temperature variations and continuous line-of-sight to Earth for communications. When landed, the crew will collect up to 35 kg of samples and work with the 100kg of science equipment that the *HLS* will carry.

In the following missions, next crews will use some of the already placed instruments and tools by *Artemis III* first astronauts.

During the first one week-long expedition the astronauts will study and document the landing site geology, using tube regolith samples to capture ancient solar wind trapped in the soil. While on the surface, crew will live in the cabin of the ascent vehicle, which is the upper portion of the HLS.

After completing this historic expedition on the lunar surface, the crew will launch from the surface to rendezvous with *Orion* and their crewmates in lunar orbit and prepare for the three-day trip back to Earth.

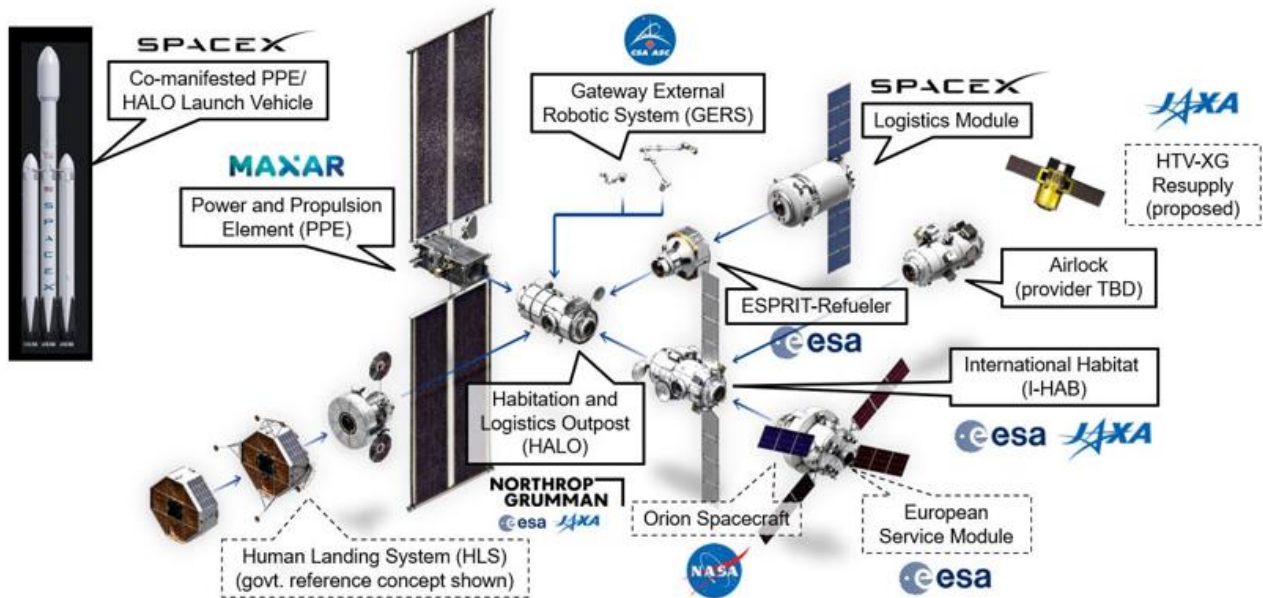


Figure 4: Lunar Gateway

A fundamental element of the Artemis program will be the Lunar Gateway (Figure 4). The 'ISS' like lunar station will be the first outpost orbiting the Moon which will provide support for long-term human missions on the lunar surface, as well as a checkpoint point for deep space exploration. The Gateway will play a vital role in the development of deep space exploration and will provide a port to transport landers to the lunar surface or spacecraft embarking to destinations beyond the Moon, like Mars [3].

At the beginning the Gateway will be composed by only two modules, the *Power and Propulsion Element (PPE)* and the *Habitation and Logistic Outpost (HALO)* that will be integrated on the ground and launched together on the same rocket in 2023. The *PPE* will provide power, communications, attitude control, and orbital transfer capabilities to the Gateway with its 60-kW solar electric propulsion.

HALO will be the first home of the astronauts visiting the Gateway, providing life support to the crew after docking with the *Orion* capsule while preparing for the descend on the lunar surface. It will also provide command, control, data handling capabilities as well as environmental control and life support systems and will feature multiple docking ports, not only for *Orion* but for other modules/capsules too.

In the future the Gateway provide fundamental contribution to the creation of a future lunar outpost, providing remote control for robotics on the lunar surface, refueling capabilities and housing for the astronauts [4].

Artemis and NASA's final goal is to lengthen the duration through the creation of a permanent base camp called *Artemis Base Camp*. This will make the crew stay on the lunar surface for up to two months at a time, using the Lunar Gateway as an intermediate check point before landing [5].

The lunar outpost (Figure 5) will even provide command-and-control for surface expeditions and an office/home for astronauts far from Earth. It will even be able to operate autonomously when no crew will be present and it will also be the stage for new science and technology demonstrations on the Moon.

At the beginning the outpost will be formed only by the Lunar Lander that will carry the astronauts to the Moon's surface but later three more pieces will be added [6]:

1. *The Lunar Terrain Vehicle (LTV)*. The LTV will be an unpressurised utility vehicle used for transport proximity of the Base Camp. It will only carry two astronauts equipped with the *Exploration Extravehicular Mobility Unit (xEMU)*, which is an innovative spacesuits.
2. *The Habitable Mobility Platform*. This will be an incredibly technological van-like vehicle that will permit to the astronauts to make further trips away from the Base Camp for periods as long as a few weeks, thanks to its pressurised cabin and robust life support systems.
3. *The Foundation Surface Habitat*. This module will be non-mobile and designed for accomodation of a few days by up to four astronauts. It will be pressurised and has integrated life support systems, allowing the astronauts to take off their suits and work with plain clothes.



Figure 5: Artemis Base Camp with the LTV (bottom-right), the Habitable Mobility Platform (center) and the Foundation Surface Habitat (top-right)

Due to these cutting-edge innovations astronauts will work on testing robotics and a wide set of new technologies identified through the *Lunar Surface Innovation Initiative*, with the main goal of developing techs for *in-situ resource utilization (ISRU)* and power systems. A variety of rovers will carry numerous instruments including ISRU experiments that will gather information on the availability of usable resources like oxygen or water.

Mastering these technologies can lead to the production of fuel, water, and oxygen from lunar materials, making possible long sustainable surface operations and lessening supply needs from Earth.

Once the system will be completed NASA will gather all the knowledge for the next big step in human space exploration: land the first humans on the surface of Mars.

The distance from Earth to the Moon is a relatively manageable 400000 km. In contrast, Mars is, on average, 225 million km from Earth. In addition to the challenges that a Martian mission requires because of its distance there are dangerous levels of radiation that permeate deep space and the challenges caused by the dusty atmosphere of the Red Planet.

To solve all these problems NASA is developing a concept of operations with the idea of significantly reduce trip time to Mars and the permanence on the surface, minimizing crew's health risks, galactic cosmic ray exposure and complexity and cost of the mission.

NASA aims to conduct a human mission to Mars that can be realized as soon as possible, but the only way to fulfill this goal is to borrow as much as possible from the know-how of the astronauts' expertise on the Moon.

OBJECTIVES AND METHODOLOGY

In the following chapter will be discussed the main goals of this thesis as well as the methodology used to achieve it. After a brief general introduction about optimization and its bond with space trajectory analysis the thesis's objective will be presented in detail along with the physical and mathematical model used in its resolution.

3.1 Optimization

The term optimization means *"finding the best possible solution by changing variables that can be controlled, often subject to constraints"* [7]

Optimization is something intrinsic in nature, as exemplified by the evolution of species, how birds optimize their wings' shape in real time for flying and dogs have been shown to find optimal trajectories. Generally, different laws of physics relate to optimization, such as the principle of minimum energy and is a human instinct too. People constantly seek to improve their lives and surroundings and, consequently, apply this concept even in the field of engineering.

3.1.1 General concept of optimization

The subject of spacecraft trajectory optimization has a long and interesting history. The problem can be defined as *"the determination of a trajectory for a spacecraft that satisfies different initial and terminal conditions while minimizing some quantity of importance"* [8].

Usually, the most common goal is to minimize propellant consumption or to maximize the dry mass of the spacecraft (payload and bus).

Obviously, it is usually necessary to provide some more practical upper or lower boundaries for the variables of the problem, for example final time or the optimizer will trade it for propellant or set limits for angle changes, like pitch between 0 and 360° to avoid singularities. Sometimes the goal is minimizing flight time but the trajectories obtained could be too steep and need boundaries on the pitch rate [9].

As stated, there are numerous types of optimal control problems, depending on the domain (continuous, discrete), the constraints and free variables, but every problem needs the following elements to be solved:

- a mathematical model of the system to be controlled;
- a specification of the performance index;
- a specification of all boundary conditions on states and constraints to be satisfied by states and controls;
- a statement of what variables are set free.

Luckily today different methods exist to deal with real world optimization problems that can be categorized in three macro-categories [10]:

- *Direct methods:* transform the optimal control problem in a nonlinear programming (NLP) problem. The trajectory is discretized in N intervals while state and control variables are approximated by a piecewise constant parameterization for each arc, resulting into a large-scale problem.

This way the problem became a parameter optimization and various discretizing approaches can be exploited depending on the nature of the problem like Convex Optimization or Quadratic Programming.

Direct methods have the big advantage to handle easily almost any problem formulation and to be robust, meaning that the algorithm performs well under different starting conditions and boundaries. On the negative side they may be computationally expensive and relatively inaccurate if compared to indirect methods.

- *Indirect methods*: they consider the problem as continuous for both state and control variables, but the trajectory can be divided into arches if the problem has to deal with discontinuities or if there is a change in the set of differential equation considered. The optimal control law is obtained from the Pontryagin's Maximum Principle (PMP).

Indirect approach leads to a smaller problem with a lower number of parameters to evaluate, leading to a shorter computational time and possibly a higher degree of accuracy compared to direct methods.

On the other hand, it relies on the determinations of the costates λ , quantities that do not have a physical significance and are difficult to determine to satisfy all the constraints and boundaries of the problem. If not carefully selected these variables can cause some troubles in convergence of the algorithms or numerical issues [11].

- *Evolutionary Algorithms*: use mechanisms derived by nature and solves problems through processes that emulate the behaviors of living organisms and are particularly inspired by the concepts of Darwinian Evolution. The first guess solutions of the problem are randomly generated and later are tested for how well they solve the problem. Next the best solutions are picked for reproduction and mutated, generating iteration after iteration better solutions [12].

There are different techniques to achieve the result, the most popular being Genetic Algorithm that can be summarized with the following image (Figure 6):

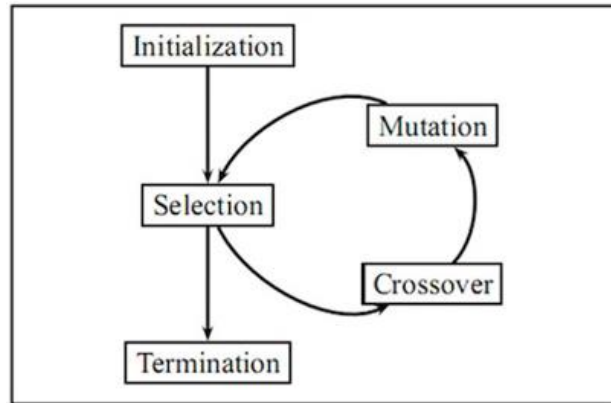


Figure 6: Genetic Algorithm functioning scheme

In general, a continuous optimal control problem is defined by a set of ordinary differential equations (ODEs), which can be expressed as [13]:

$$\dot{\mathbf{x}}(t) = \mathbf{F}[\mathbf{x}(t), \mathbf{u}(t), \mathbf{p}, t], t \in [t_0, t_f] \quad (1)$$

Where:

- $\mathbf{x} \in [t_0, t_f] \rightarrow \mathcal{R}^{N_x}$ is the state vector, i.e. the set of equations that describes the problem

- $\mathbf{u} : [t_0, t_f] \rightarrow \mathcal{R}^{N_x}$ is the control variables vector, which can freely change in order to optimize the performance index
- $\mathbf{p} \in \mathcal{R}$ is a vector of static time independent parameters
- $t \in [t_0, t_f]$ is an independent variable, usually time

A set of constraints, usually called event constraints, express the initial and final conditions as a set of inequalities:

$$\mathbf{e}_L \leq \mathbf{e}[\mathbf{x}(t_0), \mathbf{u}(t_0), \mathbf{x}(t_f), \mathbf{u}(t_f), \mathbf{p}, t_0, t_f] \leq \mathbf{e}_U \quad (2)$$

Additionally, the problem could involve time-independent constraints on the states and/or control variables, called path constraints:

$$\mathbf{h}_L \leq \mathbf{h}[\mathbf{x}(t), \mathbf{u}(t), \mathbf{p}, t] \leq \mathbf{h}_U, t \in [t_0, t_f] \quad (3)$$

There are even upper and lower boundaries on controls, states and static parameters:

$$\mathbf{u}_L \leq \mathbf{u}(t) \leq \mathbf{u}_U, t \in [t_0, t_f], \quad (4)$$

$$\mathbf{x}_L \leq \mathbf{x}(t) \leq \mathbf{x}_U, t \in [t_0, t_f], \quad (5)$$

$$\mathbf{p}_L \leq \mathbf{p} \leq \mathbf{p}_U. \quad (6)$$

It's important to notice that sometimes upper and lower boundaries can be equal (this particular condition will be used in this thesis as will be later shown).

Finally, the last element is the performance index J , which is the quantity that should be minimized:

$$J_1 = \varphi_1[\mathbf{x}(t_0), t_0, \mathbf{x}(t_f), t_f] \quad (7)$$

Where φ is the cost function, usually propellant mass consumption.

Occasionally the performance index can be written as:

$$J_1 = \varphi_1[\mathbf{x}(t_0), t_0, \mathbf{x}(t_f), t_f] + \int_{t_0}^{t_f} \mathbf{L}[\mathbf{x}(t), \mathbf{u}(t), t] dt \quad (8)$$

Where $L: \mathcal{R}^{n_x} \times \mathcal{R} \times \mathcal{R}^{n_u} \times \mathcal{R} \mapsto \mathcal{R}$ is known as running cost function

As said before, while being computationally effective and with a high level of accuracy, indirect methods need a good guess of the initial adjoint variables. This can be difficult with inequality constraints and with variables that can be subject to frequent changes, for example when a tradeoff between different controls or starting conditions is made.

Differently, direct collocation methods discretize the differential equations with different methods such as trapezoidal, Hermite—Simpson [or pseudospectral approximations, defining a grid of N points covering the time interval $[t_0, t_f]$, $t_0 = t_1 < t_2 \dots < t_N = t_f$ (Figure 7).

This operation transforms the differential equations into a finite set of equality constraints of the NLP problem.

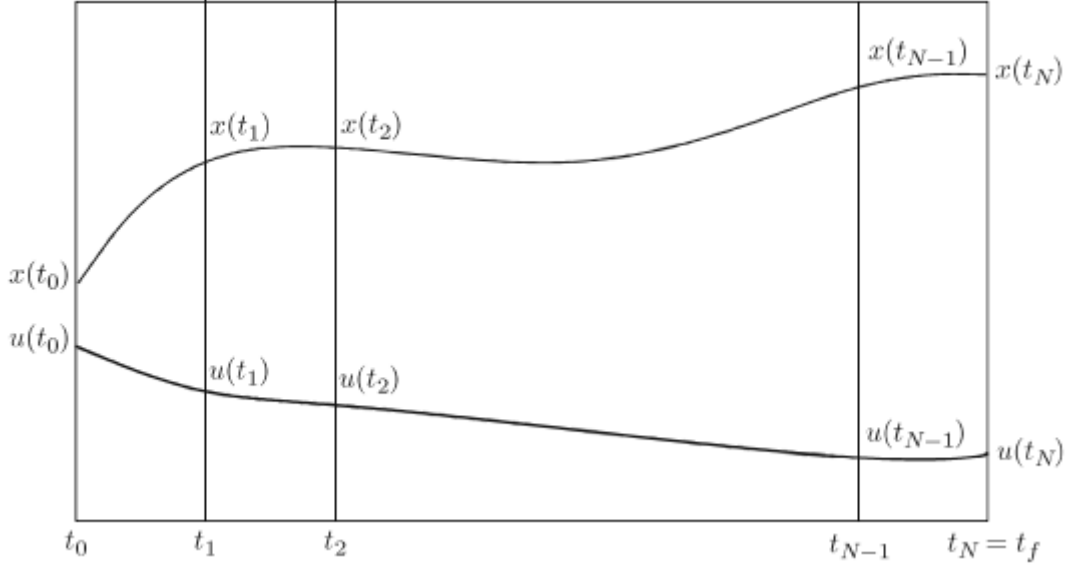


Figure 7: Discretization of u and x over the resulting grid

This usually leads to a very large nonlinear problem, with thousands of variables and constraints but even with this numbers this problem is easier to solve than a boundary-value one.

To solve it, it necessary to chose $y \in \mathfrak{R}^{N_y}$ to minimize $F(y)$ subject to:

$$\begin{bmatrix} \mathbf{0} \\ \mathbf{H}_L \\ \mathbf{e}_L \end{bmatrix} \leq \begin{bmatrix} \mathbf{Z}(y) \\ \mathbf{H}(y) \\ \mathbf{E}(y) \end{bmatrix} \leq \begin{bmatrix} \mathbf{0} \\ \mathbf{H}_U \\ \mathbf{e}_U \end{bmatrix} \quad (9)$$

$$\mathbf{y}_L \leq \mathbf{y} \leq \mathbf{y}_U \quad (10)$$

Where:

- $F : \mathfrak{R}^{N_y} \rightarrow \mathfrak{R}$ is the result from the evaluation of the performance index (eq. 7)
- $\mathbf{Z} : \mathfrak{R}^{N_y} \rightarrow \mathfrak{R}^{N_z}$ is the mapping that arises from the discretization of the constraints in the points of the grid
- $\mathbf{H} : \mathfrak{R}^{N_y} \rightarrow \mathfrak{R}^{(N+1)n_h}$ includes the path constraints associated with the lower and upper boundaries $H_L, H_U \in \mathfrak{R}^{(N+1)n_h}$ respectively (eq. 3)
- $\mathbf{E} : \mathfrak{R}^{N_y} \rightarrow \mathfrak{R}^{N_e}$ are the event constraints (eq. 2)

To further simplify the problem is possible to approximate the solution of the differential equation with a polynomial $\tilde{\mathbf{x}}(t)$ of degree M over each interval $t \in [t_k, t_{k+1}]$, $j = 0, \dots, N - 1$:

$$\tilde{\mathbf{x}}(t) = \mathbf{a}_0^{(k)} + \mathbf{a}_1^{(k)}(t - t_k) + \dots + \mathbf{a}_M^{(k)}(t - t_k)^M \quad (11)$$

With the coefficients $\mathbf{a}_0^{(k)}, \dots, \mathbf{a}_M^{(k)}$ chosen in order to match the function at the end and beginning of the k -th interval:

$$\tilde{\mathbf{x}}(t_k) = \mathbf{x}(t_k) \quad (12)$$

$$\tilde{\mathbf{x}}(t_{k+1}) = \mathbf{x}(t_{k+1}) \quad (13)$$

An the same must be for the time derivative at t_k and t_{k+1} :

$$\frac{d\tilde{\mathbf{x}}(t_k)}{dt} = \mathbf{f}[\mathbf{x}(t_k), \mathbf{u}(t_k), \mathbf{p}, t_k] \quad (14)$$

$$\frac{d\tilde{\mathbf{x}}(t_{k+1})}{dt} = \mathbf{f}[\mathbf{x}(t_{k+1}), \mathbf{u}(t_{k+1}), \mathbf{p}, t_{k+1}] \quad (15)$$

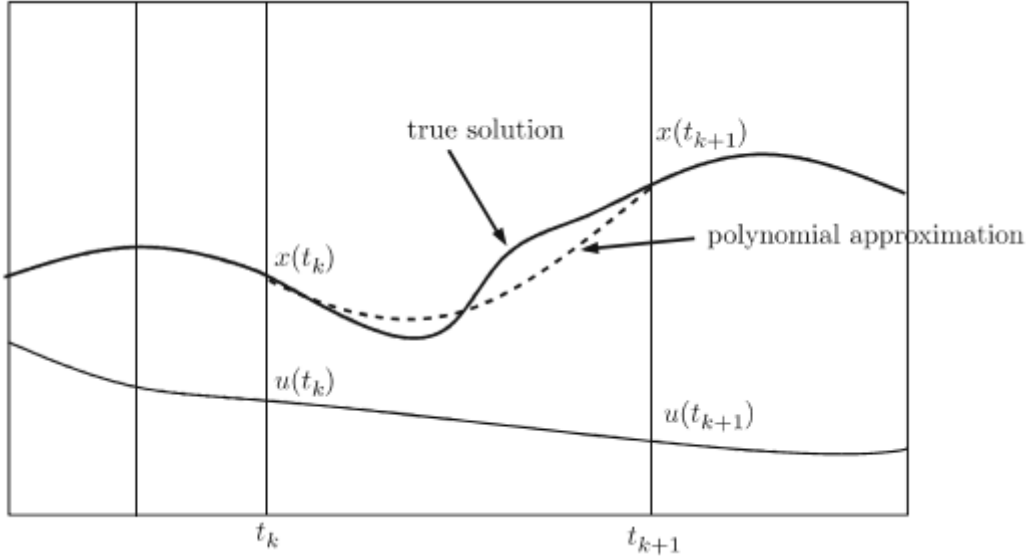


Figure 8: Polynomial approximation of the solution of the ODE

Equations 13 and 14 are called collocation conditions.

Usually, the discretization method used for solving optimal control problem relies on Runge-Kutta methods. A general formulation for a k-stage Runge-Kutta is the following (Figure 8):

$$\mathbf{x}_{k+1} = \mathbf{x}_k + h_k \sum_{i=1}^K b_i \mathbf{f}_{ki} \quad (16)$$

Where

$$\mathbf{x}_{ki} = \mathbf{x}_k + h_k \sum_{l=1}^K a_{il} \mathbf{f}_{kl} \quad (17)$$

$$\mathbf{f}_{ki} = \mathbf{f}[\mathbf{x}_{ki}, \mathbf{u}_{ki}, \mathbf{p}, t_{ki}], \quad (18)$$

Where $u_{ki} = u(t_{ki})$, $t_{ki} = t_k + h_k \rho_i$, and $\rho_i = (0,1]$.

3.1.2 Sequential Quadratic Programming

Sequential Quadratic Programming (SQP) is one of the most successful methods for the numerical solution of constrained nonlinear optimization problems and have been effectively used in the space industry for years [13]. For this reason, it was chosen as the grounding base of the algorithm developed for this thesis, as will be later explained.

This class of algorithms can almost handle any degree of non-linearity, but has the disadvantage of incorporating several derivatives, which need to be worked analytically before converging to a solution, so SQP becomes quite encumbering for large problems with numerous variables and constraints.

The method was first introduced in 1963 and was developed and refined in the 1970's. SQP combines two fundamental algorithms for solving non-linear optimization problems: an active set method and Newton's method [14].

SQP methods solve a series of optimization subproblems, each one optimizes a quadratic model of the objective function and constraints. If the problem is unconstrained the method reduces to Newton's method and if the problem has only equality constraints is equivalent to applying Newton's method to the first-order optimality conditions (or Karush–Kuhn–Tucker conditions) of the problem.

To develop a better understanding of the topic the author suggest to read about Lagrangian multipliers and Karush-Kuhn-Tucker (KKT) conditions, that will not be discussed in this thesis.

The application of the SQP to non-linear optimization problems (NLP) can be written in the form:

$$\begin{aligned} & \text{minimize } f(x) \\ & \text{over } x \in \mathbb{R}^n \\ & \text{subject to } h(x) = 0 \text{ and } g(x) \leq 0 \end{aligned}$$

where:

- $f: \mathbb{R}^n \rightarrow \mathbb{R}$ is the objective function
- $h: \mathbb{R}^n \rightarrow \mathbb{R}^n$ describe the equality constraints
- $g: \mathbb{R}^n \rightarrow \mathbb{R}^n$ describe inequality constraints

If the reader is interested, a deeper and complete explanation of the problem can be found in the work of Prof. Dr. Ronald W. Hoppe of the University of Houston [15].

3.2 Model definition

The main objective of this thesis is to create an algorithm that can perform descent trajectory optimization in the lunar environment, minimizing propellant consumption and thus maximizing mass upon landing.

To do so, it was necessary to define the problem in detail, identifying and carefully choosing the following elements:

- physics of the problem: reference system and equations describing the descent motion;
- identification of the control parameters that can be chosen to perform the optimization;

- identification of the constraints that identify the starting and ending conditions of the trajectory;
- optimization method;
- software in which to implement the problem.

The mission starts with the lander on a 100 km x 100 km circular *Low Lunar Orbit (LLO)*. Later a ΔV is applied to move the lander from the LLO to a 30 km x 100 km Elliptical Lunar Orbit (ELO). Then at the periapsis of the ELO, a Powered Descent Initialization (PDI) starts, bringing the lander on a trajectory to the designated landing site.

From the LLO to the PDI the lander will follow the elliptical ELO trajectory.

Therefore, is fundamental to perfectly match the initial condition of the PDI with the final condition of the ELO at the periapsis.

3.2.1 Equations and reference frame

For the landing trajectory from the PDI the Radial Transversal Normal (RTN) reference system is used, as suggested in the MAG document written by ESA, which was the benchmark for the validation of this software. This is a particular *satellite coordinate system* that is used to studies of relative motion and moves with the satellite. Sometimes it's called *Gaussian coordinate System* or *Local Vertica Local Horizontal (LVLH)* system, according to the direction taken as positive of the axis. The *R* axis always point out from the satellite along Earth's radius while the *S/C* moves along the orbit. The *T* axis is perpendicular to the *R* axis and in the plane defined by the velocity vector and the *R* axis along motion direction. The Normal axis *N* completes the right-handed coordinate system [16].

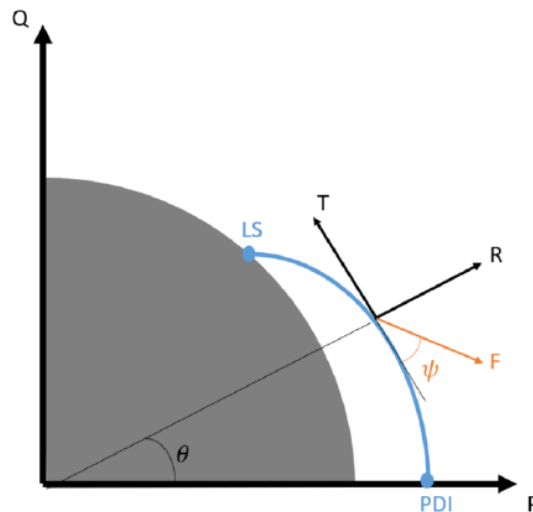


Figure 9: RTN reference system

As can be seen from Figure 9 above, the motion can be described by a 2-D dynamic equation system. A bidimensional reference has been chosen for two main reasons: the first is that the ideal trajectory, i.e. the one with the minimum fuel consumption, will always lay on a plane. This is because any out-of-the-plane components of the thrust vector will not be used to break the lander during the descent but only to steer its trajectory.

The second reason is to reduce the computational effort required by the optimization and consequently the running time of the algorithm. This choice confirmed its usefulness, especially in the first phases of the creation of the algorithm, when a lot of iterations have been necessary to correctly tune it.

IN the RTN reference frame the equations of motion are expressed as:

$$\dot{r} = V_R \quad (19)$$

$$\dot{\theta} = \frac{V_T}{r} \quad (20)$$

$$\dot{V}_R = \frac{V_T^2}{r} - \frac{\mu}{r^2} + \frac{F_R}{m} \quad (21)$$

$$\dot{V}_T = -\frac{V_R V_T}{r} + \frac{F_T}{m} \quad (22)$$

Where:

- r is the radius of the trajectory;
- θ is the cross-track angle;
- V_R is the radial component of the velocity;
- V_T is the tangential component of the velocity;
- m is the mass of the lander;
- $\mu = 4902,7779 \frac{km^3}{s^2}$ is the gravitation parameter of the moon.

The two components of the thrust can be expressed as:

$$\begin{cases} F_R = F \sin \psi \\ F_T = -F \cos \psi \end{cases} \quad (23)$$

Where F is the module of the thrust and ψ indicates the direction, as can be seen in Figure 9.

The lander considered is not equipped with thrust vectoring, which means that in order to change the direction of the thrust the spacecraft must rotate completely, varying the pitch angle α . This means that the following relationship exist between the two angles, if ψ is considered positive as represented in Figure 9:

$$\alpha = -\psi \quad (24)$$

In addition, the following relationship has been added to the system of differential equation to take into account the changes in the mass of the lander:

$$\dot{m} = -\frac{F}{I_{sp} g_0} \cdot t_f \quad (25)$$

$$\frac{dm}{dt} = -\frac{F}{I_{sp}g_0} \quad (26)$$

With the goal to transform the descent time into a variable of the problem and eliminating the need to give it an arbitrary value at the beginning of the simulation this relationship has been introduced:

$$\tau = \frac{t}{t_f} \quad (27)$$

Which implies:

$$dt = d\tau \cdot t_f \quad (28)$$

Through this transformation of the time variable, final time t_f became a parameter of the optimization, with the system of equation that changed as follows, having as the independent variable τ and not t :

$$\dot{r} = v_r \cdot t_f \quad (29)$$

$$\dot{\theta} = \frac{v_T}{r} \cdot t_f \quad (30)$$

$$\dot{v}_r = \left(\frac{v_T^2}{r} - \frac{\mu}{r^2} + \frac{F_R}{m} \right) \cdot t_f \quad (31)$$

$$\dot{v}_T = \left(-\frac{v_R v_T}{r} + \frac{F_T}{m} \right) \cdot t_f \quad (32)$$

$$\dot{m} = -\frac{F}{I_{sp}g_0} \cdot t_f \quad (33)$$

$$\dot{t}_f = 0 \quad (34)$$

3.2.2 Control variables

To optimize the landing trajectory both thrust module F and direction ψ has been set as control variable. This means that they can freely change in order to maximize landing mass.

Previously, at the beginning of the study, thrust direction has been removed by the control variables in order to simplify convergence, imposing the thrust vector tangential to the descent trajectory. This was done in order to reduce the dimension of the problem and significantly shorten computational time so that the software could have been tuned easily and validated more rapidly.

Being the thrust tangential to the trajectory implies that it is aligned with the velocity vector. Therefore, it was useful to define the elevation angles as $\gamma = \text{atan}\left(\frac{V_R}{V_T}\right)$ that can be introduced in the system of equations:

$$\dot{r} = V_R \cdot t_f \quad (35)$$

$$\dot{\theta} = \frac{V_T}{r} \cdot t_f \quad (36)$$

$$\dot{V}_R = \left(\frac{V_T^2}{r} - \frac{\mu}{r^2} + \frac{F \sin(\gamma)}{m} \right) \cdot t_f \quad (37)$$

$$\dot{V}_T = \left(-\frac{V_R V_T}{r} + \frac{f \cos(\gamma)}{m}\right) \cdot t_f \quad (38)$$

$$\dot{m} = -\frac{F}{I_{sp} g_0} \cdot t_f \quad (39)$$

$$\dot{t}_f = 0 \quad (40)$$

3.2.3 Boundary conditions and constraints

The algorithm was created making it able to handle a set of boundary conditions at the initiation and termination of the descent trajectory. Specifically, ESA required the following constraints to be met, which have been reported in the following table (Table 1) Table 1: Descent starting and final conditions:

Table 1: Descent starting and final conditions

Initial conditions		Final conditions	
Starting altitude	$r_0 = 30 \text{ km} + R_{moon}$	Final altitude	$r_f = 30 \text{ m} + R_{moon}$
Starting radial velocity	$V_{R_0} = 0 \frac{m}{s}$	Final radial velocity	$V_{R_f} = -2 \frac{m}{s}$
Starting tangential velocity	$V_{T_0} = 1680 \frac{m}{s}$	Final tangential velocity	$V_{T_f} = 0 \frac{m}{s}$
Starting elevation angle/thrust direction	$\gamma_0 = \psi_0 = -0^\circ$	Final elevation angle/thrust direction	$\gamma_f = \psi_f = -90^\circ$
Starting mass	$m_0 = 7350 \text{ kg}$	Final mass	$m_f > 3400 \text{ kg}$

Additionally, two technological limits have been imposed by ESA on the derivative of the thrust module and pitch angle that the system must satisfy:

$$-0.02F_{max} \leq \dot{T} \leq 0.02F_{max} \quad (41)$$

And

$$-\psi_{lim} \leq \dot{\psi} \leq \psi_{lim} \quad (42)$$

To implement this control on the derivative the equations 41 and 42 have been rewritten as:

$$\left| \frac{F(t+dt) - F(t)}{dt} \right| \leq 0.02F_{max} \quad (43)$$

And

$$\left| \frac{\psi(t+dt) - \psi(t)}{dt} \right| \leq \psi_{lim} \quad (44)$$

Then it is possible to introduce the variable $dt = d\tau \cdot t_f$ obtaining:

$$\left| \frac{F(\tau + d\tau) - F(\tau)}{d\tau} \right| \leq 0.02 F_{max} t_f \quad (45)$$

And

$$\left| \frac{\psi(\tau + d\tau) - \psi(\tau)}{d\tau} \right| \leq \psi_{lim} t_f \quad (46)$$

3.2.4 Algorithm and tool architecture

With the physics of the problem now well defined, as well as the constraints, the final step was to choose an optimization strategy that will suit the problem in the best possible way.

With the goal of making a tool that will perform well in a commercial reality like *Thales* and that could be reused for different mission, it was necessary to put first the robustness of the algorithm. This means that the tool must converge even if the starting conditions will change, such as altitude, velocity, or the configuration of the thrusters.

To do so direct optimisation methods have been chosen for the optimization.

The platform identified for the implementation of direct methods applied to this optimal descent problem was *MATLAB* [17]. It was picked because today it is a consolidated reality in the space field and because of two particular routines, *fmincon* and *multistart*.

Fmincon is a subroutine part of the *optimization toolbox* [18] that can find a minimum of a constrained nonlinear multivariable function and therefore is ideal for this problem.

Fmincon solver finds the minimum of a cost function $J = f(x)$ part of a problem specified by:

$$\min f(x) \text{ such that } = \begin{cases} c(x) \leq 0 \\ c_{eq}(x) = 0 \\ A \cdot x \leq b \\ A_{eq} \cdot x = b_{eq} \\ lb \leq x \leq ub \end{cases} \quad (47)$$

Where:

- $c(x) \leq 0$ expresses nonlinear inequality constraints
- $c_{eq}(x) = 0$ expresses nonlinear equality constraints
- $A \cdot x \leq b$ expresses linear inequality constraints
- $A_{eq} \cdot x = b_{eq}$ expresses linear equality constraints
- $b \leq x \leq ub$ expresses the upper and lower boundaries

Fmincon can used different algorithms to directly solve di optimisation problems such as interior-point (default), trust-region-reflective, SQP and SQP-legacy'. The Sequential Quadratic Programming was picked due to its proven effectiveness in the space field.

To 'feed' a direct optimisation method like the SQP the problem must be discretized in a series of N arches defined by N+1 nodes in which the differential equation system will be solved (Figure 10). These arches have the same length, defined by the value of the dt considered in the problem.

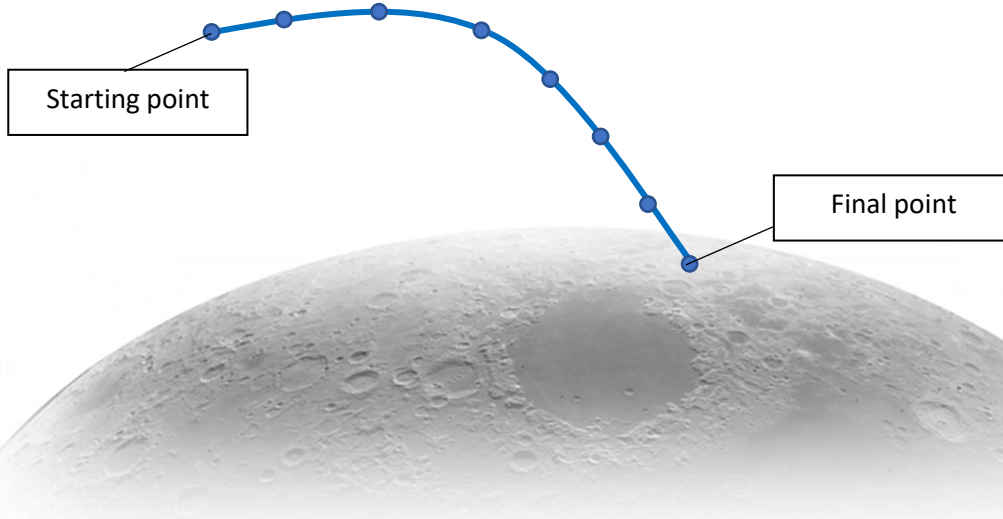


Figure 10: Discretized Landing Trajectory

The final step to make the function ready to perform the analysis is to implement all the constraints previously described.

For the starting and final points of the landing trajectory the constraint listed in Table 1 have been implemented as upper and lower boundaries in the first and last node. This may seem counterintuitive, but it gives the ability to the user to set a tolerance to the constraint. For example, considering the starting altitude $r_0 = 30 \text{ km}$ it possible to set $ub_{r_0} = r_0 + 500\text{m}$ and $lb_{r_0} = r_0 - 500\text{m}$, giving this way a $\pm 500\text{m}$ tolerance on the starting point. On the other hand, if the user desire to precisely set the starting altitude as 30 km, just have to set the two boundaries as coincident $ub_{r_0} = lb_{r_0} = r_0$.

The same concept has been applied to the maximum and minimum values of the control variable trust module $T_{min} \leq T \leq T_{max}$.

For the constraints on the derivatives \dot{T} and $\dot{\psi}$, the $c(x) \leq 0$ relationship has been exploited.

Starting from the equations 45 e 46, knowing that for a discretized dominium they can be rewritten as:

$$\left| \frac{F(i) - F(i+1)}{d\tau} \right| \leq 0.02 F_{max} t_f \quad \forall i = 1, \dots, N \quad (48)$$

And

$$\left| \frac{\psi(i) - \psi(i+1)}{d\tau} \right| \leq \psi_{lim} t_f \quad \forall i = 1, \dots, N \quad (49)$$

With i that identifies the i -th arch of the trajectory, the equations have been re-written the following quadratic form:

$$\left(\frac{F(i) - F(i+1)}{d\tau} \right)^2 - (0.02 F_{max} t_f)^2 \leq 0 \quad \forall i = 1, \dots, N \quad (50)$$

And

$$\left(\frac{\psi(i) - \psi(I + 1)}{d\tau}\right)^2 - (\psi_{lim} t_f)^2 \leq 0 \quad \forall i = 1, \dots, N \quad (51)$$

Both of them now resemble the relationship $c(x) \leq 0$ that allows the user to impose nonlinear inequalities to the solver.

Lastly, for the integration of the differential equations that describe the dynamics of the landing, the trapezoidal method was identified. This was due its shorter computational time compared to MATLAB native routines like ODE45 [18] or ODE113 [19].

Fmincon alone is not sufficient to guarantee the optimal solution, being a local optimizer. As can be seen from Figure 11 its necessary to use another routine that will cooperate with fmincon to ensure that the absolute minimum is achieved.

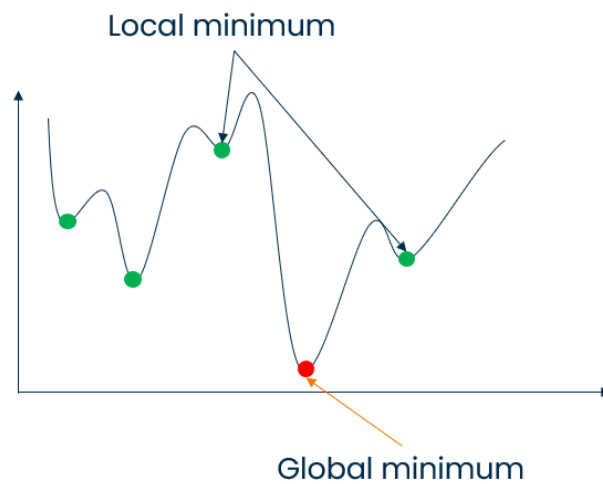


Figure 11: Local and Global minimum of a function

To achieve the desired goal the *multistart* [21] function was chosen. This function, part of the *Global Optimization Toolbox*, was created work jointly with fmincon and extends its ability to reach the global minimum. In particular, the solver attempts to find multiple local solutions to a problem by starting from various points, repeatedly calling fmincon.

RESULTS

In the following paragraphs are reported all the analysis made with the algorithm. Initially, only the thrust module was used as a control variable to validate the software against the guide values expected by ESA.

Later thrust direction control was implemented to improve the software and therefore the results obtained, subsequently making a trade-off between different propulsion architectures that were selected for the mission

4.1 Only thrust module control

As mentioned earlier, the first software validation analysis was done using only thrust as a control parameter, still setting a limit value to the pitch/elevation rate of $5 \frac{deg}{s}$. Moreover, the descent trajectory was discretized only into 40 arches to reduce computational time. This allowed for an easier tuning of the software to make it converge.

Furthermore, a small gap was left in the boundary conditions in the first and last point of the trajectory, as can be seen in Table 3, simplifying convergence.

Thrust direction was supposed tangential with trajectory, and therefore aligned with velocity vector but with opposite direction (see chapter 3.2.2 *Control variables*)

In the table below (Table 2) are listed the characteristics of propulsion architecture used in this analysis:

Table 2: Engine architecture

Engine	Number of engines	Tmax [kN]	Tmin [kN]	Isp [sec]	\dot{T}_{max} [N/sec]
Proto-0	4	5 x 4 = 20	2.5 x 4 = 10	325	0.02 x Tmax = 400

Later, the same thrusters' configuration was used for an analysis with different starting altitudes. For all these simulations the trial values assumed by the variables are supposed to be linear but, since the first iterations, the algorithm easily started producing feasible solutions.

4.1.1 Fixed altitude of 30000 meters

In Table 3 are reported all the constraint and boundaries imposed for this simulation. As reported, a little margin is left for the starting and final altitudes, as well as for the velocities and thrust direction to facilitate convergence.

Table 3: Results fixed starting altitude

	<i>Mission requirements</i>	<i>Simulation values</i>	<i>Upper boundary</i>	<i>Lower Boundary</i>
Initial mass	7350 kg	7350 kg	7350 kg	7350 kg
Final mass	> 3400 kg	4049.43 kg	-	-
Delta V	< 2457.15 m/s	1876.63 m/s	-	-
Maneuver time	-	597.07 sec	-	-
Initial altitude	30000 m	29050 m	30050 m	29050 m
Final altitude	30 m	25 m	35 m	25 m
Initial vertical speed	0 m/s	2 m/s	2 m/s	-2 m/s
Final vertical speed	-2 m/s	-3 m/s	-3 m/s	-1 m/s
Initial tangential speed	1680 m/s	1660 m/s	1700 m/s	1660 m/s
Final tangential speed	0 m/s	0.2 m/s	0.5 m/s	- 0.5 m/s
Initial thrust direction ψ	-	0° (horizontal)	0.1 °	- 0.1 °
Final thrust direction ψ	90° (vertical)	93.8° (vertical)	99 °	81 °

From the obtained results it can be observed that the optimizer tries to shift toward the most favorable boundary to maximize the mass at the end of the descent, which has a value of 4049.43 kg, significantly higher than the minimum value required by ESA of 3400 kg.

Down below have been reported all the feasible solution for a starting altitude of 30000 m that meet all the imposed constraints. As can be seen, 36 solutions out of the 100 iterations performed by the software satisfy all the boundary conditions, leading to slightly different trajectories and maneuver time (Figure 12, Figure 13 and Figure 14).

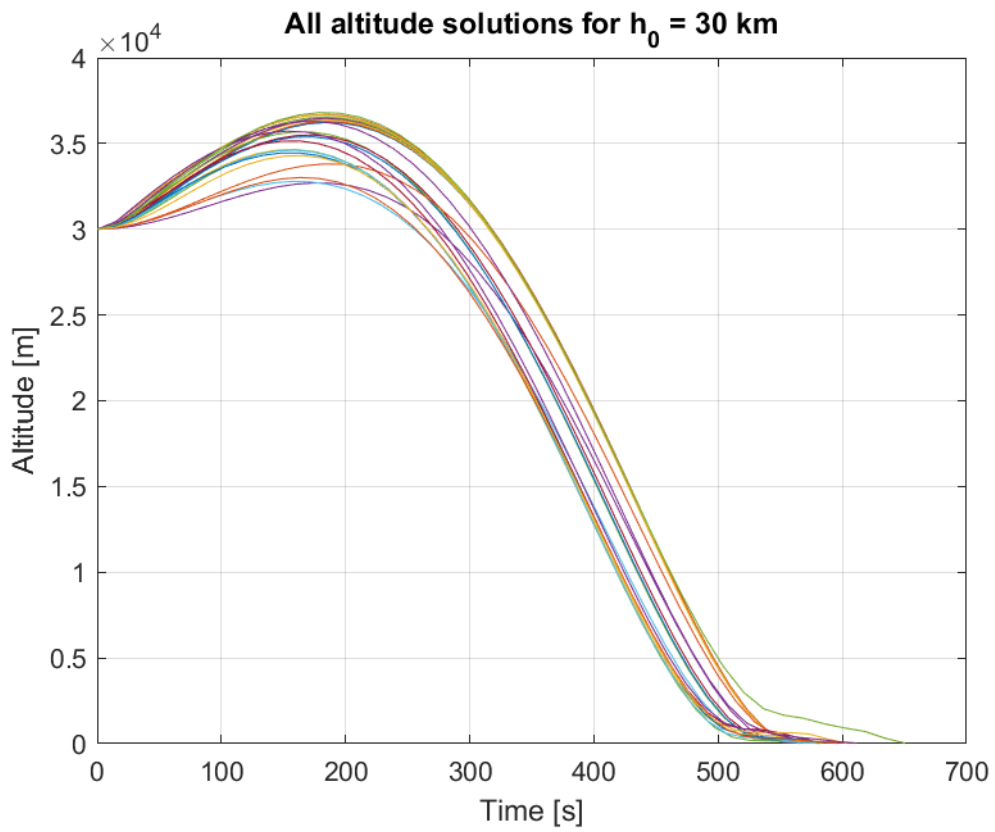


Figure 12: Altitude - Time for all feasible solutions

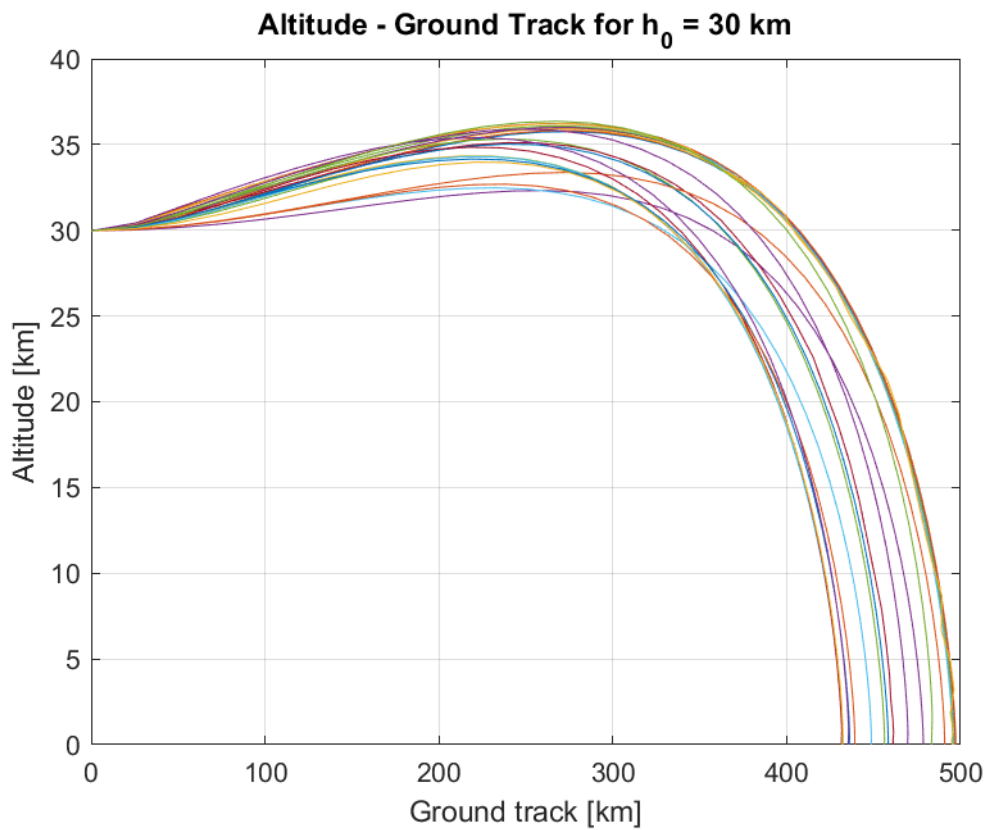


Figure 13: Altitude - Ground Track for all feasible solutions

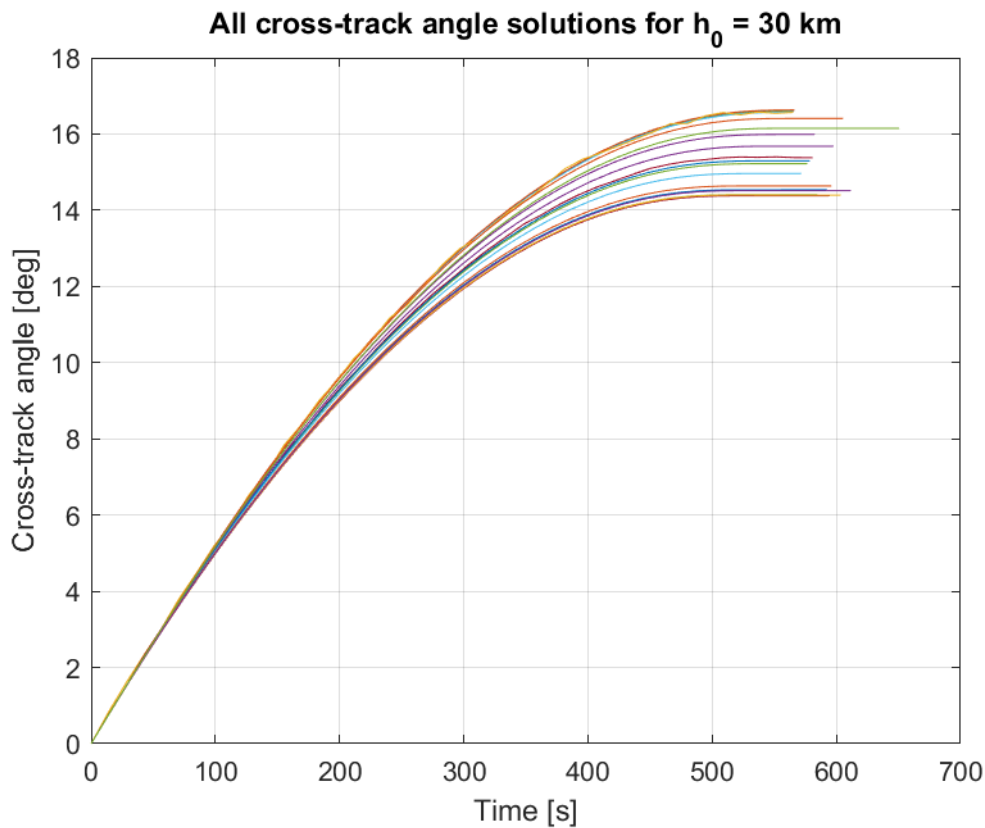


Figure 14: Cross-track Angle - Time for all feasible solutions

All trajectories are quite similar and show a tendency to raise altitude in the first part of the maneuver in order to earn enough time to break horizontal velocity and minimize gravity losses.

This is due the low level of *thrust to mass ratio* of the lander but, whether it would be possible to reach progressively greater values of thrust, this trend would gradually reduce until it disappears (*Dong-Hyun Cho, 2015*).

A similar phenomenon can be observed during the launch of rockets that use gravity turn as a steering mechanism.

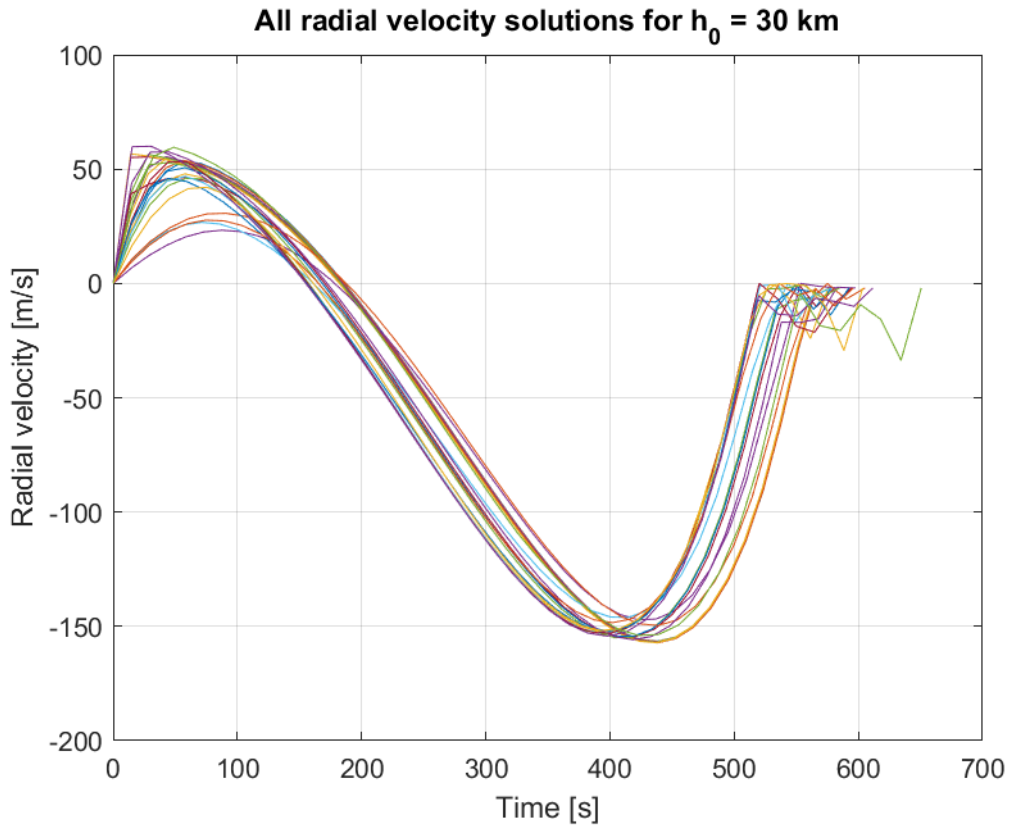


Figure 15: Radial Velocity - Time for all feasible solutions

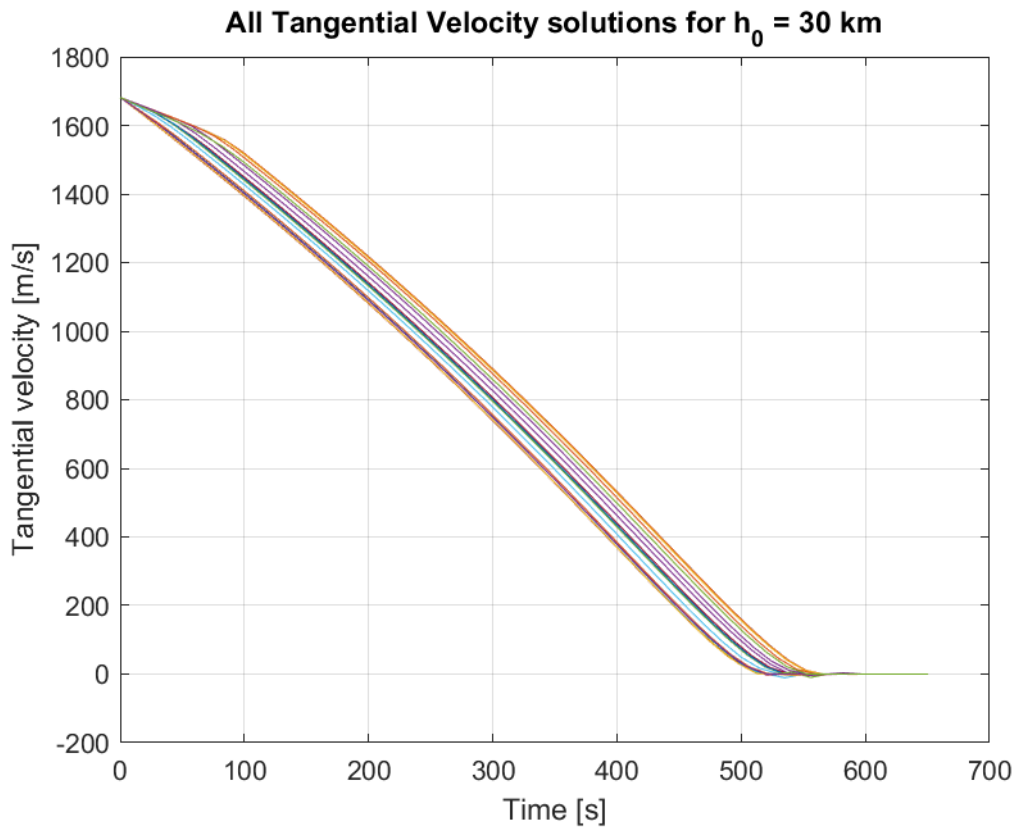


Figure 16: Tangential Velocity - Time for all feasible solutions

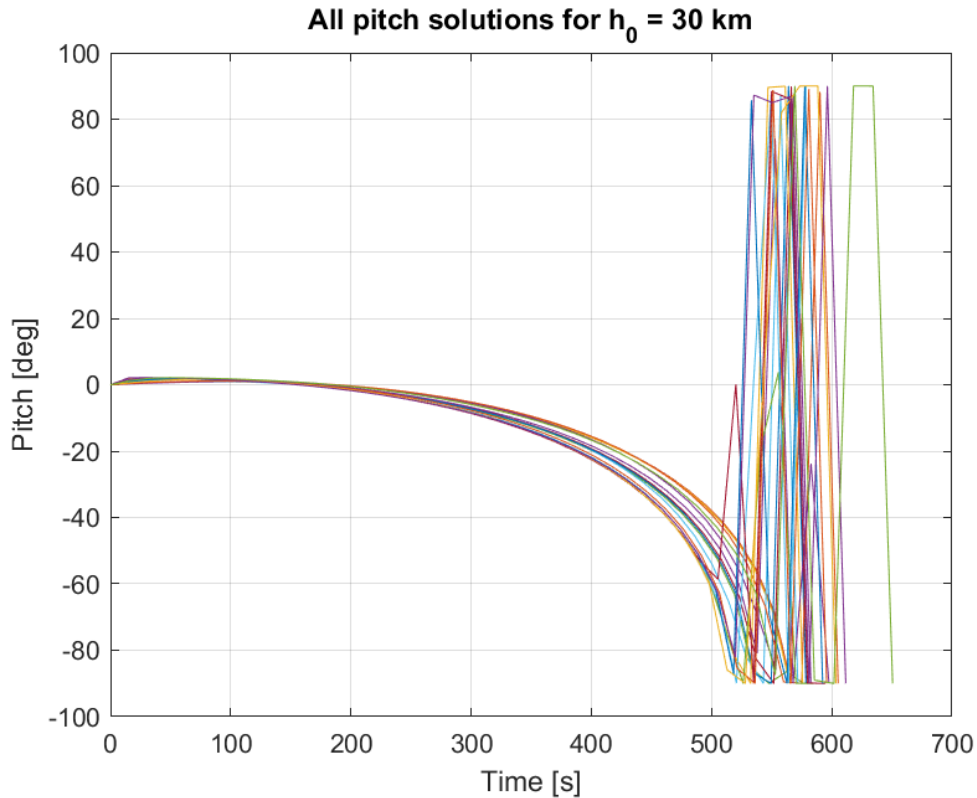


Figure 17: Pitch - Time for all feasible solutions

For some trajectories, as can be seen from the previous image, the pitch angle suddenly became positive (Figure 17) close to the end of the landing. This is because for this analysis the pitch angle coincides with the elevation angle, which is defined as:

$$\gamma = \text{atan}\left(\frac{V_R}{V_T}\right)$$

For several simulations, the lander reaches a small value of positive vertical velocity (Figure 15, Figure 16) before becoming negative or null again in the final point of the descent and this cause a change in the sign of the elevation angle γ .

This does not influence the results of the simulation and the optimal solution is not characterized by this phenomenon (Figure 25). In fact, having a small vertical velocity close to the arrival means that the lander ‘braked’ too hard on the vertical component and had to gain altitude again.

Obviously, this leads to a waste of propellant, especially considering that the ascent is made against the force of gravity, increasing gravity losses.

An important result can be extrapolated by the Figure 18 and Figure 19 in which it possible to identify a cluster of remarkably similar landing mass values all close to the absolute maximum. This means that the algorithm frequently converges to the best solution, proving its reliability.

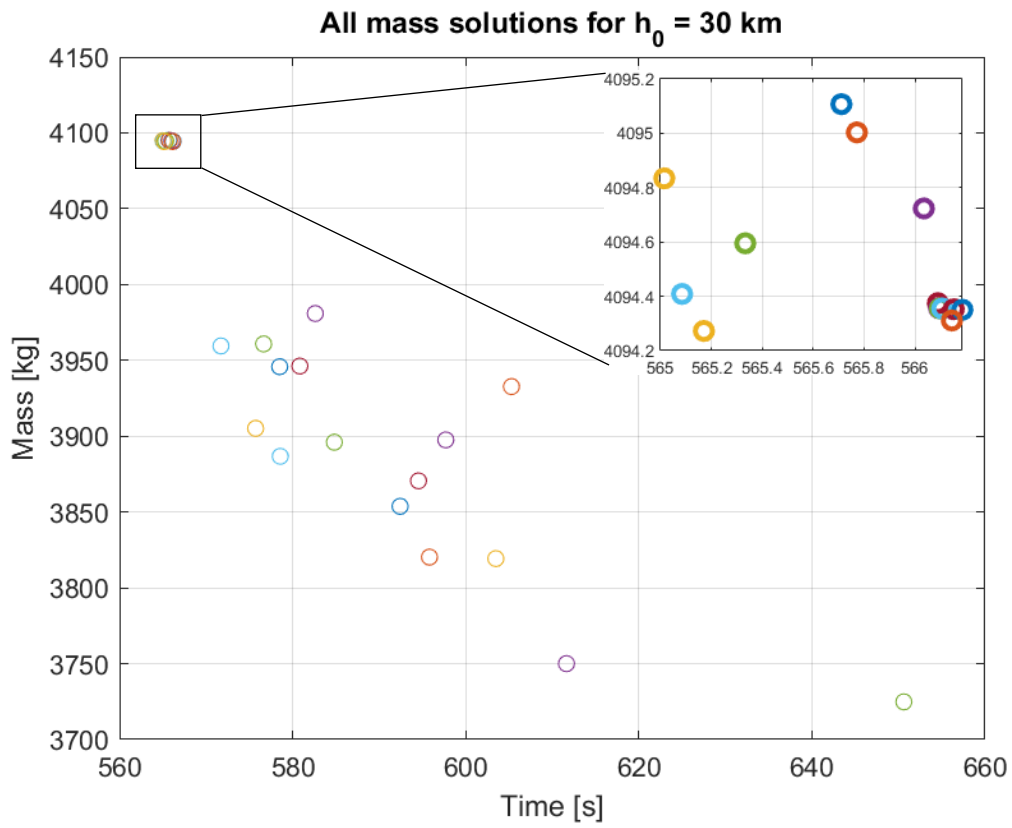


Figure 18: Landing masses - time for all feasible solutions

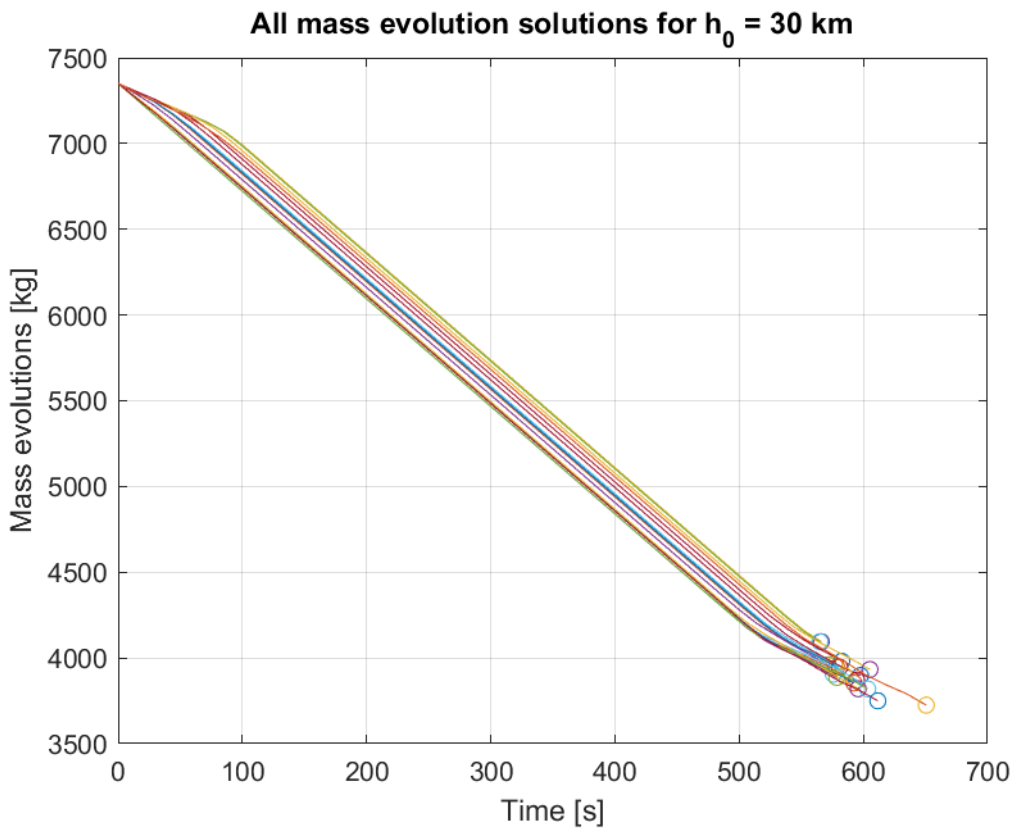


Figure 19: Mass evolution - Time for all feasible solutions

In Figure 20 are reported the values of the module of the thrust for the different trajectories:

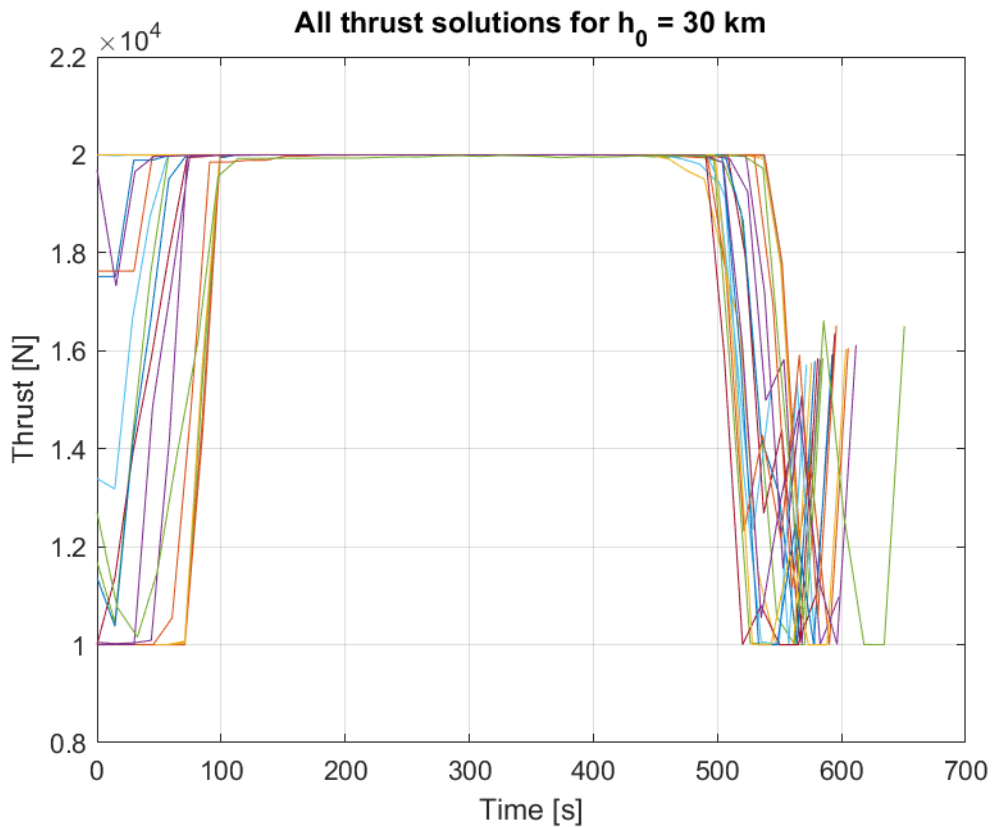


Figure 20: Thrust - time for all feasible solutions

In Figure 21, Figure 22, Figure 23, Figure 24, Figure 25, Figure 26 and Figure 27 are reported all the trends of the variables for the best case, i.e. the one with the highest landing mass; as stated before it's possible to observe that the global optimum does not show the tendency to regain altitude in proximity of the end of the trajectory and therefore there are no inversions in the sign of the pitch angle (Figure 25).

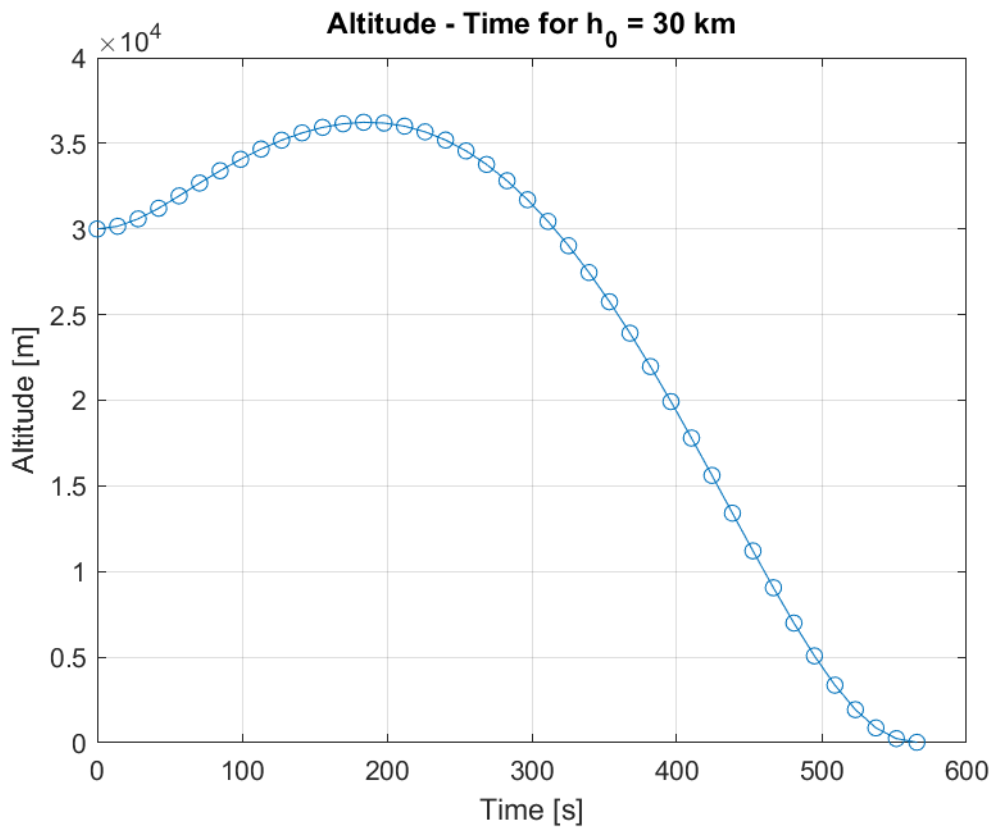


Figure 21: Altitude - Time best case

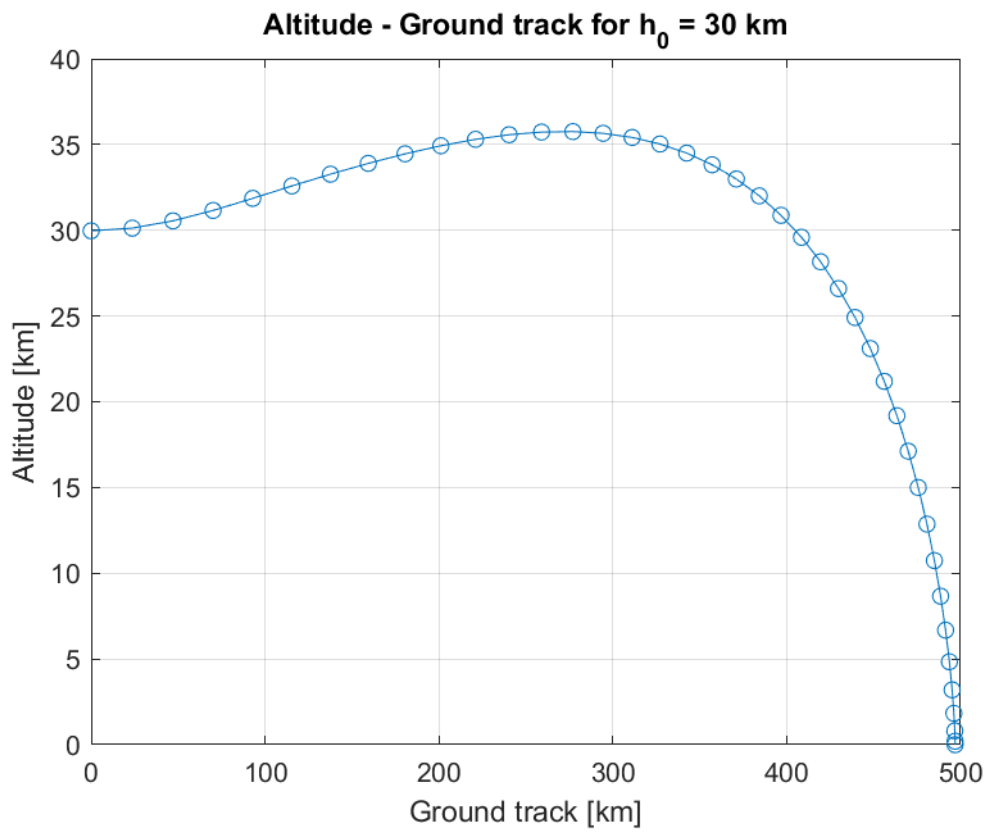


Figure 22: Altitude - Ground track best case

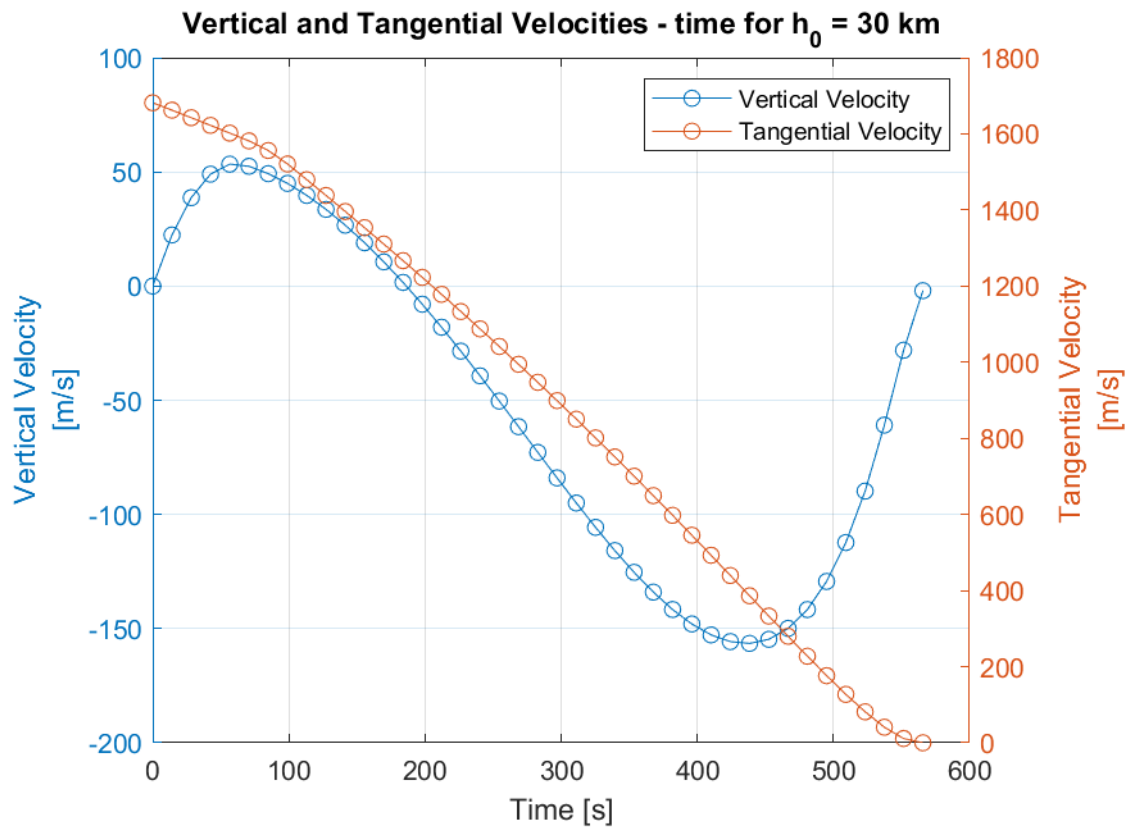


Figure 23: Tangential and Vertical Velocities best case

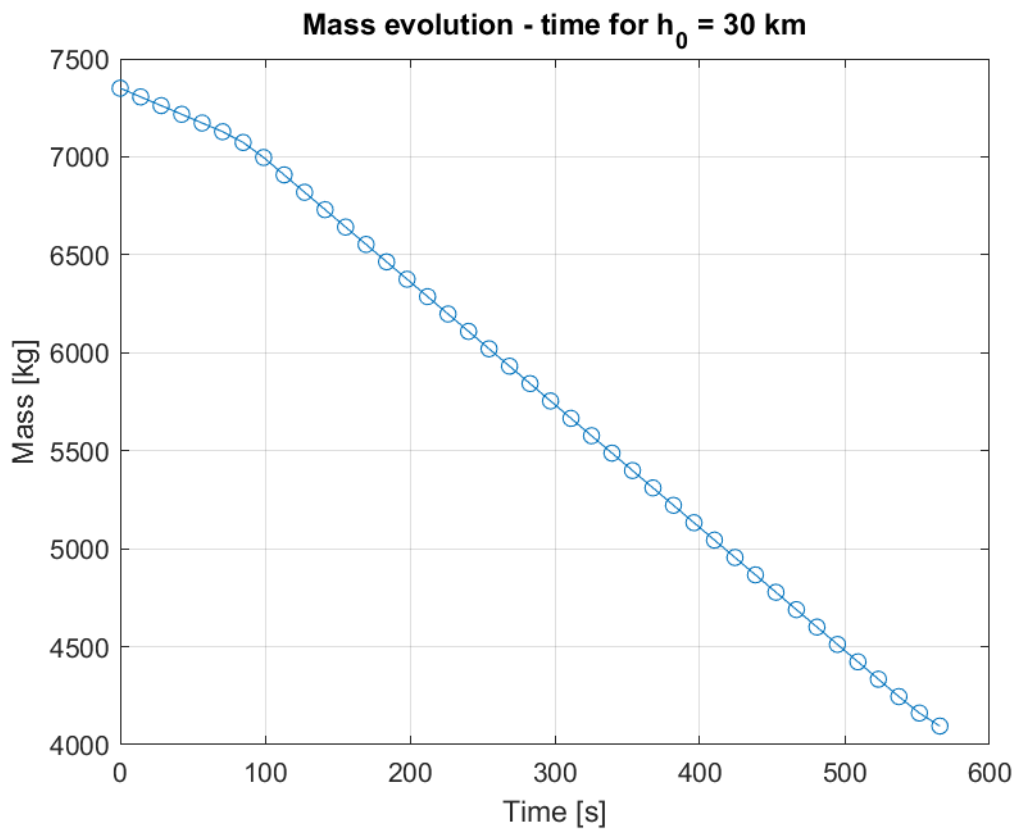


Figure 24: Mass evolution - Time best case

From the graph of the thrust module (Figure 25), is possible to observe that the trend resemble a step, with the thrust that is at the lowest level at the beginning and only later jumps to the maximum level. This suggest that the S/C waits to have the ideal pitch angle before firing at T_{max} .

For comparison, this does not happen if the pitch angle became a control variable that can freely change, as will be shown in the next chapter.

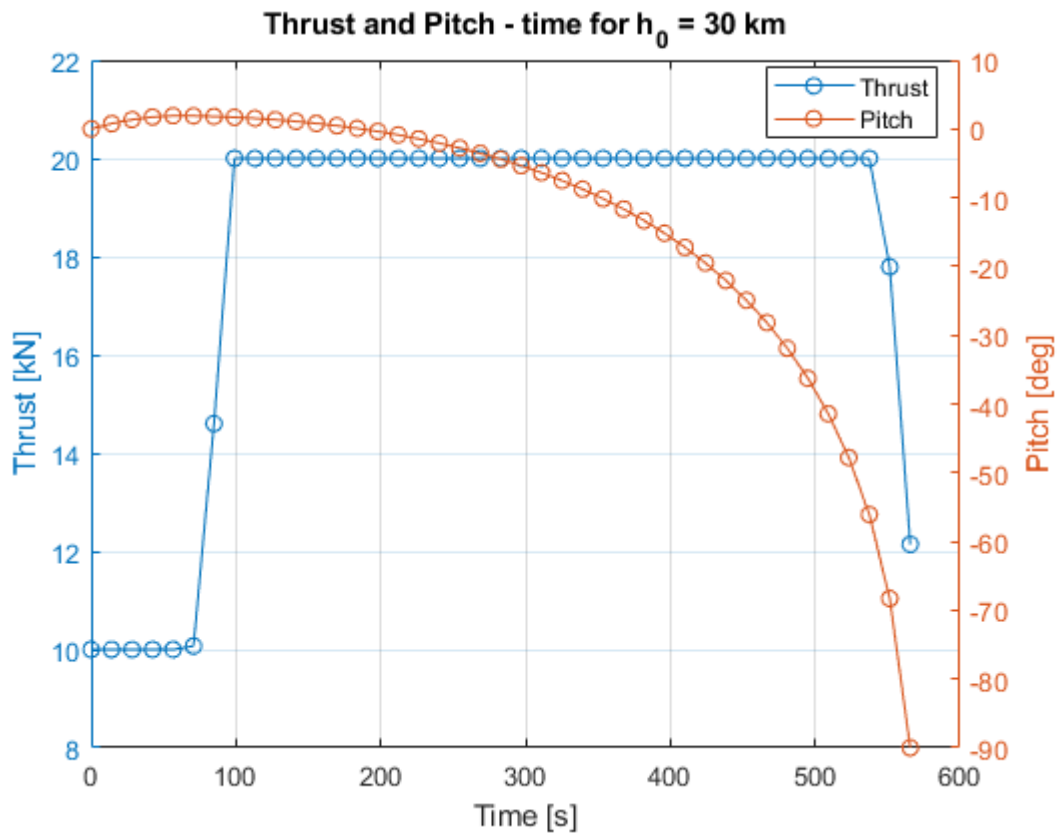


Figure 25: Thrust and Pitch - Time best case

In Figure 26 and Figure 27 are reported the trends of the derivative of the thrust module \dot{T} and pitch/elevation angle $\dot{\gamma}$ with the maxim values they are allowed to reach. Both are contained between the upper and lower imit, with \dot{T} that reaches the extremes while $\dot{\gamma}$ stays close to zero.

This is caused by the distinct roles that these two terms have: T is a control variable free to change accordingly to the imposed limits and uses all its capability to maximize the landing mass, while γ is a variable subjected by the equations that regulate the physic of the problem.

Additionally, \dot{T} is zero for almost all the descent, with two peaks that confirm the resemblance of the control variable to a step (in red and yellow are shown the upper and lower boundaries of the derivates respectively).

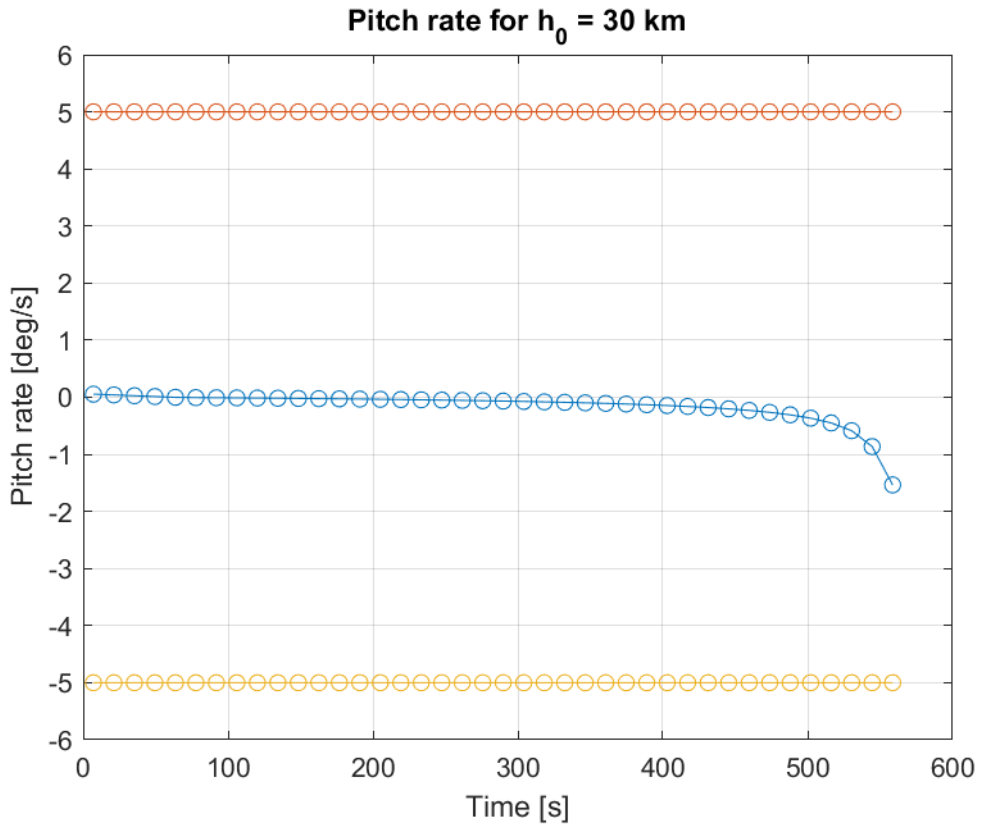


Figure 26. Pitch rate - Time best case

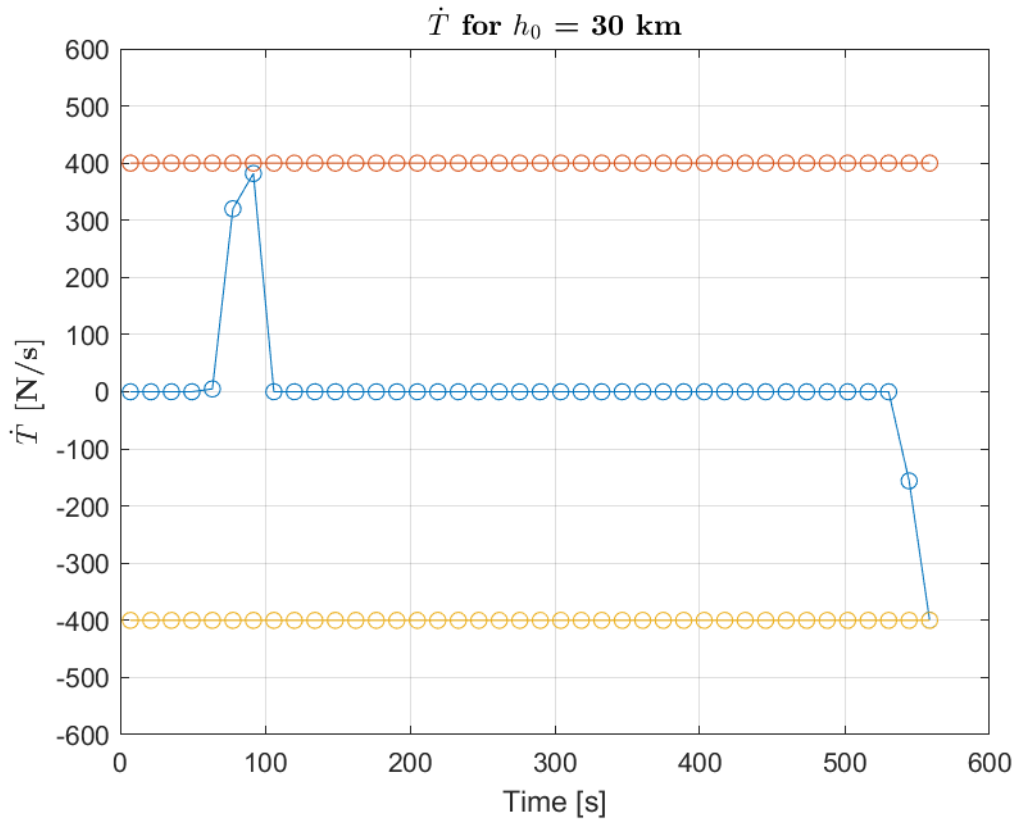


Figure 27: T_{dot} - time best case

4.1.2 Variable altitude with fixed starting mass

In this section an analysis at different starting quotes has been performed with a fixed starting mass of 7350 kg. This was made for two main reasons: one was the necessity to perform a sensitivity analysis of the tool and the other was to evaluate the effect of a different starting point on the landing mass and descent trajectory.

The procedure used is the same as the previous case, where a family of trajectories have been obtained and the best one is picked and compared with the other best solutions at different altitudes. The optimal trajectories are reported in Figure 28 and Figure 29, with the final masses related to time of flight and starting altitude (Figure 30).

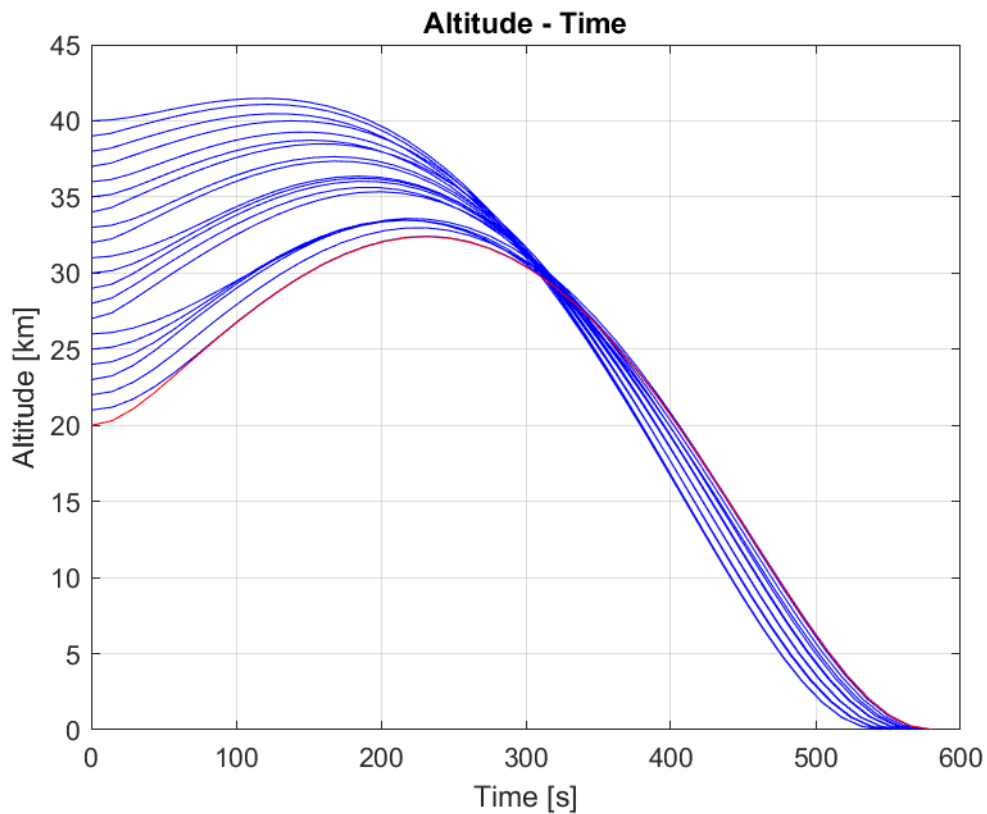


Figure 28: Altitude - Time for different starting altitudes

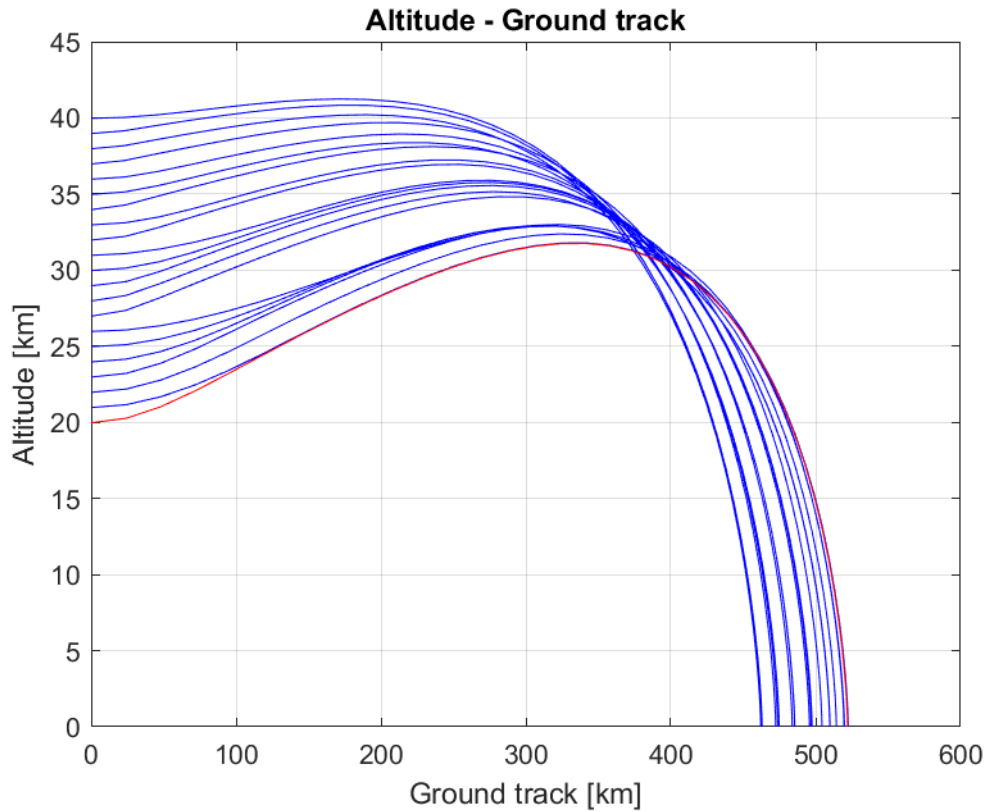


Figure 29: Altitude - Ground Track for different starting altitudes

As shown in Figure 28 and Figure 29 for a higher starting altitude there is a smaller ascent in the first part of the maneuver. This leads to a steeper and more vertical trajectory in the final part of the descent, increasing safety and simplifying obstacle detection and avoidance.

From Table 4 it can be seen that the tool responds well to the changes in the altitude. In fact, the total variation in landing mass between the cases at 20000 m and 40000 m is only 20 kg due to the tool's ability to optimize the thrust accordingly (Figure 32). As the starting altitude increases, there is a growth in average thrust value (Figure 31) while both landing mass and descent time decrease.

This is because the smaller ascent at the beginning of the maneuver makes the thrusters align sooner with the ideal direction, allowing them to fire at T_{max} earlier and this leads to a greater braking action and shorter descent time.

Lastly the reduction in maneuvering time is only 35 seconds between the highest starting trajectory and the lowest, which alone is not enough to justify the loss of 20 kg of useful mass at the landing. It is important to remember that, as said before, a higher PDI lead to a steeper and therefore safer trajectory and this will have an important weight in the choice of the starting point.

Table 4: Results for different starting altitudes

Starting altitude [m]	Final Mass [kg]	Time [s]	Average thrust value [N]
20000	4104.02	580.23	17666.24
21000	4103.86	580.45	17660.73
22000	4102.48	579.11	17708.19
23000	4101.23	579.39	17706.27
24000	4101.17	572.68	17910.65
25000	4101.06	572.61	17913.44
26000	4100.86	575.85	17814.41
27000	4097.26	570.25	18006.69
28000	4096.59	565.70	18153.29
29000	4095.67	565.88	18152.71
30000	4095.11	565.71	18161.01
31000	4094.67	565.04	18184.62
32000	4092.82	558.76	18396.05
33000	4092.11	558.86	18396.90
34000	4090.54	558.28	18424.34
35000	4089.92	552.42	18620.24
36000	4088.83	552.08	18637.78
37000	4087.52	551.51	18663.94
38000	4086.59	545.21	18881.52
39000	4085.65	545.22	18886.61
40000	4084.64	545.48	18883.45

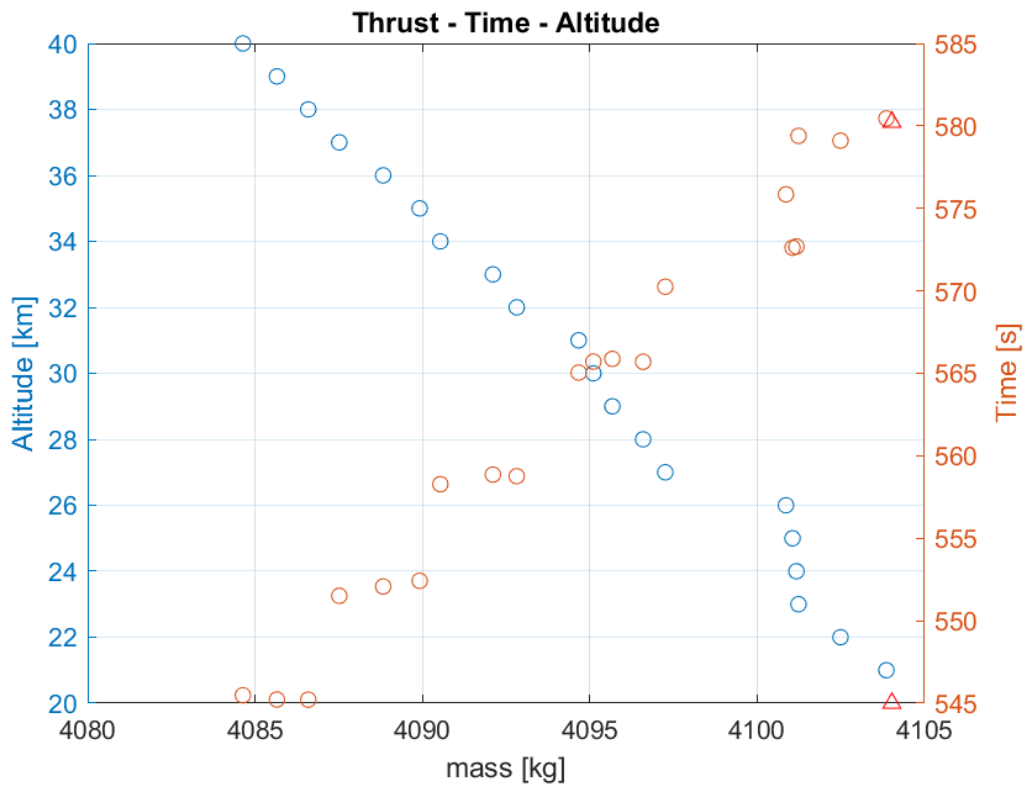


Figure 30: Final mass with descent time and starting altitude

Thrust - time @ different altitudes

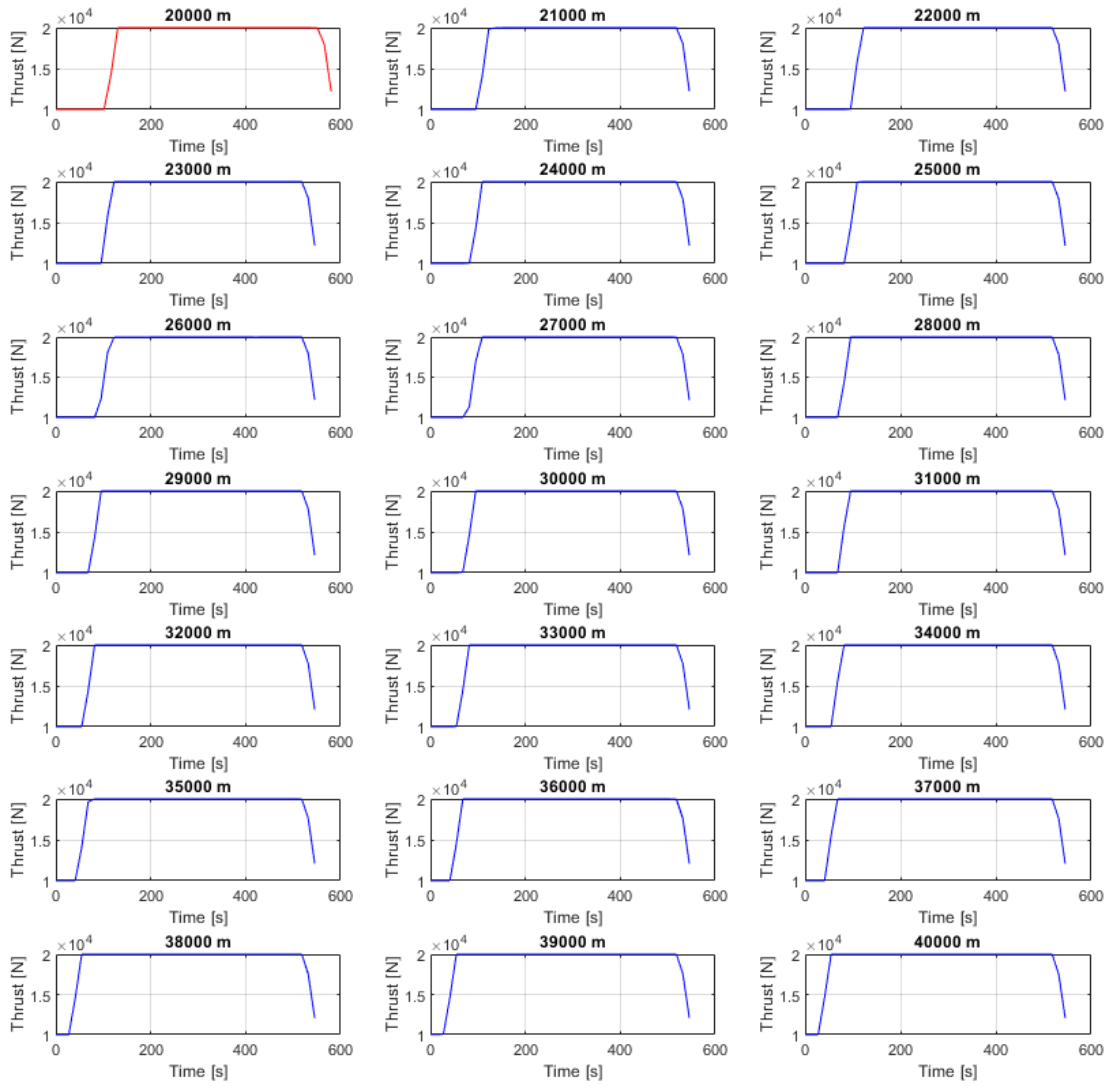


Figure 31: Thrust trends - Time for different starting altitudes

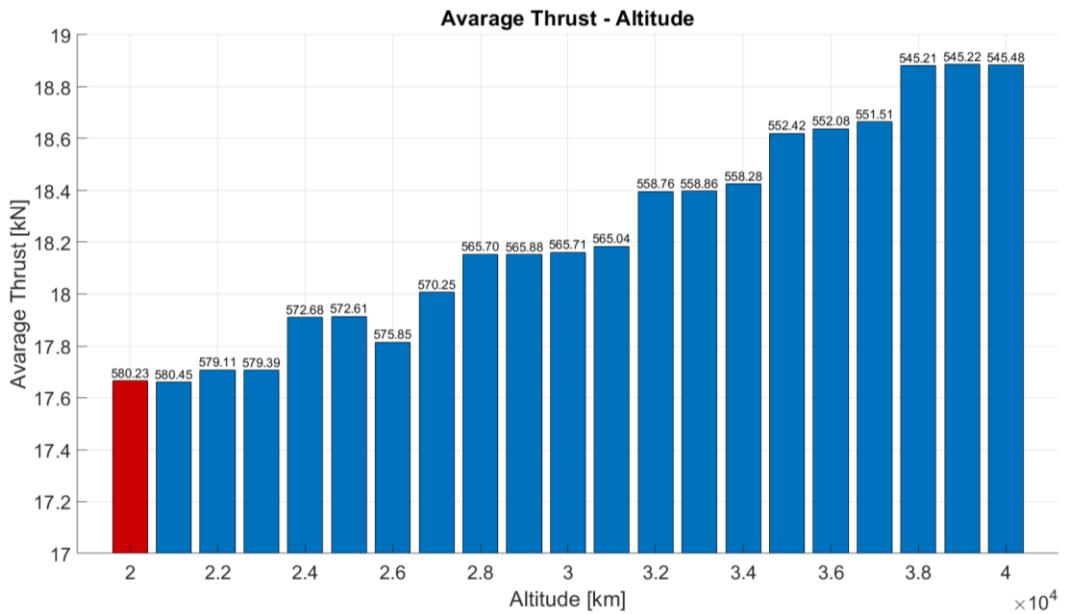


Figure 32: Average thrust and descent time for different starting altitude

4.2 Thrust module and pitch control

Once the software reliability has been proven in the previous study cases, the tool has been updated with the ability to use pitch/thrust direction ψ as a control variable to perform a tradeoff between four different engines architectures for a real mission.

Now the pitch angle ψ is a control variable being free to change with a limit on $\dot{\psi}$ and it is not forced to being coincident with the elevation angle γ , increasing the degrees of freedom of the system and therefore improving its performances.

For each of the four architectures, three different control configurations have been considered:

- **One control variable** → Thrust module T with an elevation/pitch rate limit of $5 \frac{deg}{s}$. This is the same kind of analysis performed in chapters [1] and [2].
- **Two control variables** → Thrust module T and direction ψ with pitch rate limit of $\dot{\psi} = 5 \frac{deg}{s}$;
- **Two control variables** → Thrust module T and direction ψ with pitch rate limit of $\dot{\psi} = 0.5 \frac{deg}{s}$.

The values of $\dot{\psi}_{max}$ were given by ESA's preliminary analysis, which identified $5 \frac{deg}{s}$ as a technological limit and $0.5 \frac{deg}{s}$ to obtain smother solutions.

For commercial reasons the name of the engines and their real performances (T_{max} , T_{min} and I_{sp}) will be concealed, but the results shown in the following paragraph are sufficiently in line with the real ones to be accepted as representative of the actual study.

As said, four different engine architectures have been compared: case 1.1 and 1.2 use the same engine but in different numbers, 4 for the first and 5 for the second case, while 2.1 and 2.2 both use 3 identical engines but with different values of \dot{T} .

All the data about these configurations are listed in Table 5, Table 6, Table 7 and Table 8:

Table 5: Four Proto-1 engine architecture

Engine	Number of engines	T_{max} [kN]	T_{min} [kN]	I_{sp} [sec]	\dot{T}_{max} [kN/sec]
Proto-1	4	$5.25 \times 4 = 18$	$4 \times 4 = 13.6$	321	$0.02 \times T_{max} = 0.421$

Table 6: 5 Proto-1 engine architecture

Engine	Number of engines	T_{max} [kN]	T_{min} [kN]	I_{sp} [sec]	\dot{T}_{max} [kN/sec]
Proto-1	5	$5.25 \times 5 = 22.5$	$4 \times 5 = 17$	321	$0.02 \times T_{max} = 525$

Table 7: 3 Proto-2 engine architecture with $T_{\dot{}} = 2000 \text{ N/s}$ each

Engine	Number of engines	T_{max} [kN]	T_{min} [kN]	I_{sp} [sec]	\dot{T}_{max} [kN/sec]
Proto-2	3	$7 \times 3 = 21$	$3.5 \times 3 = 10.5$	325	$2 \times n^{\circ} \text{ engines} = 6$

Table 8: 3 Proto-2 engine architecture with $T_{\dot{}} = 1000 \text{ N/s}$ each

Engine	Number of engines	T_{max} [kN]	T_{min} [kN]	I_{sp} [sec]	\dot{T}_{max} [kN/sec]
Proto-2	3	$7 \times 3 = 21$	$3.5 \times 3 = 10.5$	325	$1 \times n^{\circ} \text{ engines} = 3$

For all these twelve analyses the tolerance between the upper and lower boundaries has been reduced to zero, making them coincident (for example, the starting altitude is exactly 30000 m, while in the previous chapter $\pm 50 \text{ m}$ were allowed). Moreover, the mesh has been thickened, increasing the number of arches from 40 to 50, improving accuracy but significantly raising computational times.

4.2.1 Architectures comparison

In order to simplify the comparison between the outcomes of the various studies four summary tables (Table 9, Table 10, Table 11 and Table 12) have been made.

From their observation is noticeable that for all four architectures the best cases are those with a $5 \frac{\text{deg}}{\text{s}}$ pitch rate limit which are the ones with the greatest control ability. They are followed by the ones with only thrust module control and the worst are those with $0.5 \frac{\text{deg}}{\text{s}}$ of maximum pitch rate.

Interestingly, this implies that it is better to have a higher value of maximum pitch rate and only one control (thrust module) than controlling both thrust module and direction but with a lower pitch rate.

Table 9: Results case 1.1

	<i>Mission requirements</i>	<i>No pitch control</i>	<i>Pitch rate < 5 $\frac{deg}{sec}$</i>	<i>Pitch rate < 0.5 $\frac{deg}{sec}$</i>
Initial mass	7350 kg	7350 kg	7350 kg	7350 kg
Final mass	> 3400 kg	4049.43 kg	4096.10 kg	3979.12 kg
Delta V	< 2457.15 m/s	1876.63 m/s	1840.55 m/s	1931.77 m/s
Maneuver time	-	597.07 sec	570.38 sec	613.54 sec
Initial altitude	30000 m	30000 m	30000 m	30000 m
Final altitude	30 m	30 m	30 m	30 m
Initial vertical speed	0 m/s	0 m/s	0 m/s	0 m/s
Final vertical speed	-2 m/s	-2 m/s	-2 m/s	-2 m/s
Initial tangential speed	1680 m/s	1680 m/s	1680 m/s	1680 m/s
Final tangential speed	0 m/s	0 m/s	0 m/s	0 m/s
Initial thrust direction ψ	-	0° (horizontal)	-2.96°	8.84°
Final thrust direction ψ	90° (vertical)	90° (vertical)	90° (vertical)	90° (vertical)
BEST CASE				

Table 10: results case 1.2

	<i>Mission requirements</i>	<i>No pitch control</i>	<i>Pitch rate < 5 $\frac{deg}{sec}$</i>	<i>Pitch rate < 0.5 $\frac{deg}{sec}$</i>
Initial mass	7350 kg	7350 kg	7350 kg	7350 kg
Final mass	> 3400 kg	4110.06 kg	4138.14 kg	3943.64 kg
Delta V	< 2457.15 m/s	1882.88 m/s	1808.41 m/s	1959.96 m/s
Maneuver time	-	462.36 sec	493.25 sec	528.25 sec
Initial altitude	30000 m	30000 m	30000 m	30000 m
Final altitude	30 m	30 m	30 m	30 m
Initial vertical speed	0 m/s	0 m/s	0 m/s	0 m/s
Final vertical speed	-2 m/s	-2 m/s	-2 m/s	-2 m/s
Initial tangential speed	1680 m/s	1680 m/s	1680 m/s	1680 m/s
Final tangential speed	0 m/s	0 m/s	0 m/s	0 m/s
Initial thrust direction ψ	-	0° (horizontal)	-5.78°	17.85°
Final thrust direction ψ	90° (vertical)	90° (vertical)	90° (vertical)	90° (vertical)
BEST CASE				

Table 11: results case 1.2

	<i>Mission requirements</i>	<i>No pitch control</i>	<i>Pitch rate < 5 $\frac{deg}{sec}$</i>	<i>Pitch rate < 0.5 $\frac{deg}{sec}$</i>
Initial mass	7350 kg	7350 kg	7350 kg	7350 kg
Final mass	> 3400 kg	4060.39 kg	4126.16 kg	4029.36 kg
Delta V	< 2457.15 m/s	1891.39 m/s	1840.18 m/s	1915.85 m/s
Maneuver time	-	645.80 sec	573.72 sec	622.08 sec
Initial altitude	30000 m	30000 m	30000 m	30000 m
Final altitude	30 m	25 m	30 m	30 m
Initial vertical speed	0 m/s	0 m/s	0 m/s	0 m/s
Final vertical speed	-2 m/s	-1 m/s	-2 m/s	-2 m/s
Initial tangential speed	1680 m/s	1680 m/s	1680 m/s	1680 m/s
Final tangential speed	0 m/s	0 m/s	0 m/s	0 m/s
Initial thrust direction ψ	-	0° (horizontal)	-3.39°	3.31°
Final thrust direction ψ	90° (vertical)	90° (vertical)	90° (vertical)	90° (vertical)
BEST CASE				

Table 12: results case 2.2

	<i>mission requirements</i>	<i>No pitch control</i>	<i>Pitch rate < 5 $\left[\frac{deg}{sec}\right]$</i>	<i>Pitch rate < 0.5 $\left[\frac{deg}{sec}\right]$</i>
Initial mass	7350 kg	7350 kg	7350 kg	7350 kg
Final mass	> 3400 kg	4037.38 kg	4128.27 kg	4029.38 kg
Delta V	2457.15 m/s	1909.51 m/s	1838.55 m/s	1915.83 m/s
Maneuver time	-	652.10 sec	573.34 sec	625.52 sec
Initial altitude	30000 m	30000 m	30000 m	30000 m
Final altitude	30 m	25 m	35 m	30 m
Initial vertical speed	0 m/s	0 m/s	0 m/s	0 m/s
Final vertical speed	-2 m/s	-1 m/s	-4 m/s	-2 m/s
Initial tangential speed	1680 m/s	1680 m/s	1680 m/s	1680 m/s
Final tangential speed	0 m/s	0 m/s	0 m/s	0 m/s
Initial thrust direction ψ	-	0° (horizontal)	-3.25°	3.16°
Final thrust direction ψ	90° (vertical)	90° (vertical)	90° (vertical)	90° (vertical)
BEST CASE				

From the study of the trajectories reported in Figure 33, Figure 34, Figure 35, Figure 36, Figure 37, Figure 38, Figure 39 and Figure 40 it is observable that for cases 1.1, 2.1 and 2.2, when the thrust module is the only control, the S/C raises its altitude at the beginning of the descent to gain enough time to nullify horizontal velocity. This does not happen when the second control is introduced freeing pitch angle ψ .

Contrarily case 1.2 is different: thanks to its high value of T_{max} there is no ascent even with only one control variable, but this happens if a pitch rate limit of 0.5 deg/s is imposed. This means that for such high values of T_{min} and T_{max} the downgrading effect of reducing the pitch rate is higher than the added ability to freely commute it but to a lower degree.

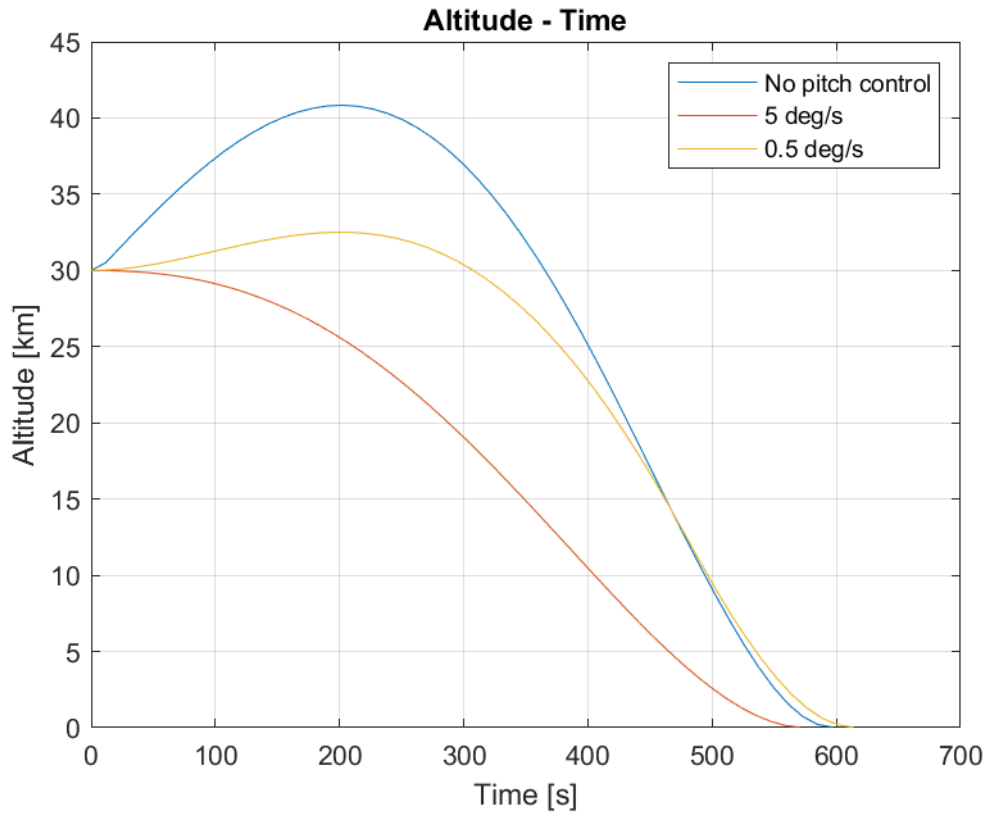


Figure 33: Altitude - Time for case 1.1

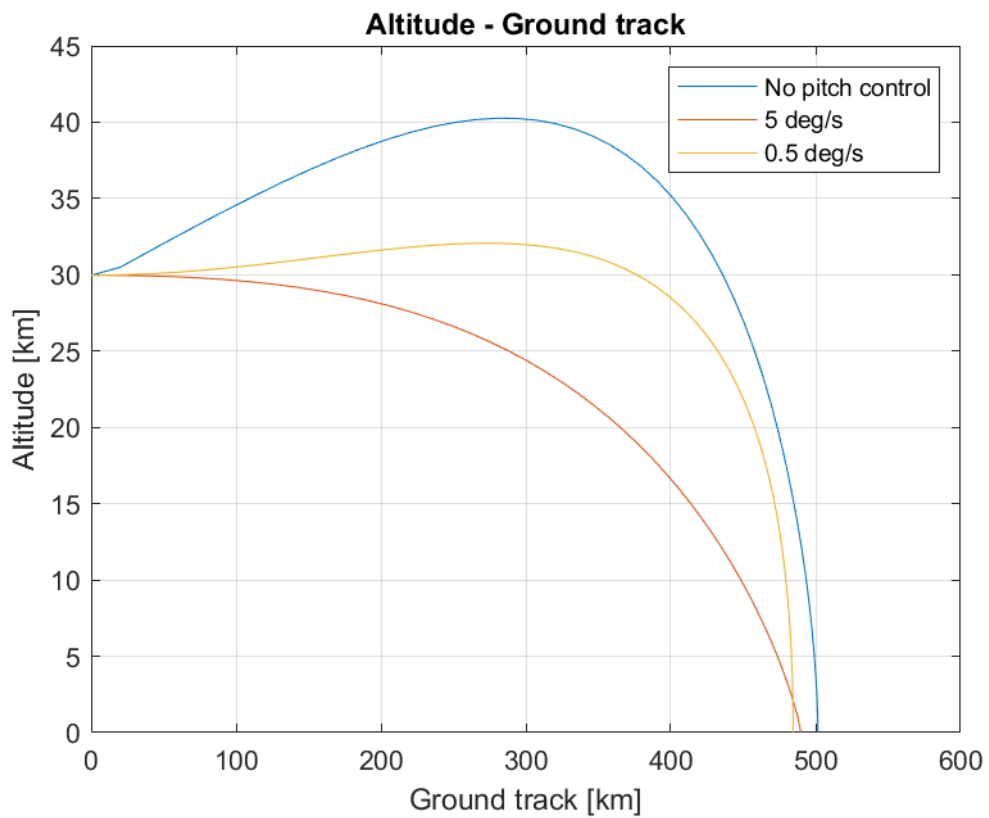


Figure 34: Altitude - Ground track for case 1.1

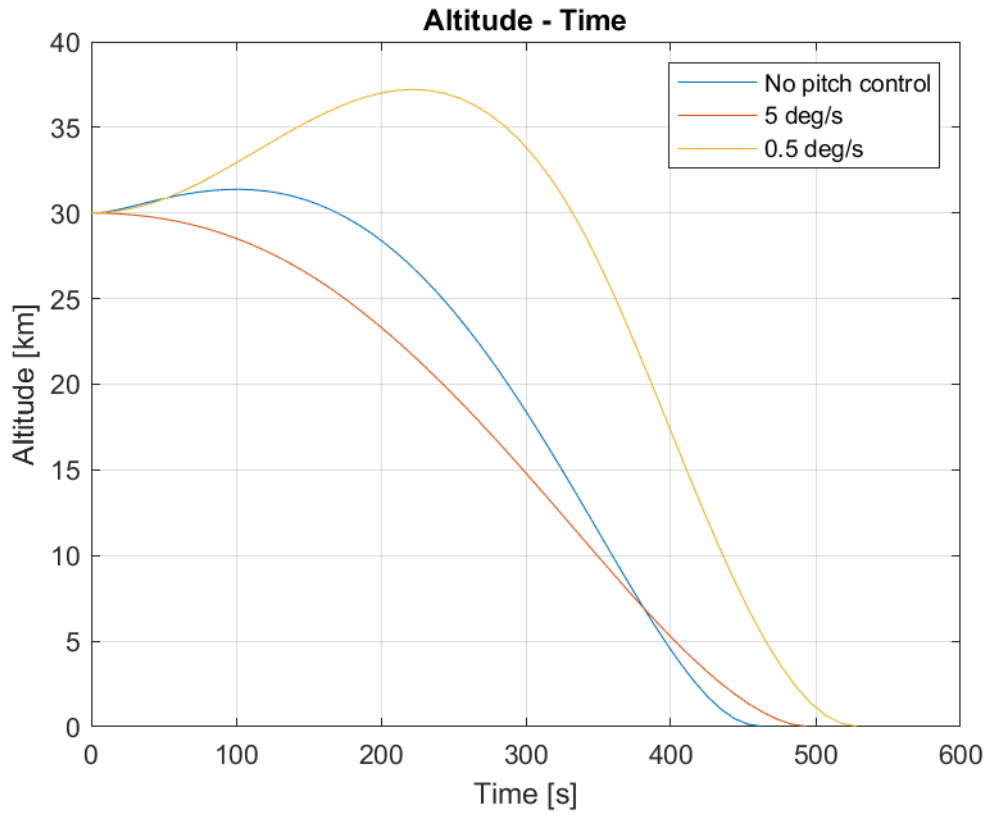


Figure 35: Altitude - Time for case 1.2

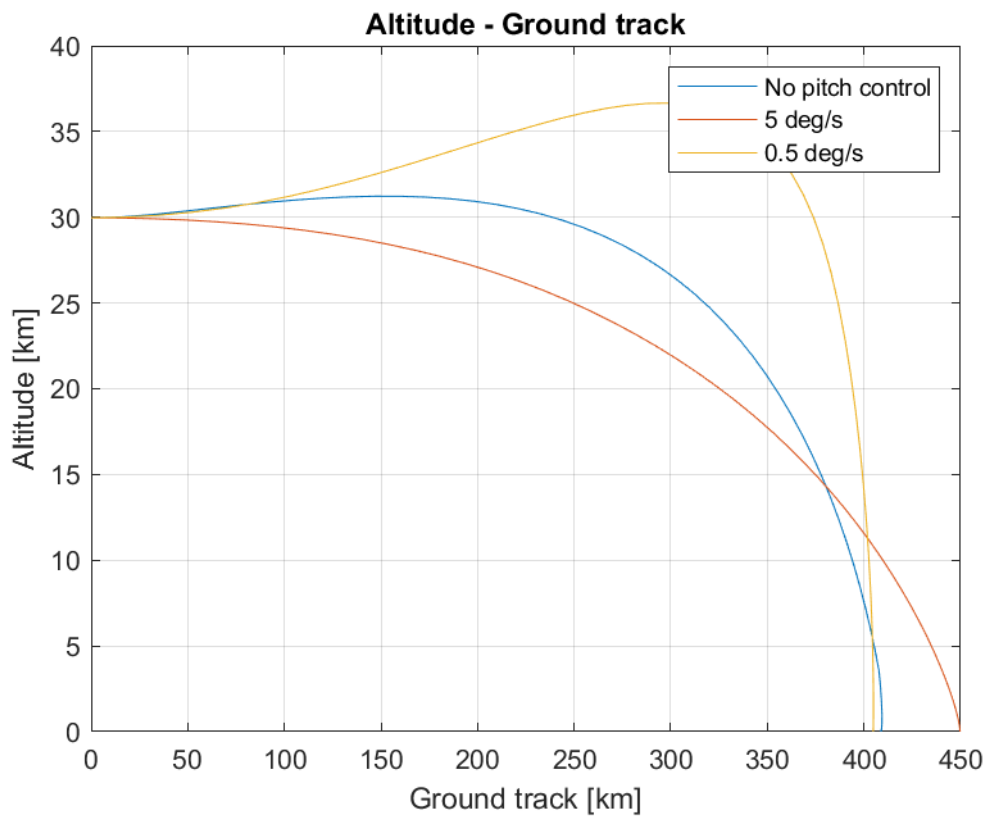


Figure 36: Altitude - Ground track for case 1.2

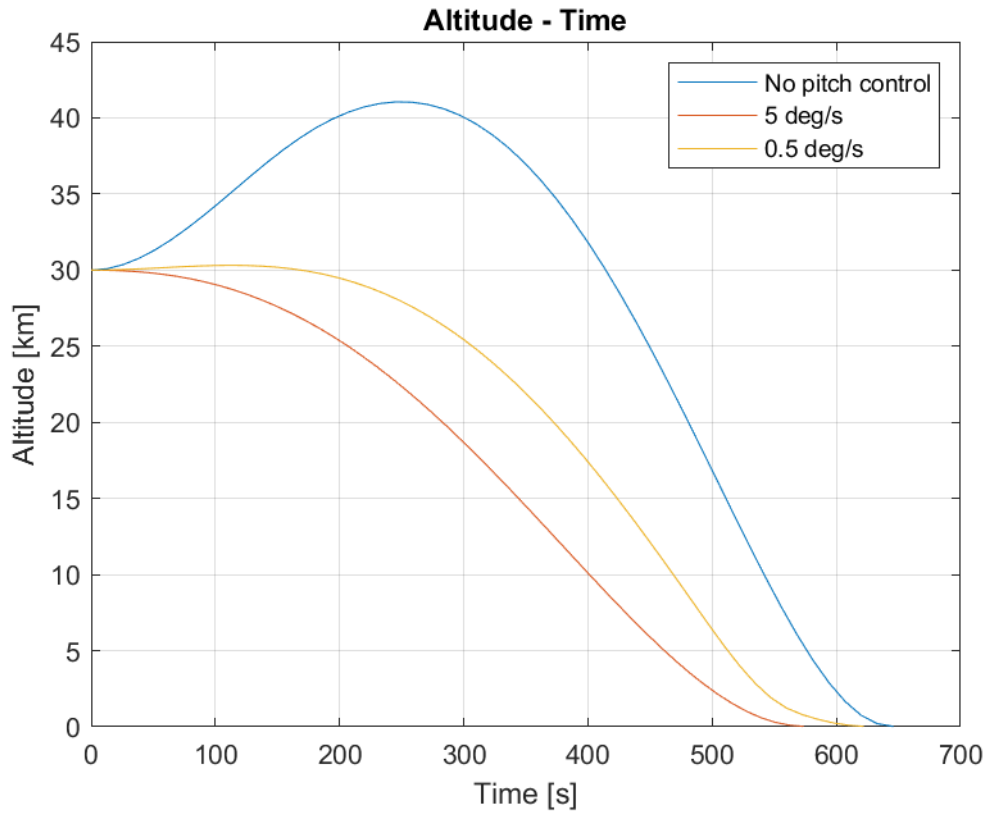


Figure 37: Altitude - Time for case 2.1

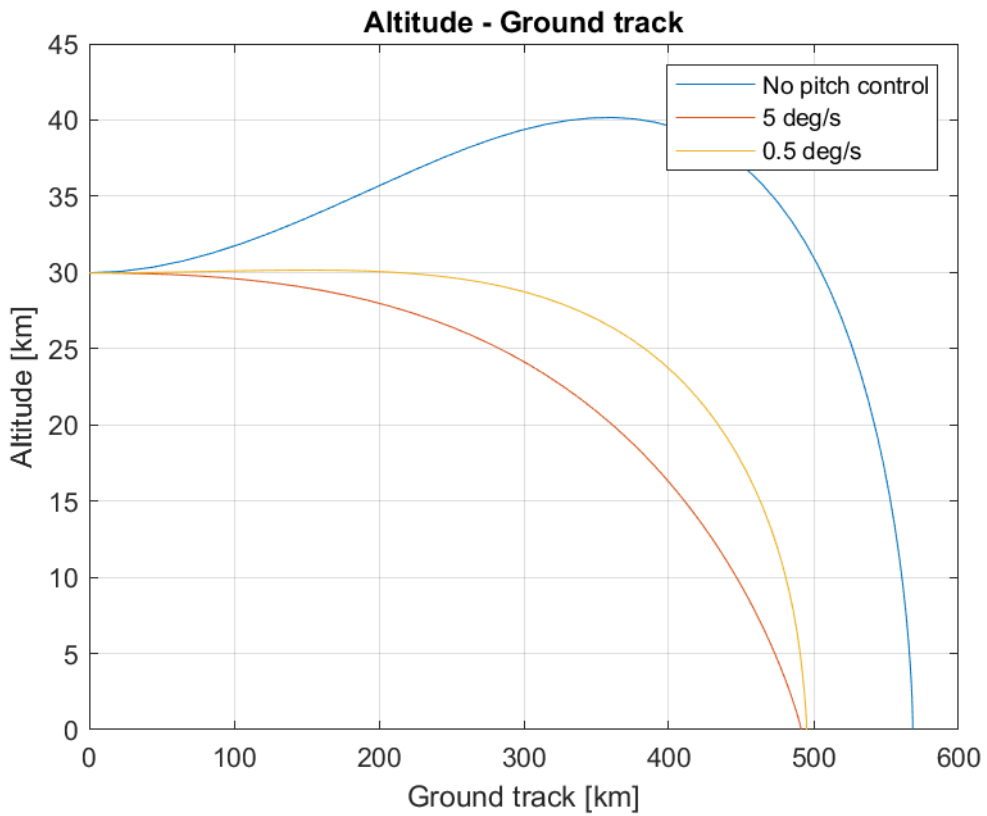


Figure 38: Altitude - Ground track for case 2.1

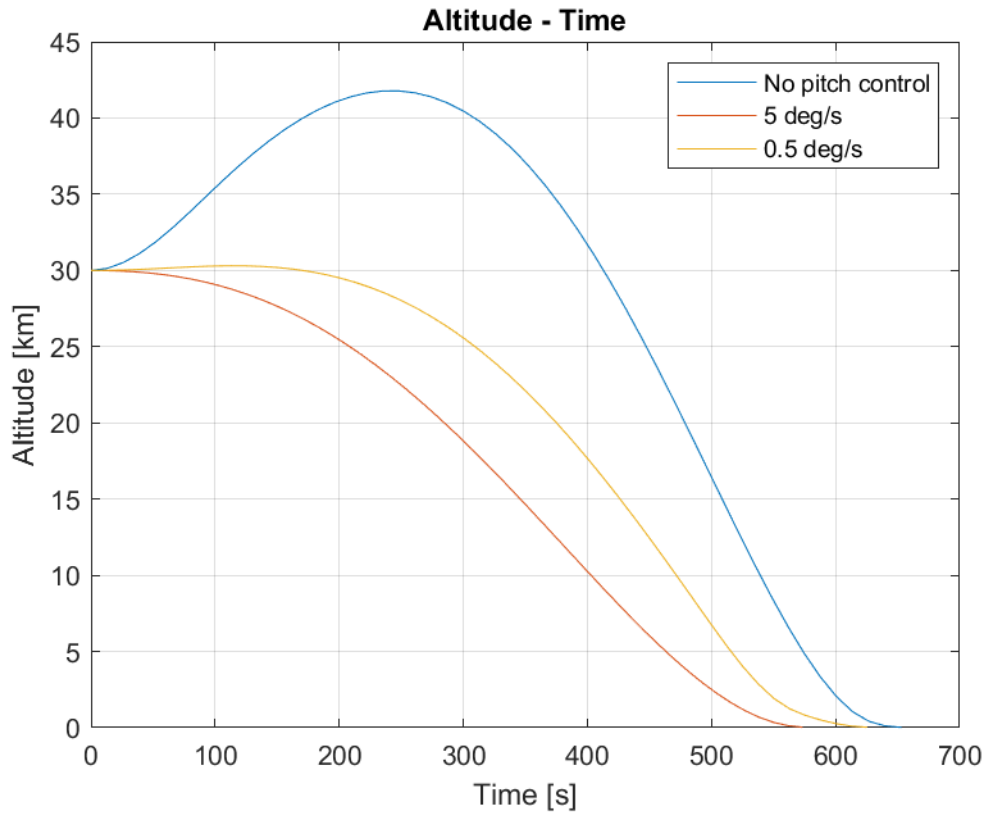


Figure 39: Altitude - Time for case 2.2

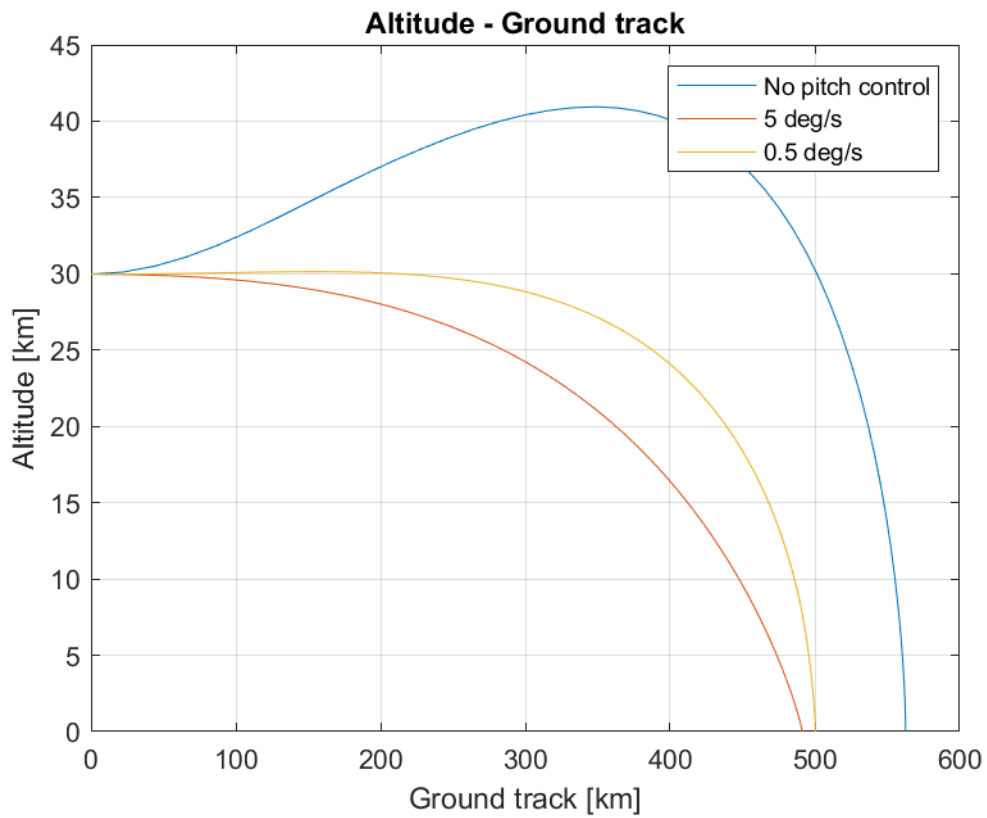


Figure 40: Altitude - Ground track for case 2.2

Generally, the $5 \frac{\text{deg}}{\text{s}}$ pitch rate limit case is the one with the lowest landing time, except in case 2.1. Here the optimizer prefers to descend for a longer time with a lower thrust level, having this architecture higher values of T_{max} and T_{min} .

For a better understanding of the landing trajectories in *Appendix A1* are reported the values of the tangential and radial velocities for all four cases.

Figure 41, Figure 42, Figure 43 and Figure 44 show that there is only a slightly difference between the elevation angle γ and pitch ψ .

This leads to the conclusion that the case in which there is only one control (thrust module) and $\gamma = -\psi$ is not too far from the result that can be obtained with two control variables. In fact, the landing mass is not that different in these two cases. For example, in case 1.1 there is an improvement of 50 kg (Table 9), which is one order of magnitude smaller than the total.

Obviously being able to carry more payload to the lunar surface with the same starting mass will lead to an enormous reduction of mission costs and it is a significant improvement, but for a quick preliminary analysis using only one control variable is sufficient, remembering that the computational time difference is significant.

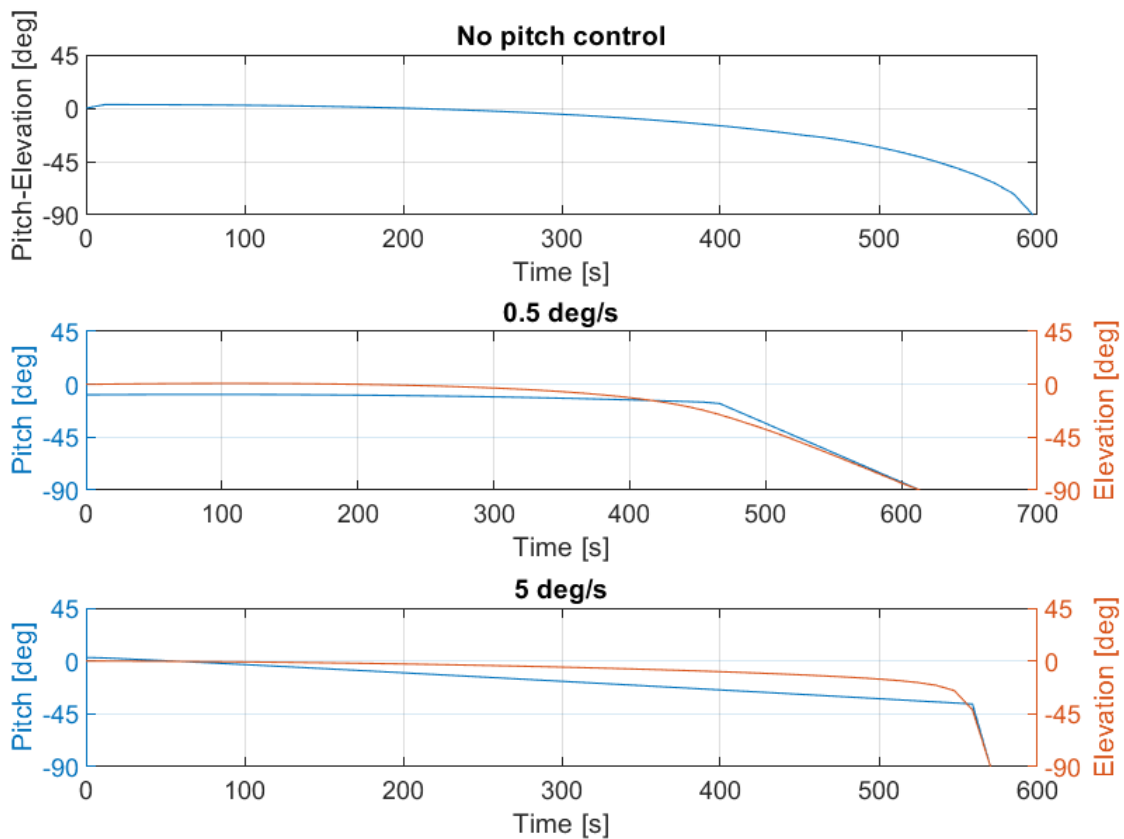


Figure 41: Pitch and Elevation angles for case 1.1

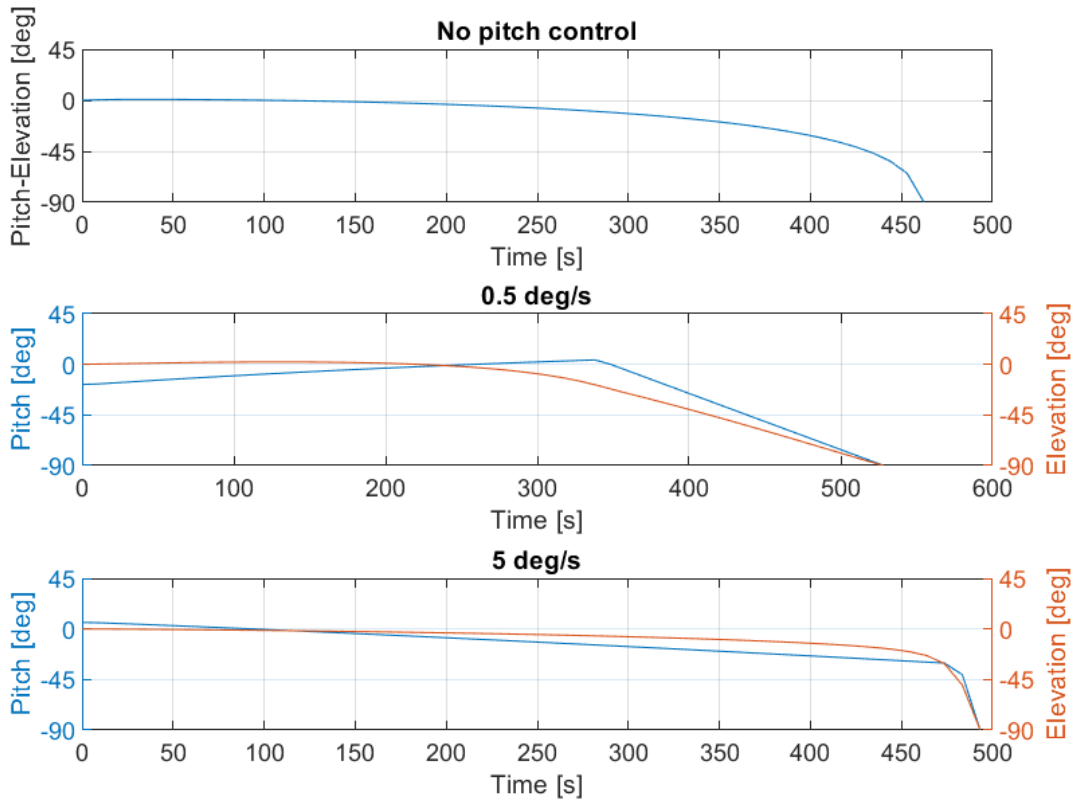


Figure 42: Pitch and Elevation angles for case 1.2

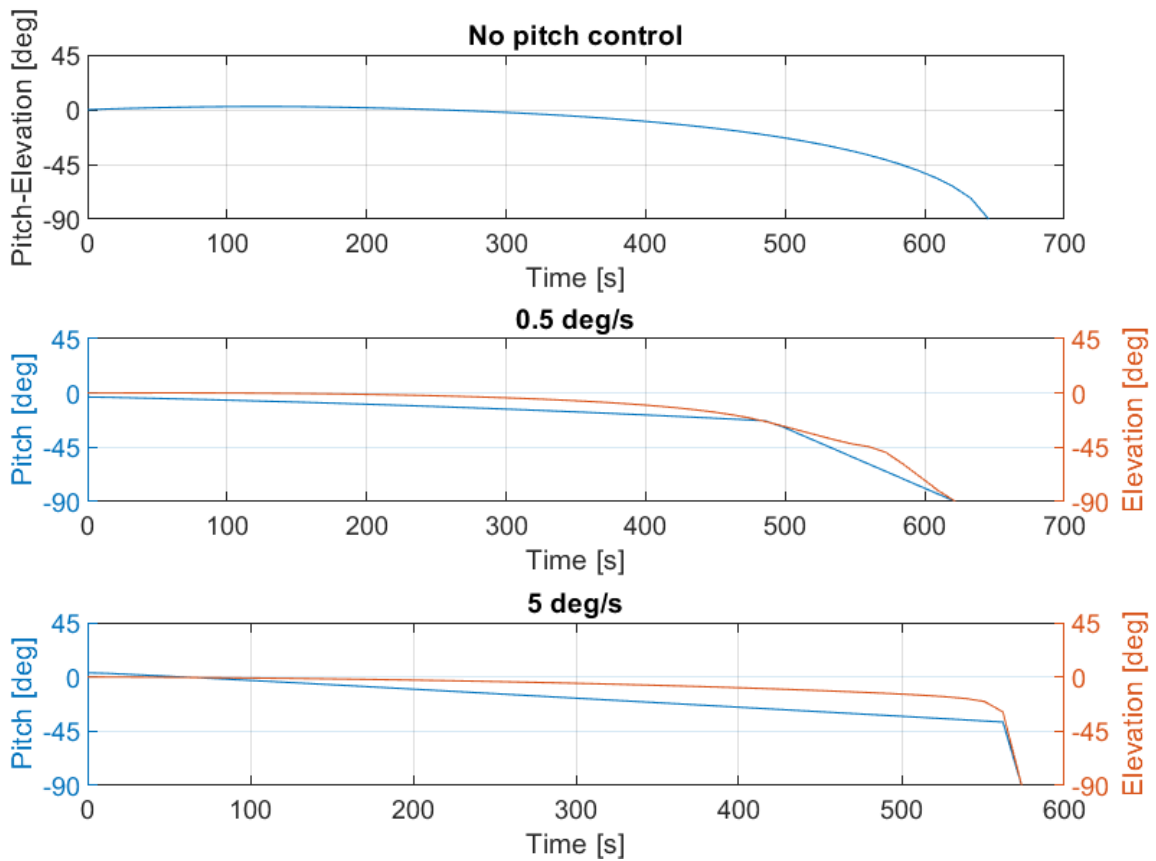


Figure 43: Pitch and Elevation angles for case 2.1

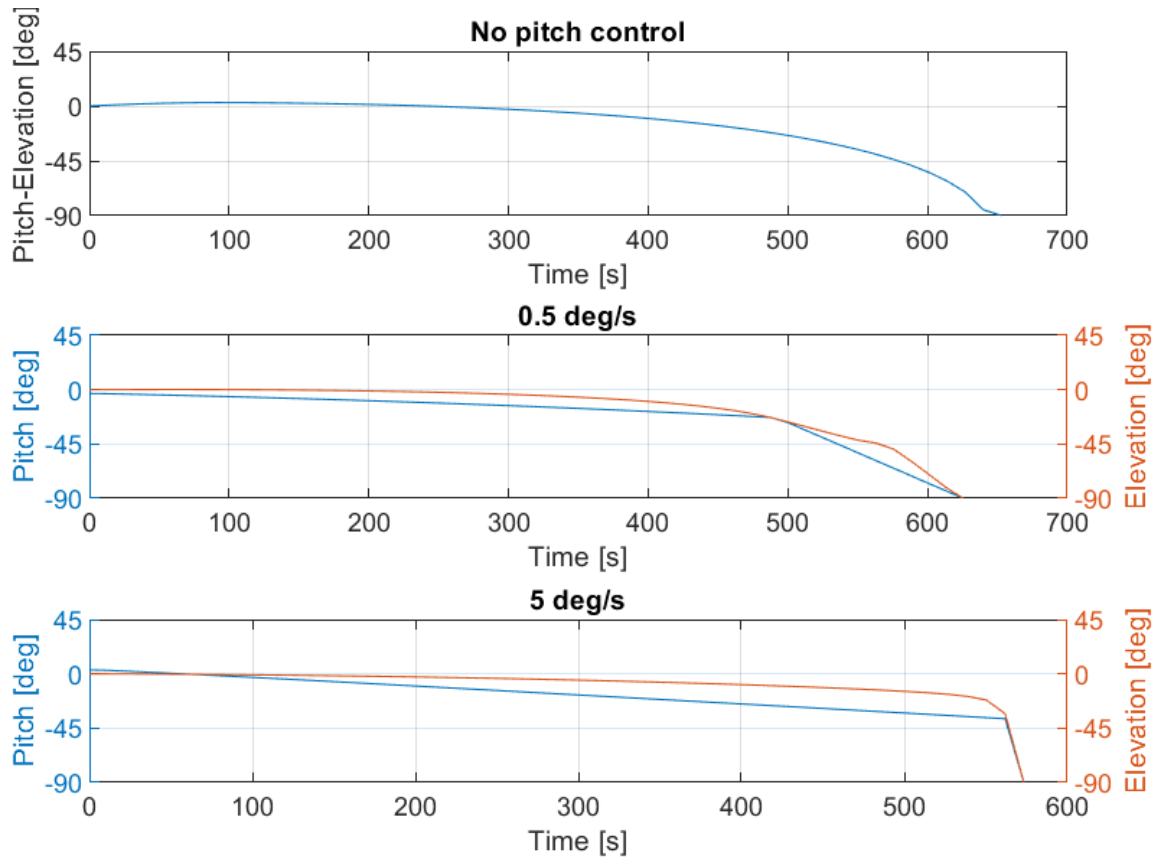


Figure 44: Pitch and Elevation angles for case 2.2

From the observation of the values that the thrust assumes in the four configurations (Figure 45, Figure 47, Figure 49 and Figure 51) it can be noticed that the $5 \frac{deg}{s}$ pitch rate limit case is always the one with the lowest variation of the thrust module during descent. This is due to the spacecraft's ability to point the engines in the optimal direction during the entire landing phase and this allows a longer usage of all the available thrust.

In Figure 46, Figure 48, Figure 50 and Figure 52 are reported the trends of the derivatives of the control variables.

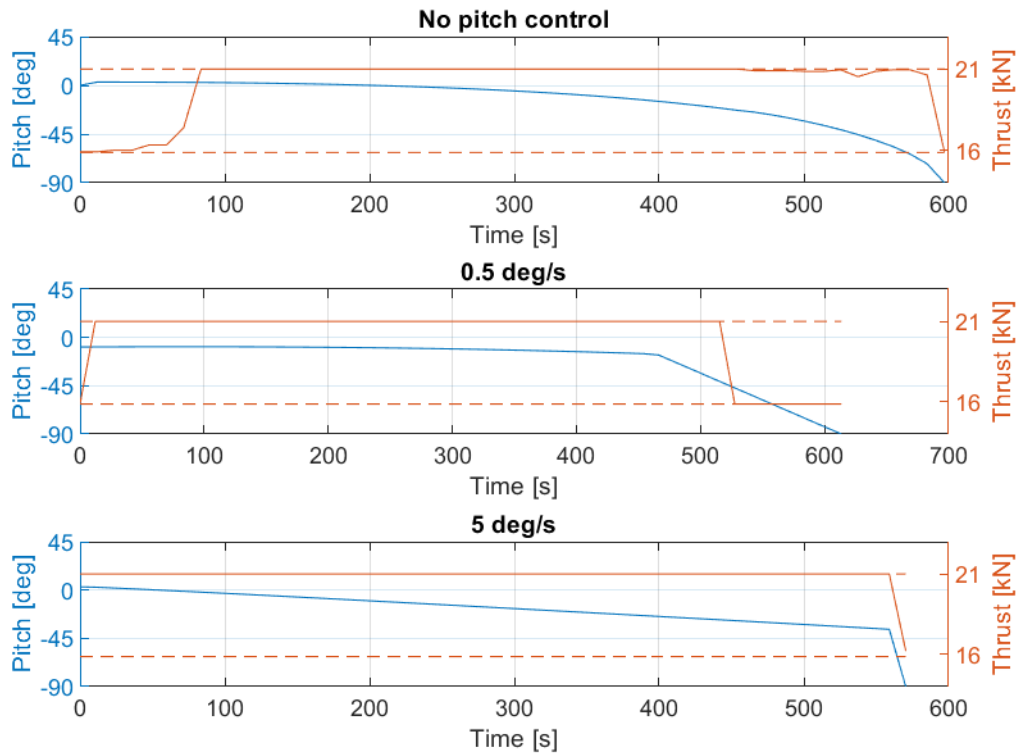


Figure 45: Pitch and Thrust module for case 1.1

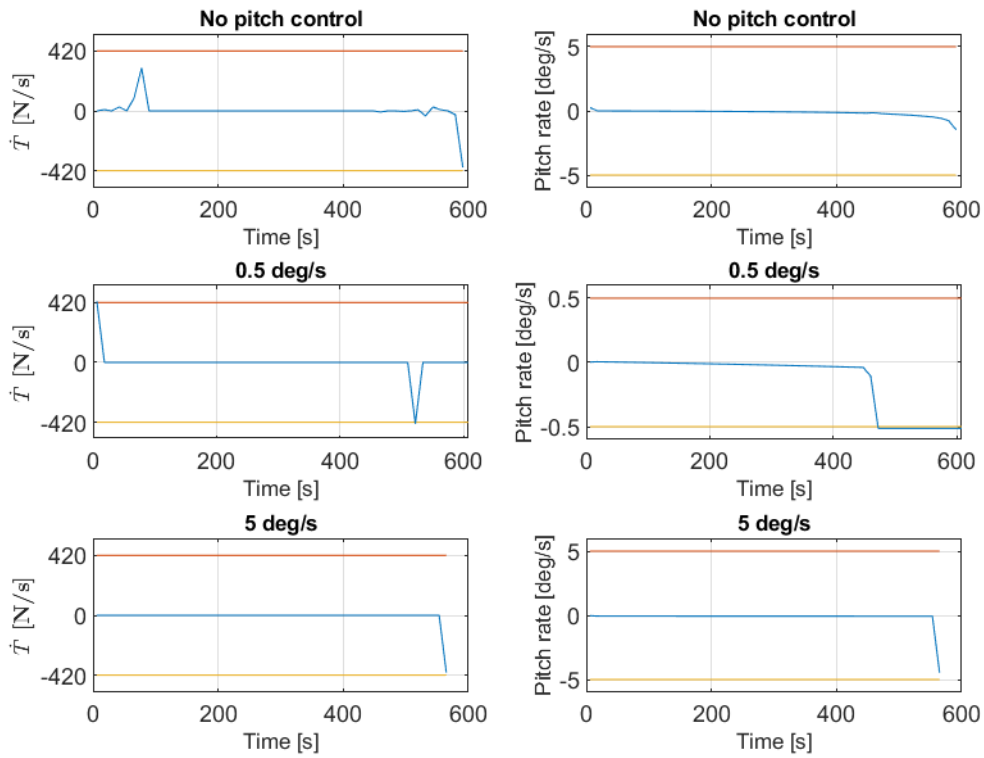


Figure 46: Pitch rate and Thrust rate for case 1.1

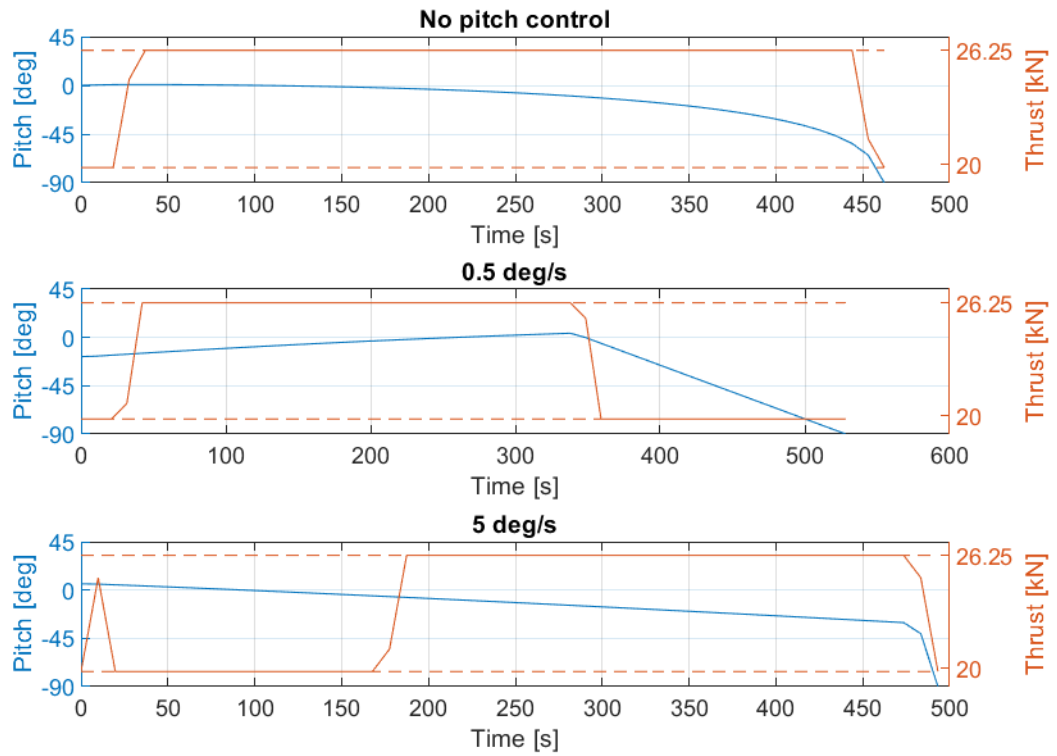


Figure 47: Pitch and Thrust module for case 1.2

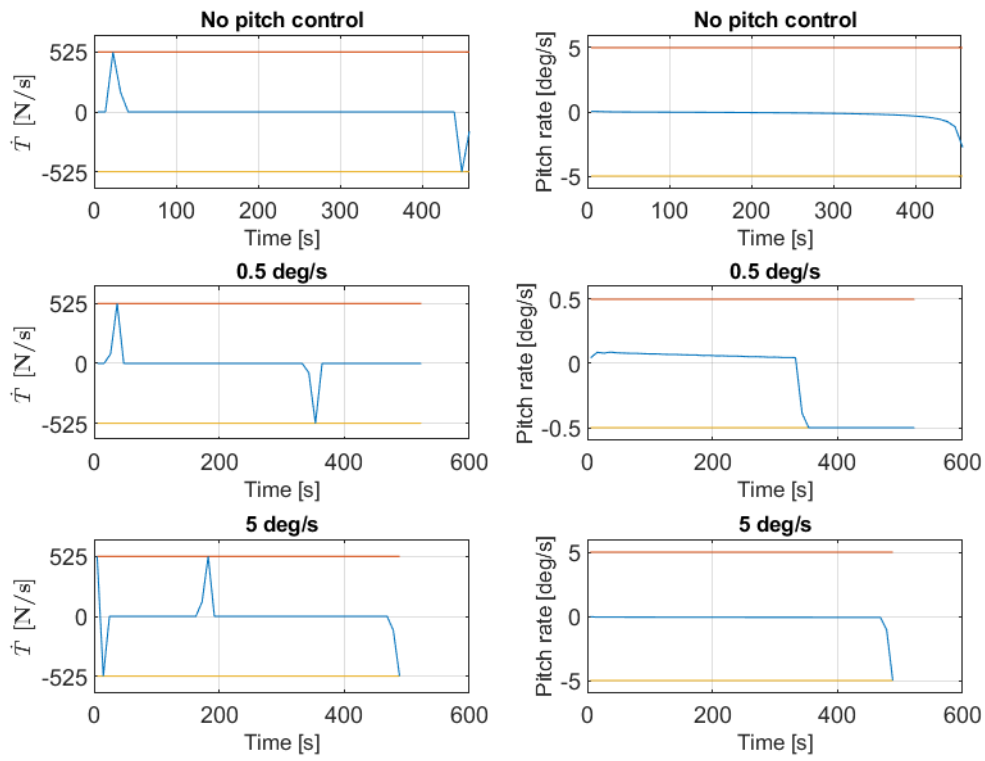


Figure 48: Pitch rate and Thrust rate for case 1.2

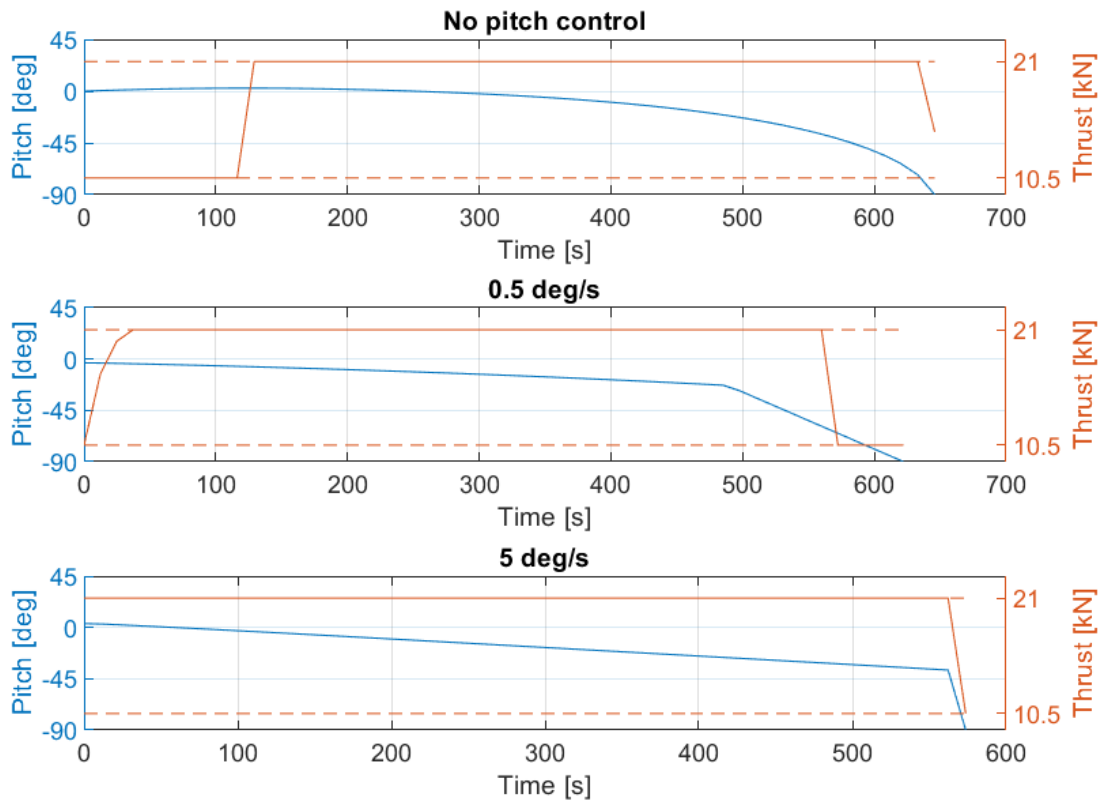


Figure 49: Pitch and Thrust module for case 2.1

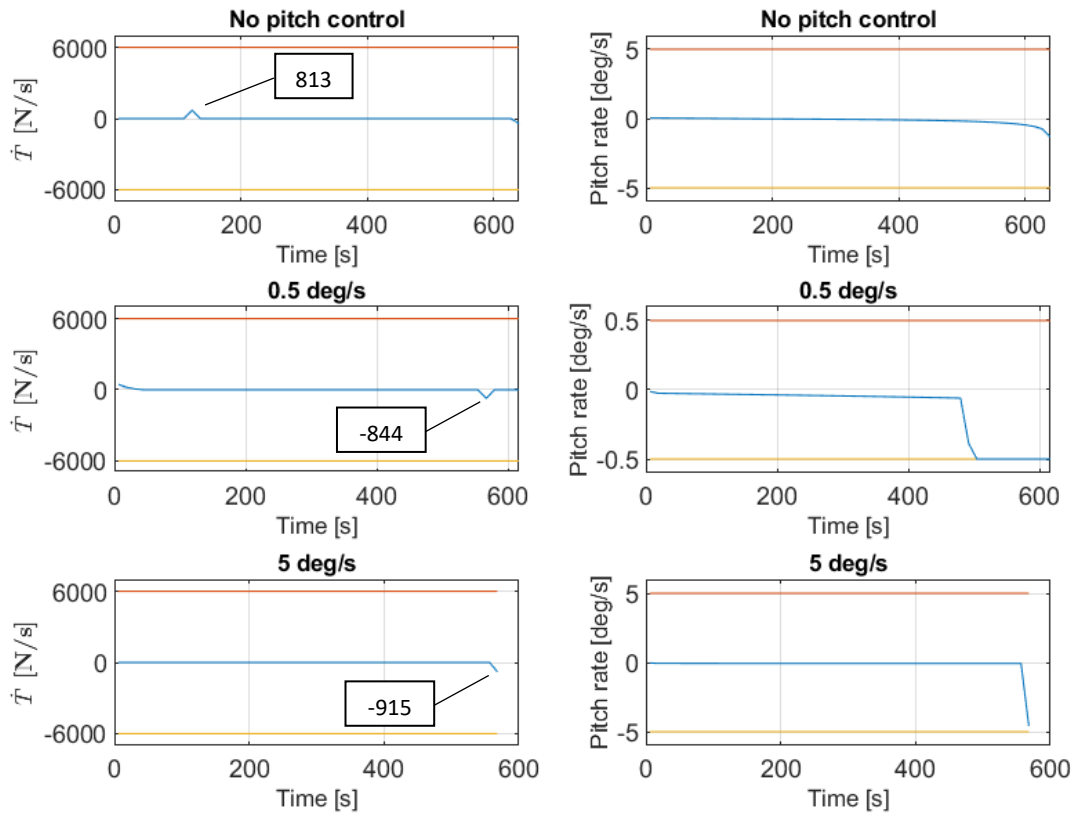


Figure 50: Pitch rate and Thrust rate for case 2.1

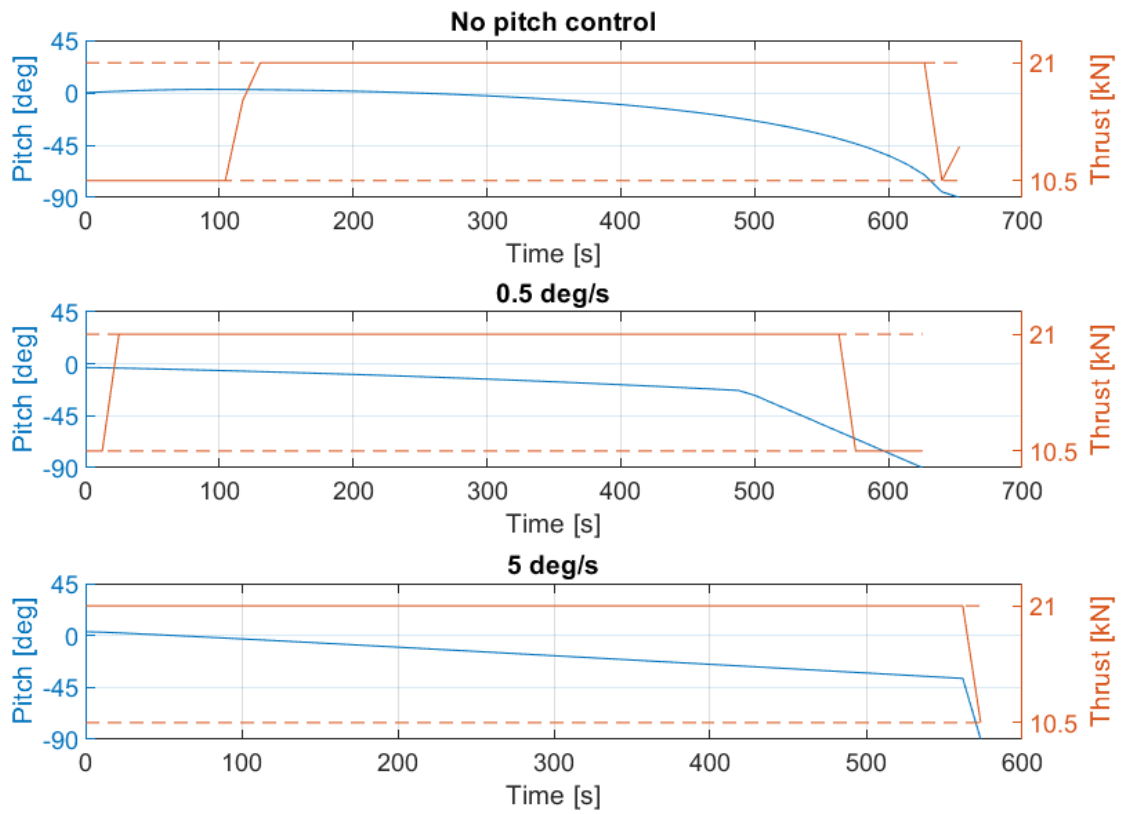


Figure 51: Pitch and Thrust module for 2.2 case

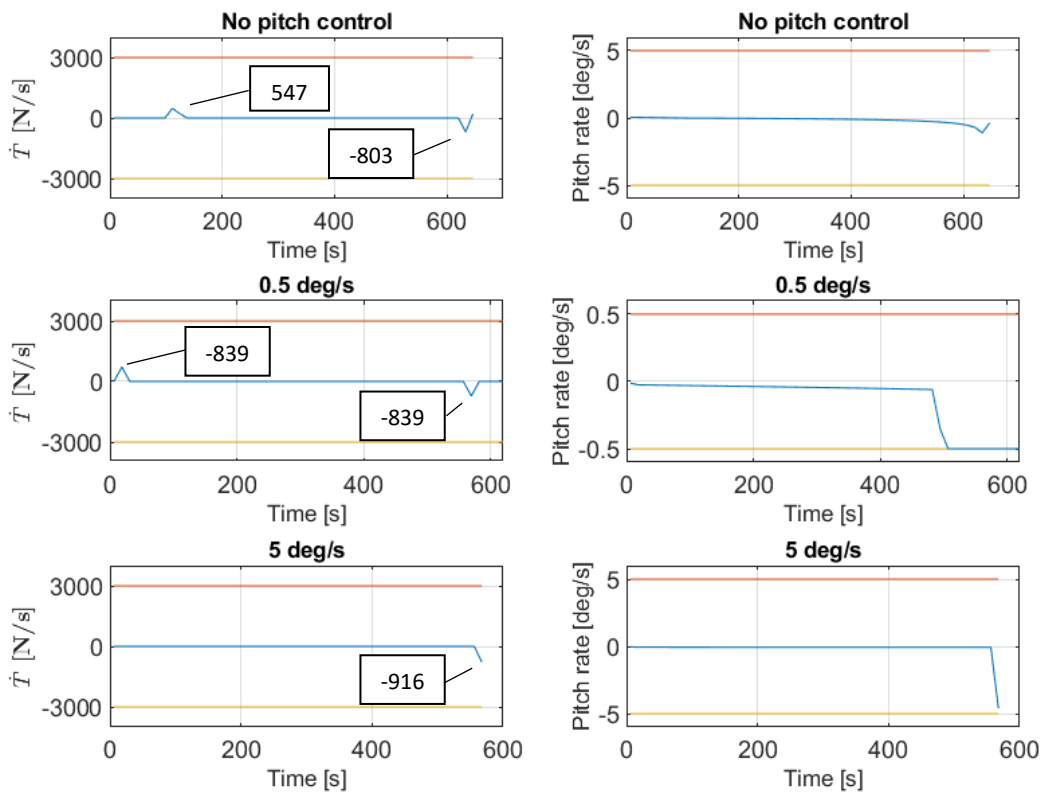


Figure 52: Pitch rate and Thrust rate for case 2.2

To give to the reader a better view of the scale of the trajectories in Appendix A2 are reported their three-dimensional representations.

4.2.2 Comparison best cases

In this section the best control configurations of the 4 architectures, i.e. those with higher landing mass, are compared. As can be seen for all 4 architectures these are cases with two controls and a maximum pitch rate of $5 \frac{deg}{s}$ and the results are summarized in Table 13.

Table 13: best cases

		4 x Proto-1	5 x Proto-1	3 x Proto-2	3 x Proto-2
	<i>mission requirements</i>	<i>Case 1.1</i>	<i>Case 1.2</i>	<i>Case 2.1</i>	<i>Case 2.2</i>
<i>T_{max} [kN]</i>	-	4 x 5.25 = 21	5 x 5.25 = 26.25	3 x 7 = 21	3 x 7 = 21
<i>T_{min} [kN]</i>	-	4 x 4 = 16	5 x 4 = 20	3 x 3.5 = 10.5	3 x 3.5 = 10.5
<i>\dot{T}_{max} [kN/sec]</i>	-	0.420	0.525	3 x 2 = 6	3 x 1 = 3
<i>Isp [sec]</i>	-	321	321	325	325
<i>Initial mass</i>	7350 kg	7350 kg	7350 kg	7350 kg	7350 kg
<i>Final mass</i>	> 3400 kg	4096.10 kg	4138.14 kg	4126.16 kg	4128.27 kg
<i>Delta V</i>	< $2457.15 \frac{m}{sec}$	$1840.55 \frac{m}{sec}$	$1808.41 \frac{m}{sec}$	$1840.18 \frac{m}{sec}$	$1838.55 \frac{m}{sec}$
<i>Maneuver time</i>	-	570.38 sec	493.25 sec	573.72 sec	573.34 sec
<i>Initial altitude</i>	30000 m	30000 m	30000 m	30000 m	30000 m
<i>Final altitude</i>	30 m	30 m	30 m	30 m	35 m
<i>Initial vertical speed</i>	0 m/s	0 m/s	0 m/s	0 m/s	0 m/s
<i>Final vertical speed</i>	-2 m/s	-2 m/s	-2 m/s	-2 m/s	-4 m/s
<i>Initial tangential speed</i>	1680 m/s	1680 m/s	1680 m/s	1680 m/s	1680 m/s
<i>Final tangential speed</i>	0 m/s	0 m/s	0 m/s	0 m/s	0 m/s
<i>Initial thrust direction</i>	-	-2.96°	-5.78°	-3.39°	-3.25°
<i>Final thrust direction</i>	90° (vertical)	90° (vertical)	90° (vertical)	90° (vertical)	90° (vertical)

The main factor affecting descent performance is the maximum available thrust.

Indeed, the best case is 2.1 with $T_{max} = 26.25 \text{ kN}$, while 1.1, 1.2 and 2.2, which have the same total $T_{max} = 21 \text{ kN}$, have almost the same landing mass, descent time and trajectory (Table 13, Figure 53, Figure 54, Figure 55, Figure 56 and Figure 72). The improvement however has almost the same value of the weight of the added engine (4096.10 kg vs 4138.14 kg) and therefore the additional engine seems unnecessary.

The only real advantage is the shorter landing time (493.25 sec vs 570.38 sec).

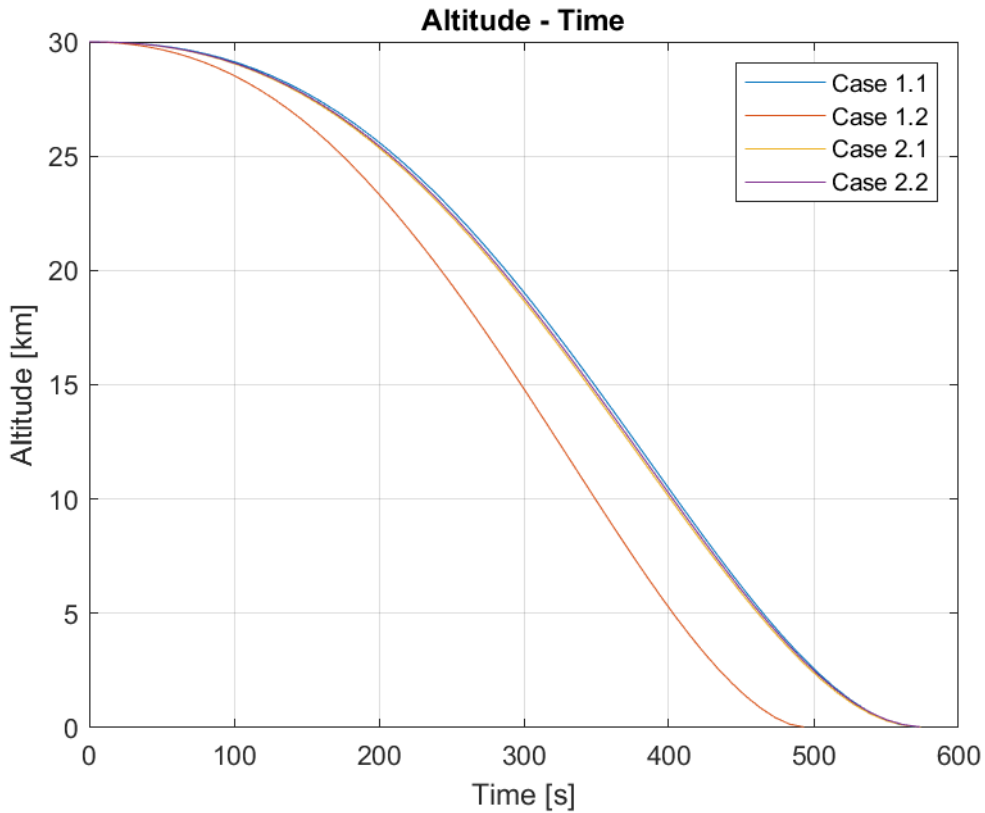


Figure 53: Altitude - Time best cases comparison

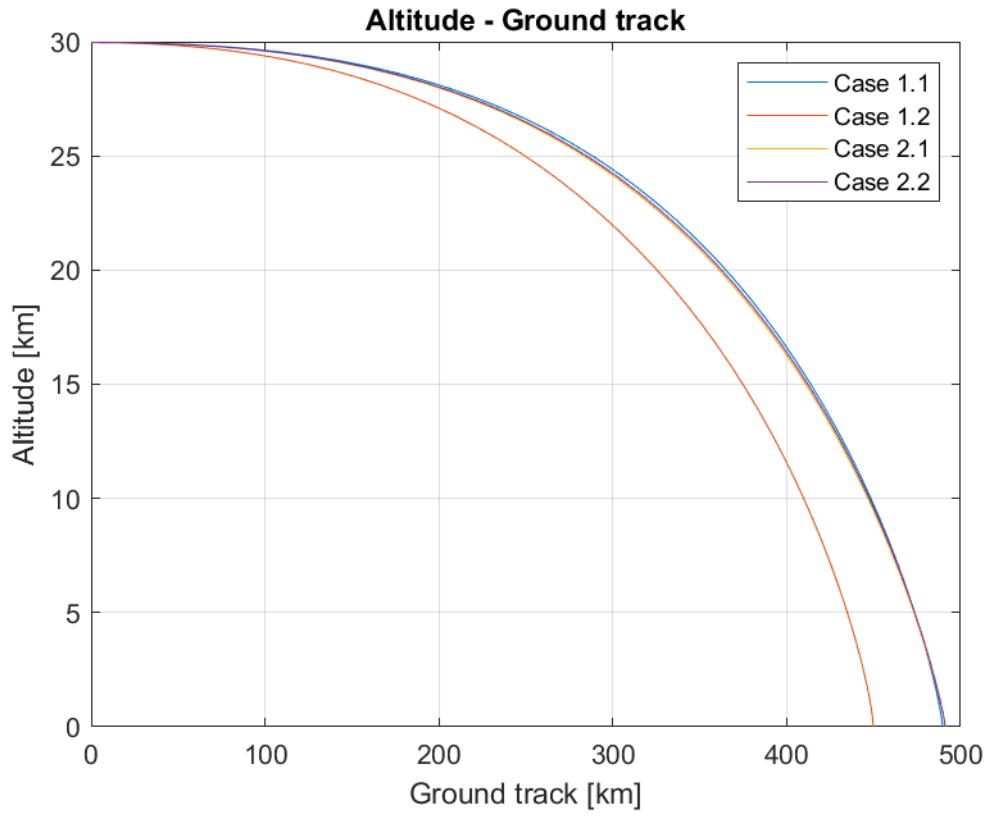


Figure 54: Altitude - Ground track best cases comparison

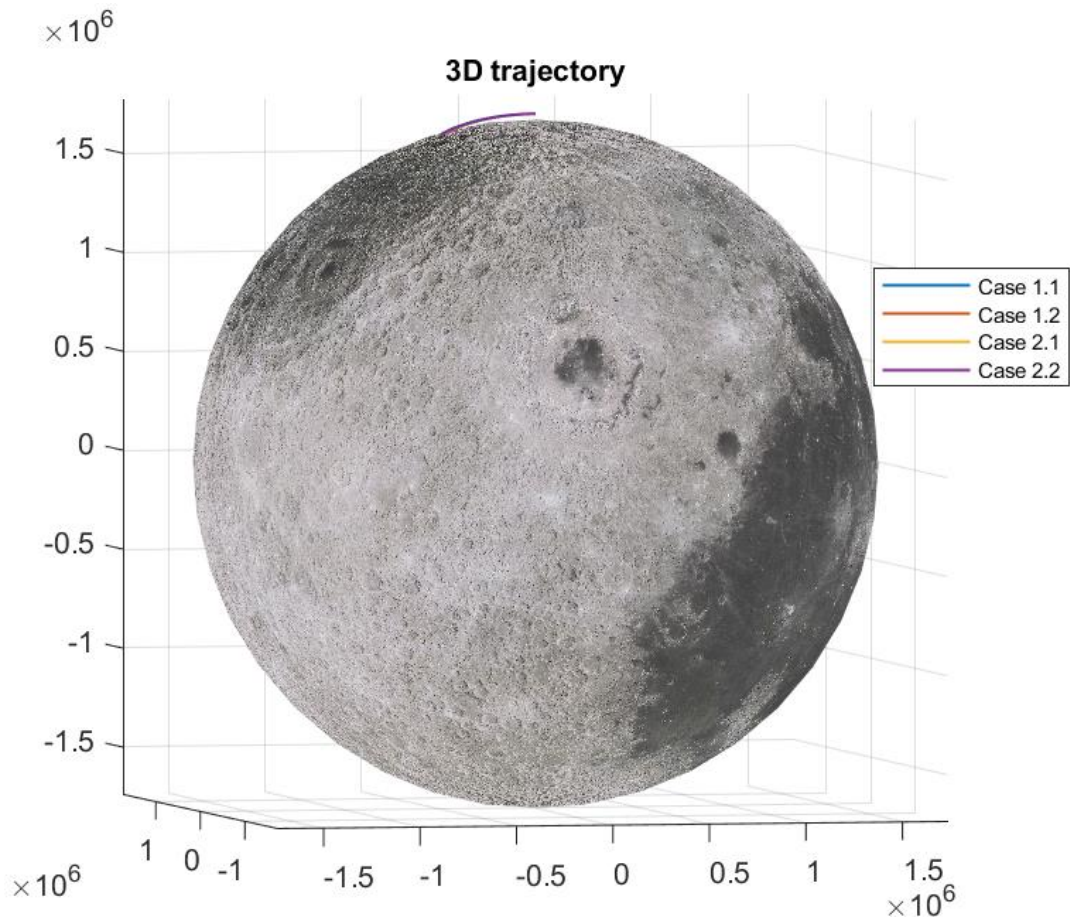


Figure 55: 3D trajectory best cases comparison

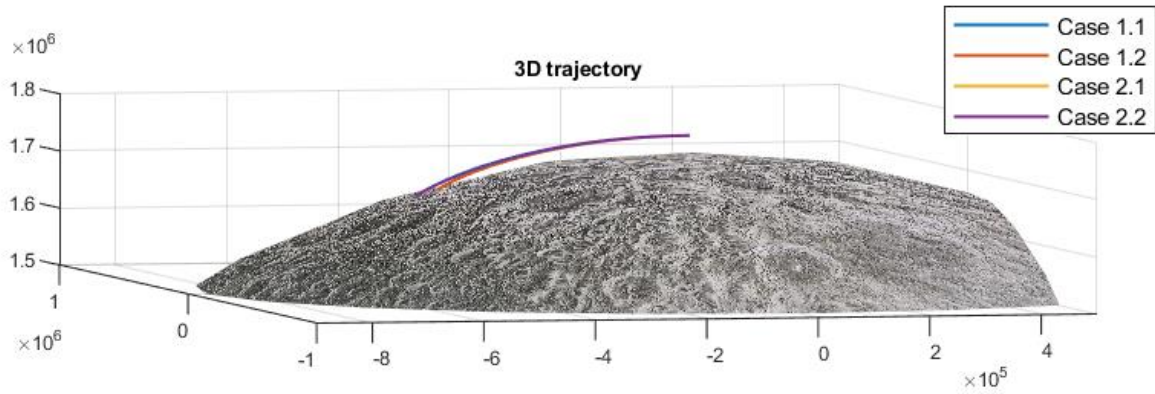


Figure 56: zoomed 3D trajectory best cases comparison

As before, the graphics of the components of the velocity can be found in Appendix A3.

For all four cases the difference between pitch and elevation angle is minimum, in particular with architecture 1.2 (Figure 57).

Moreover case 1.1, 2.1 and 2.2 have almost the same trends, which implies that the maximum and minimum levels of thrust have an influence even on the second control variable ψ .

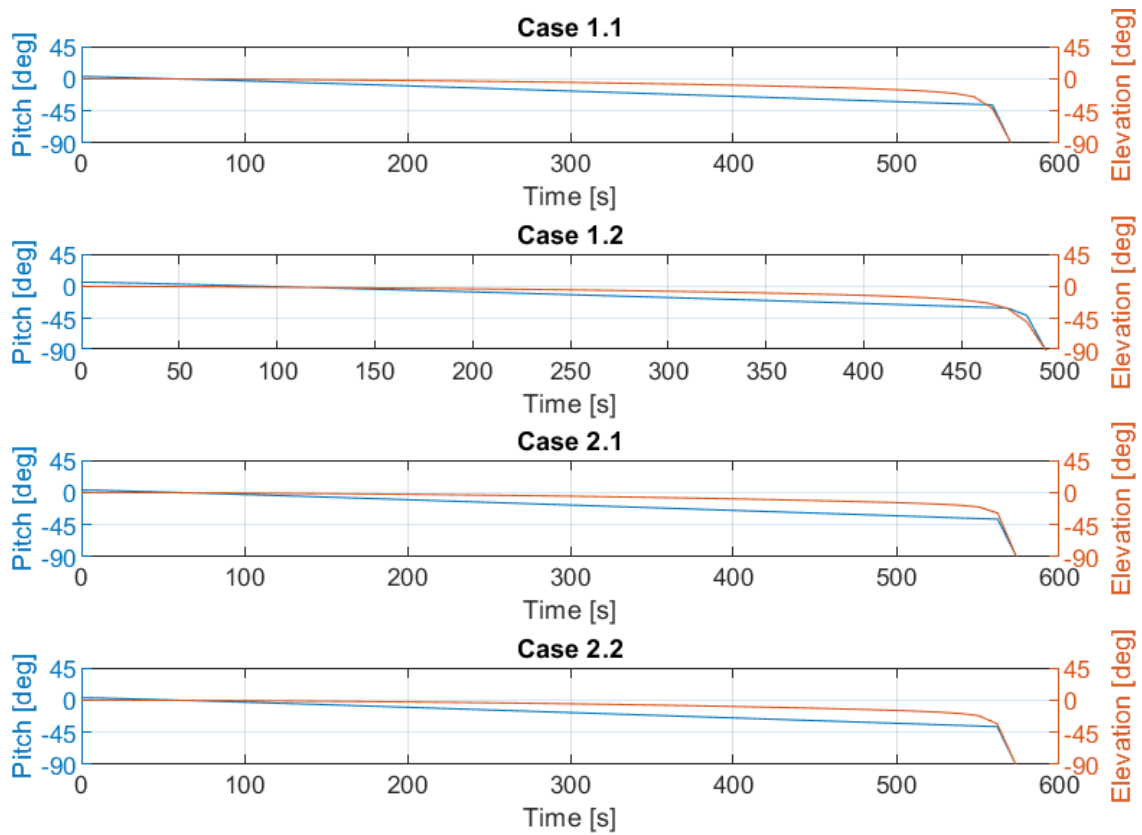


Figure 57: Pitch and Elevation angles best cases comparison

From the comparison between the thrust profiles of the best cases of architectures 1.1 and 1.2 (Figure 58), it can be observed that the maximum thrust is used for almost the same time as the minimum thrust in the 5 *Proto-1* configuration, while T_{max} is used for nearly all descent in the 4 *Proto-1* engine architecture.

This leads to the conclusion that having such high values of total T_{min} and T_{max} make impossible to use them at their full potential. In particular, the problem seems to be T_{min} which does not allow sufficient thrust reduction when needed being this case the only one in which T_{min} is saturated for a long time.

This would be different if it was possible to temporary turn off and on again the engines. Through this operation the total T_{min} would have been significantly smaller and the simulation would have produced even better results compared to the other architectures.

While not being beneficial for the optimization, the five-engine architecture has other advantages such as redundancy, cost etc. that must be taken into account.

From the observations of the values of \dot{T} of the cases 2.1 and 2.2 (Figure 59), the ability of the 3 *Proto-2* engines to modulate the thrust for a total value of $6 \frac{kN}{s}$ or $3 \frac{kN}{s}$ is not used.

Indeed, in case 2.1 the maximum value of \dot{T} reached is $915 \frac{kN}{s}$, which is only 4.36 % of the total T_{max} and 15.25 % of \dot{T}_{max} , while in case 2.2 the maximum value of \dot{T} reached is $916 \frac{kN}{s}$, which is 4.36 % of the total T_{max} and 30.53 % of \dot{T}_{max} (Figure 59).

It can be stated that having such a large value of \dot{T} is not beneficial for landing mass maximization and therefore this characteristic should not be taken too much into account during the engines' trade-off.

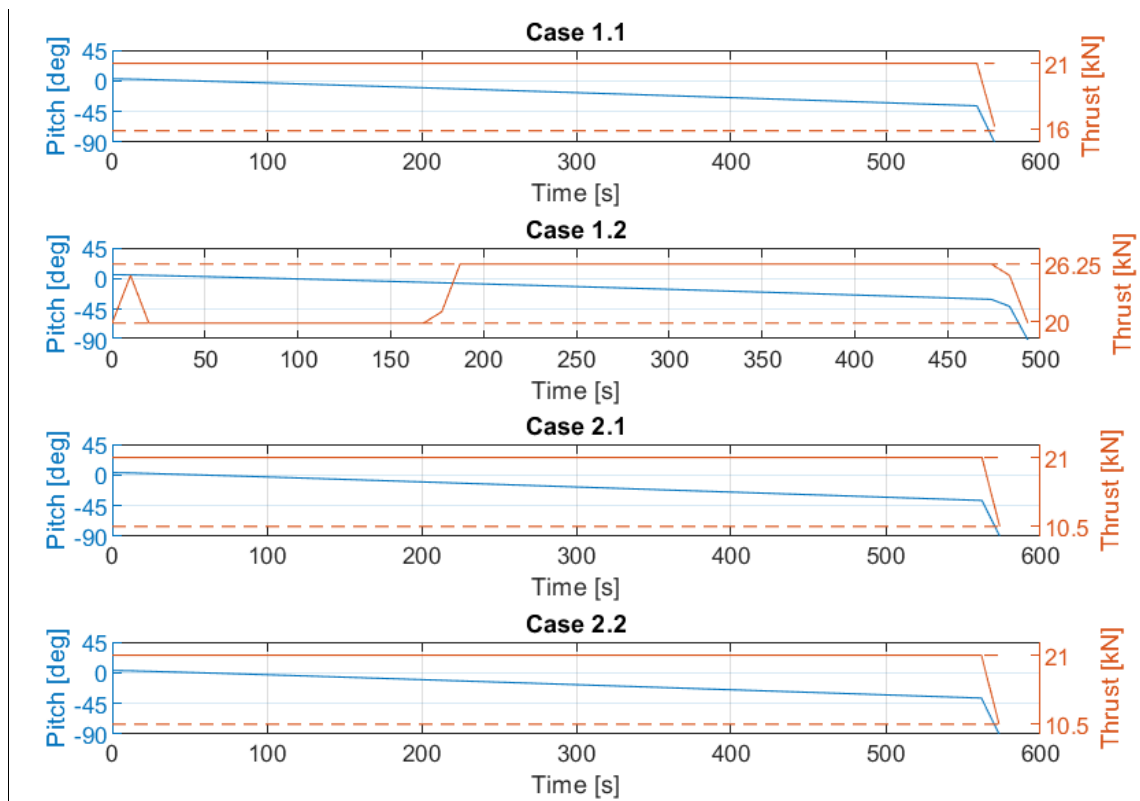


Figure 58: Pitch and Thrust module best cases comparison

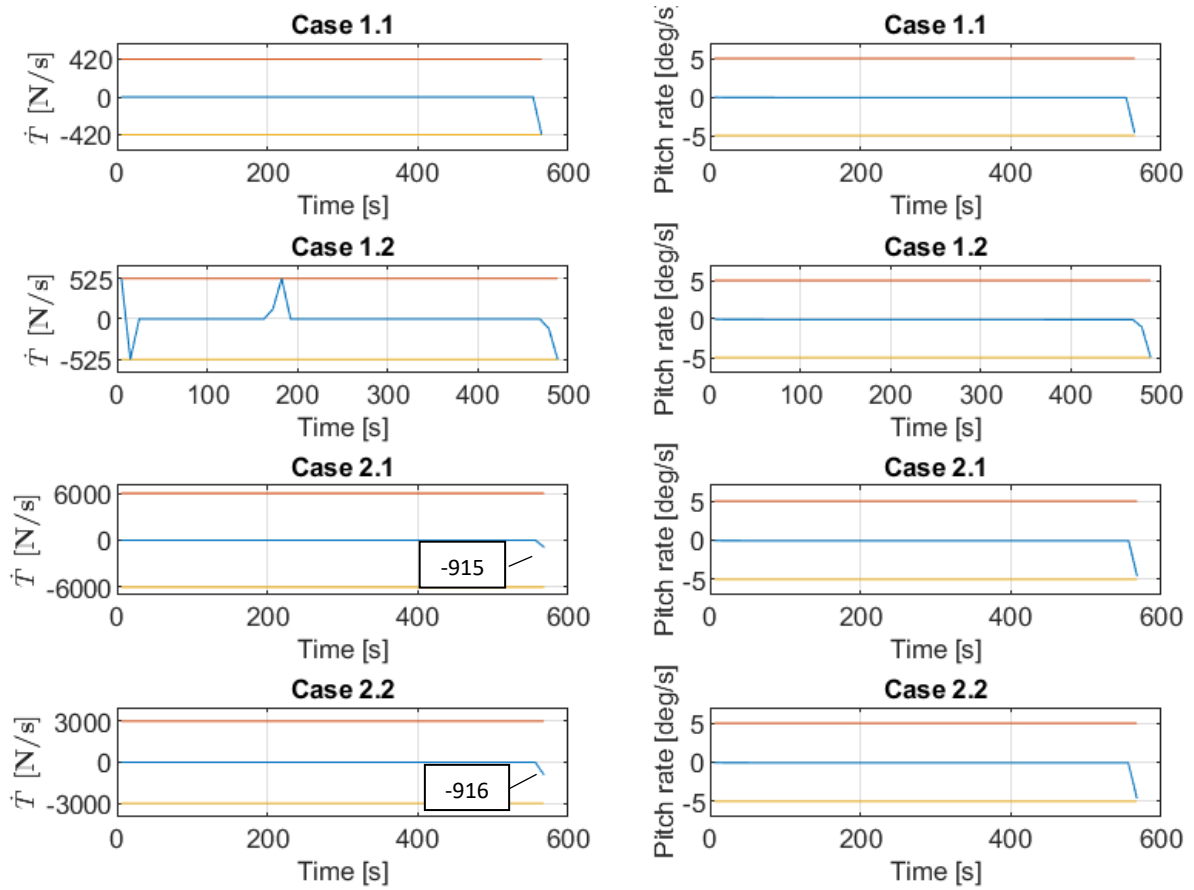


Figure 59: Pitch rate and Thrust rate best cases comparison

In conclusion, having five Proto-1 engines do not lead to a significant improvement in the maximization of the landing mass compared with the use of 4 engines and Proto-2 high \dot{T} is never fully used.

This hints that the four Proto-1 configuration could be the most suitable although other considerations must be taken into account such as redundancy, cost and complexity of the system.

CONCLUSIONS

With the following thesis, it was shown that direct methods can be effectively applied to the optimization of descent trajectories in the lunar environment. In addition, the developed tool demonstrated its possible commercial applications by displaying good robustness and adaptability.

In particular the algorithm obtained values in line with the directions given by ESA, which has far superior computational tools than those used in this thesis.

In addition, the results obtained in the thruster trade-offs were useful to select the best possible architecture and to identify which variables and parameters of the engines most affect descent performance. For example, it was shown how high values of \dot{T} have no positive impact on the propellant consumption and that the main drivers are T_{max} and T_{min} .

While high values of T_{max} allow to perform a more powerful break and eliminate the necessity to increase the altitude at the beginning of the descent, small values of T_{min} permit to better distribute the thrust during flight minimizing wasted propellant.

In the future the algorithm can be further improved including the possibility of implementing gates, i.e. points along the descent where a certain condition (for example pitch angle) must be met. Moreover, with the right arrangements and adaptations, this tool can be extended to simulate and optimize an atmospheric re-entry.

To do so, it is necessary to make it compatible with the atmospheric models provided by NASA (SPICE toolkit [24]) and to include aerodynamic forces in the model, using, for example, the set of equations derived by Avanzini in the *Entry, Descent, Landing and Ascent* document [25].

The final upgrade to this tool would be the implementation of a three-dimensional trajectory. This will allow to simulate additional analysis, for example to simulate the maximum ability of the lander to steer its trajectory to correct errors in the initialization of the PDI, or to simulate the optimal obstacle avoidance manoeuvre in the terminal phase of the descent.

Obviously, this will require a more powerful device where to run the simulation in order to have feasible simulation times due to the huge amount of new variables that the system will have to compute.

APPENDIX A1

In Figure 60, Figure 61, Figure 62 and Figure 63 are shown the four trends of the vertical and horizontal velocities for each of the four architectures:

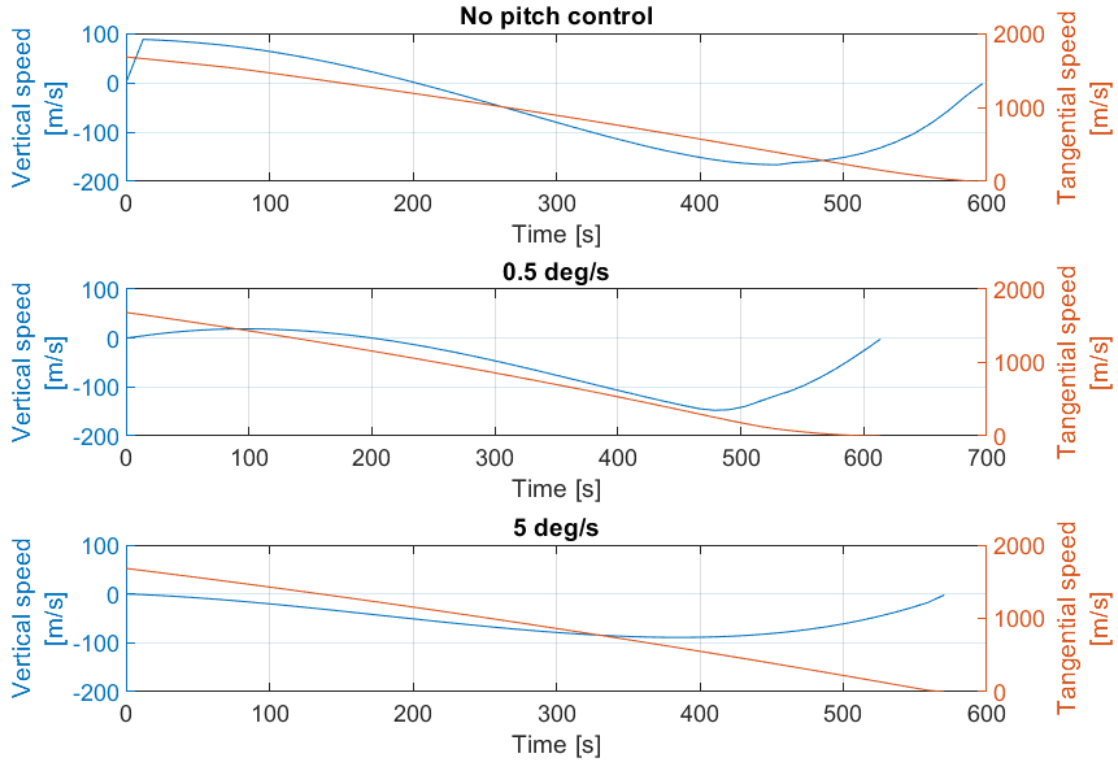


Figure 60: Vertical and Tangential velocity for case 1.1

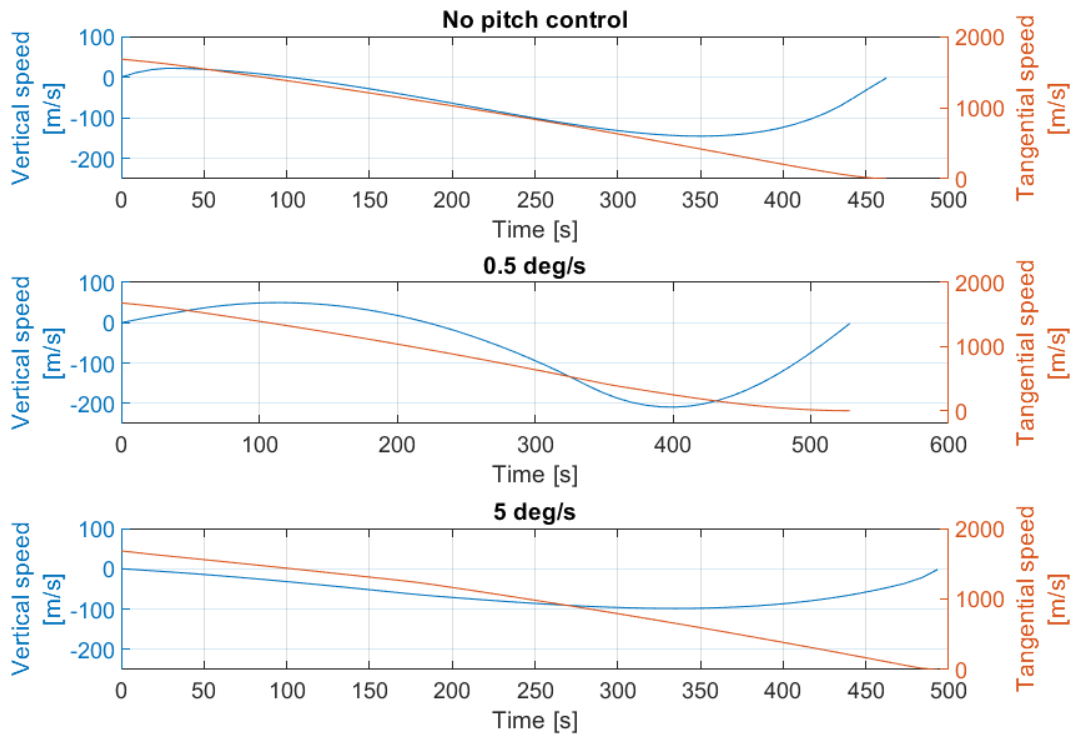


Figure 61: Vertical and Tangential speed for case 1.2

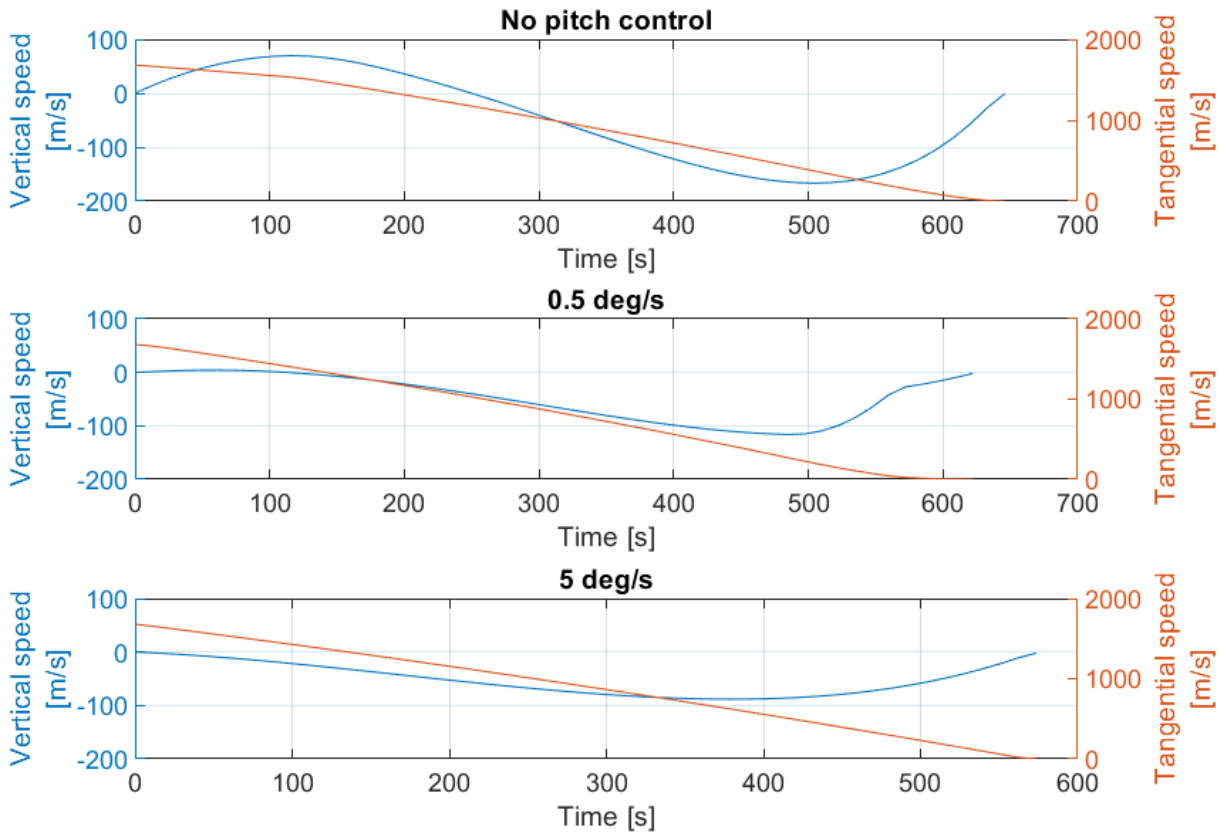


Figure 62: Vertical and Tangential velocity for case 2.1

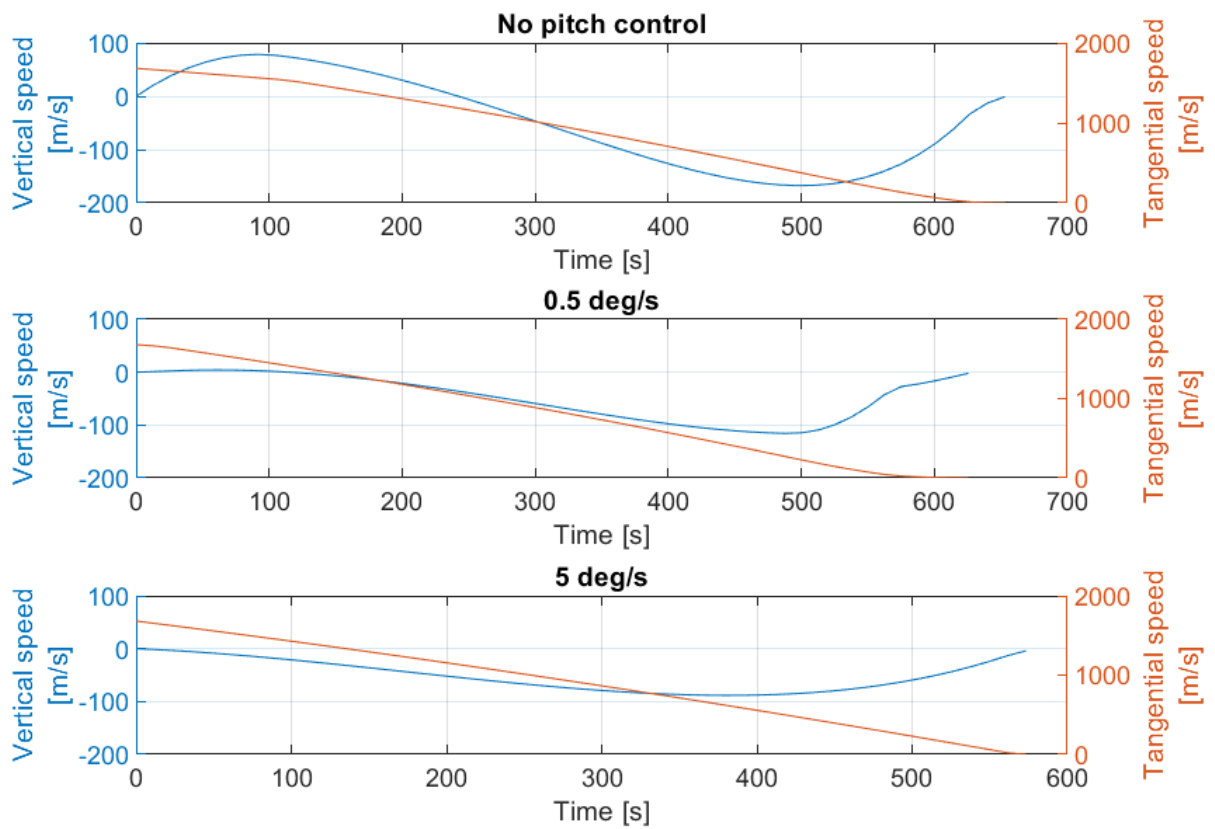


Figure 63: Vertical and Tangential speed for case 2.2

APPENDIX A2

Three-dimensional representation of the descent trajectories for the four cases in Figure 64, Figure 65, Figure 66, Figure 67, Figure 68, Figure 69, Figure 70 and Figure 71:

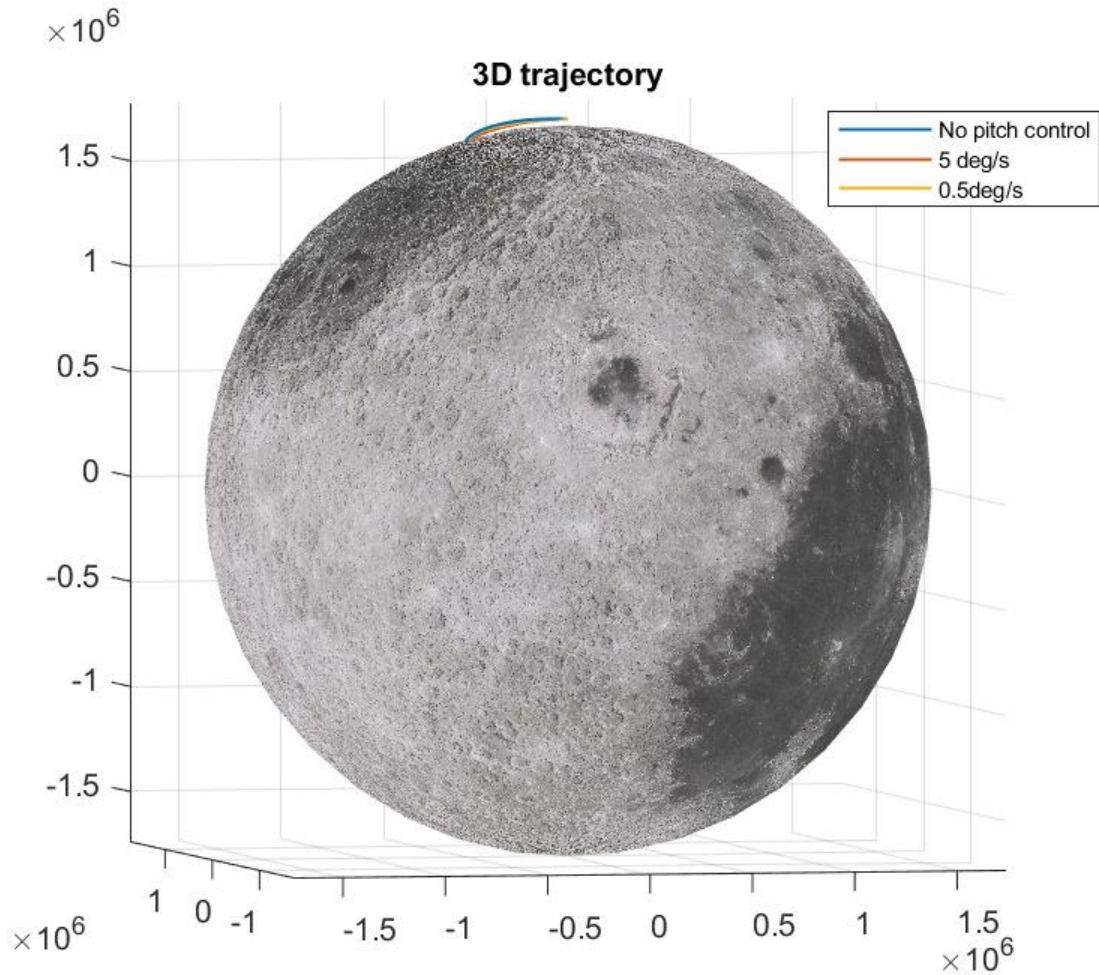


Figure 64: 3D trajectory for case 1.1

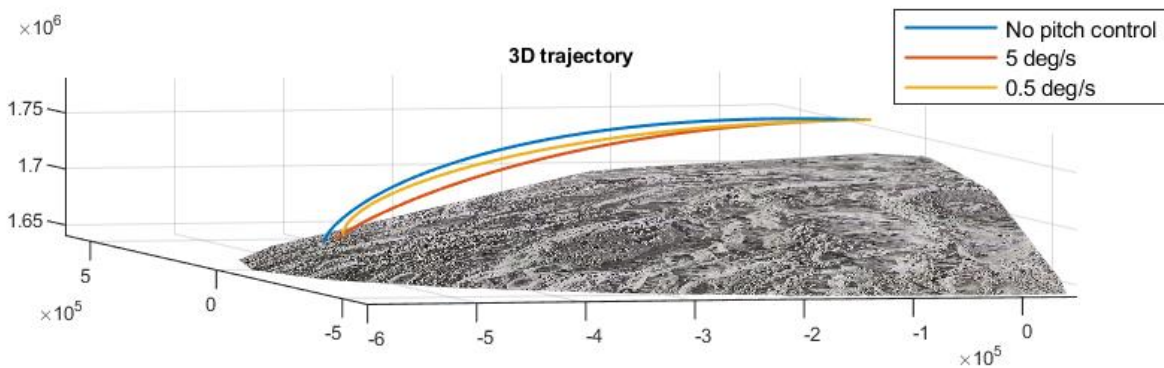


Figure 65: zoomed 3D trajectory for case 1.1

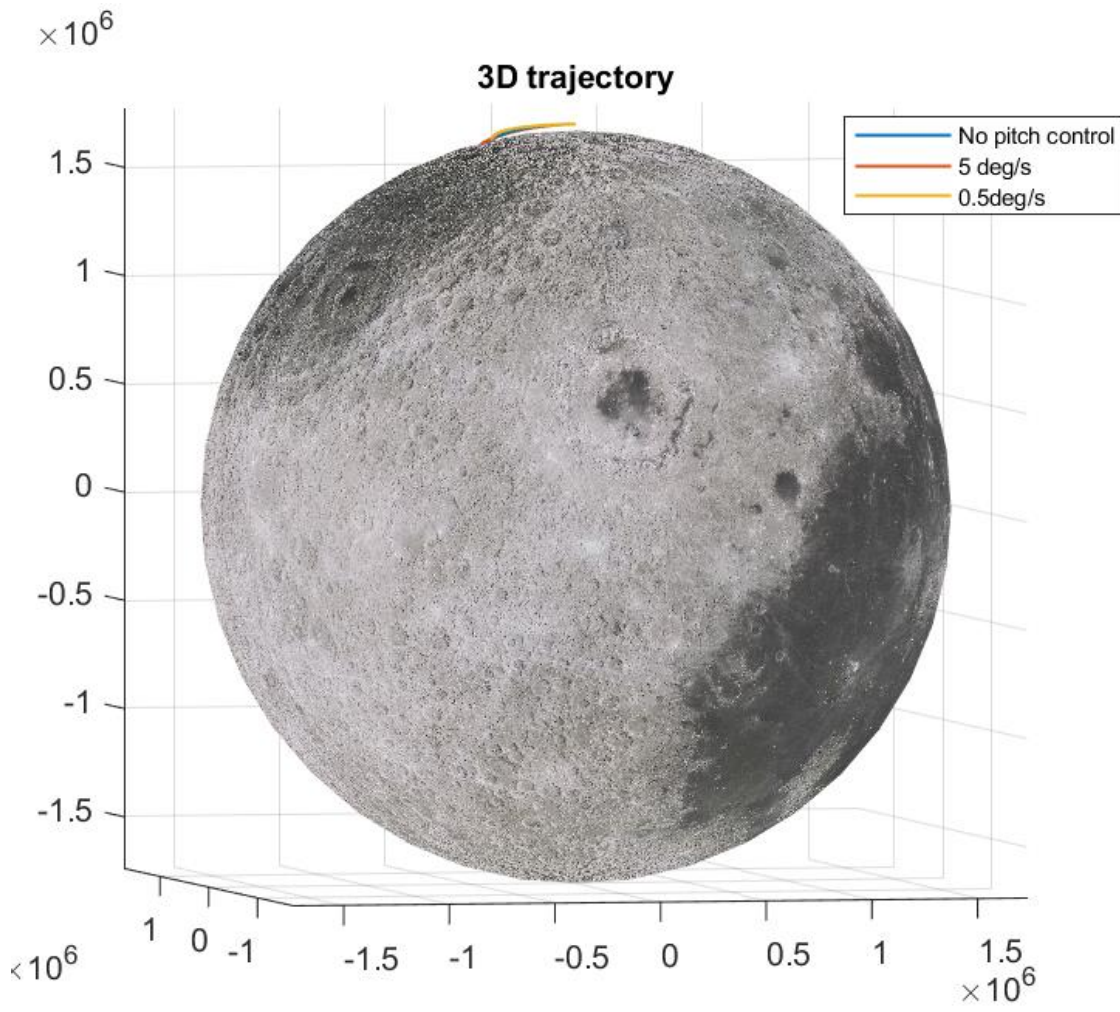


Figure 66: 3D trajectory for case 1.2

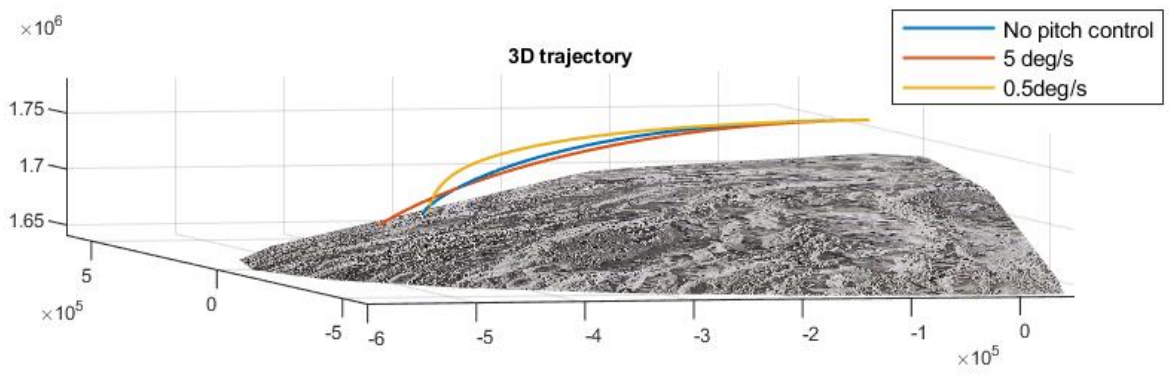


Figure 67: zoomed 3D trajectory for case 1.2

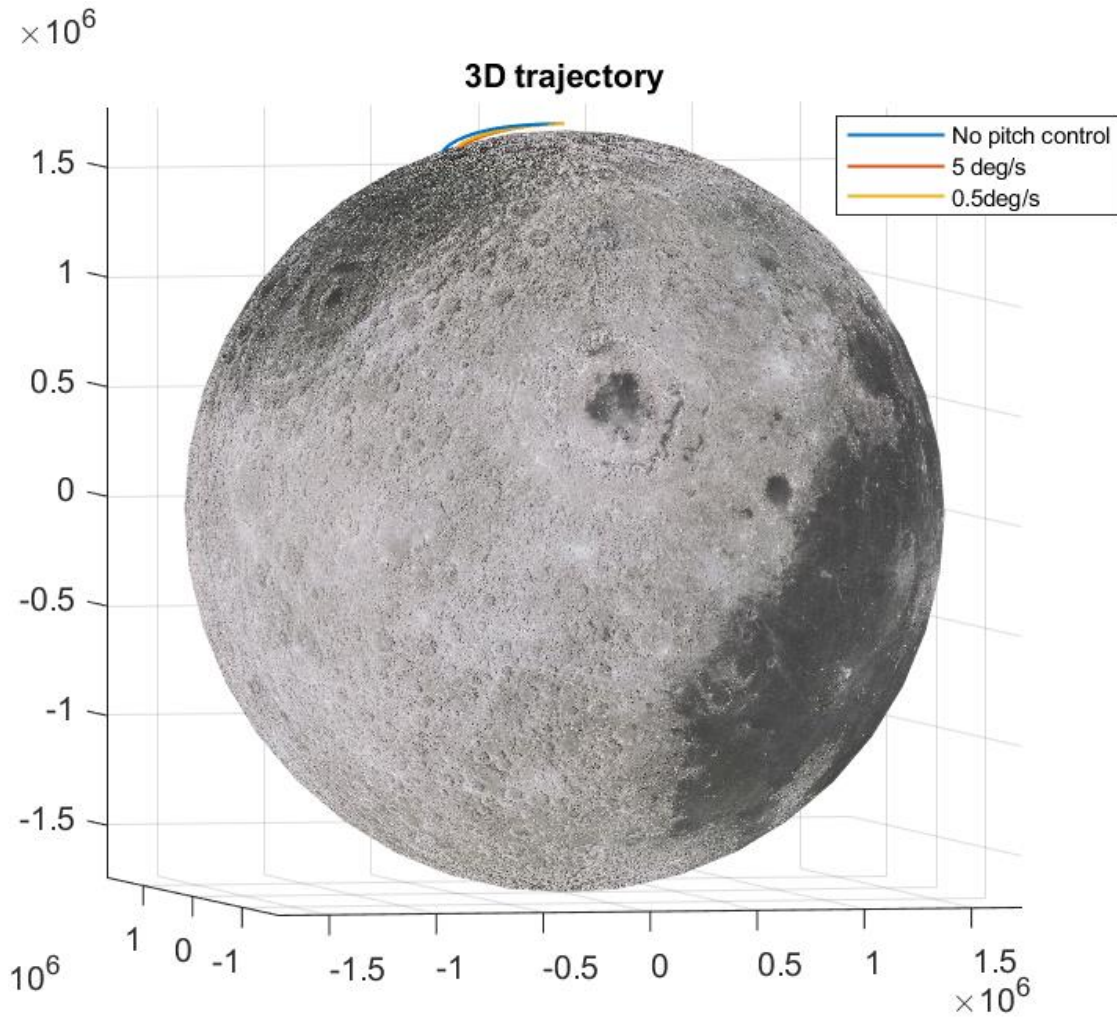


Figure 68: 3D trajectory for case 2.1

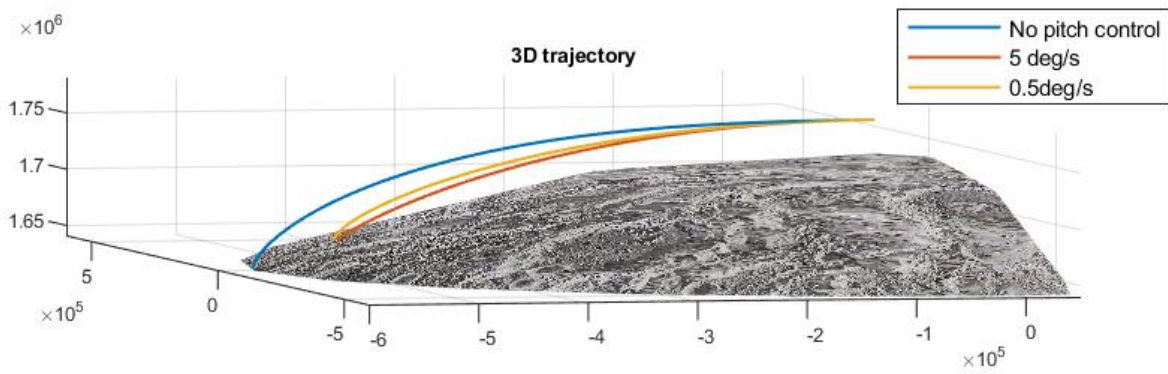


Figure 69: zoomed 3D trajectory for case 2.1

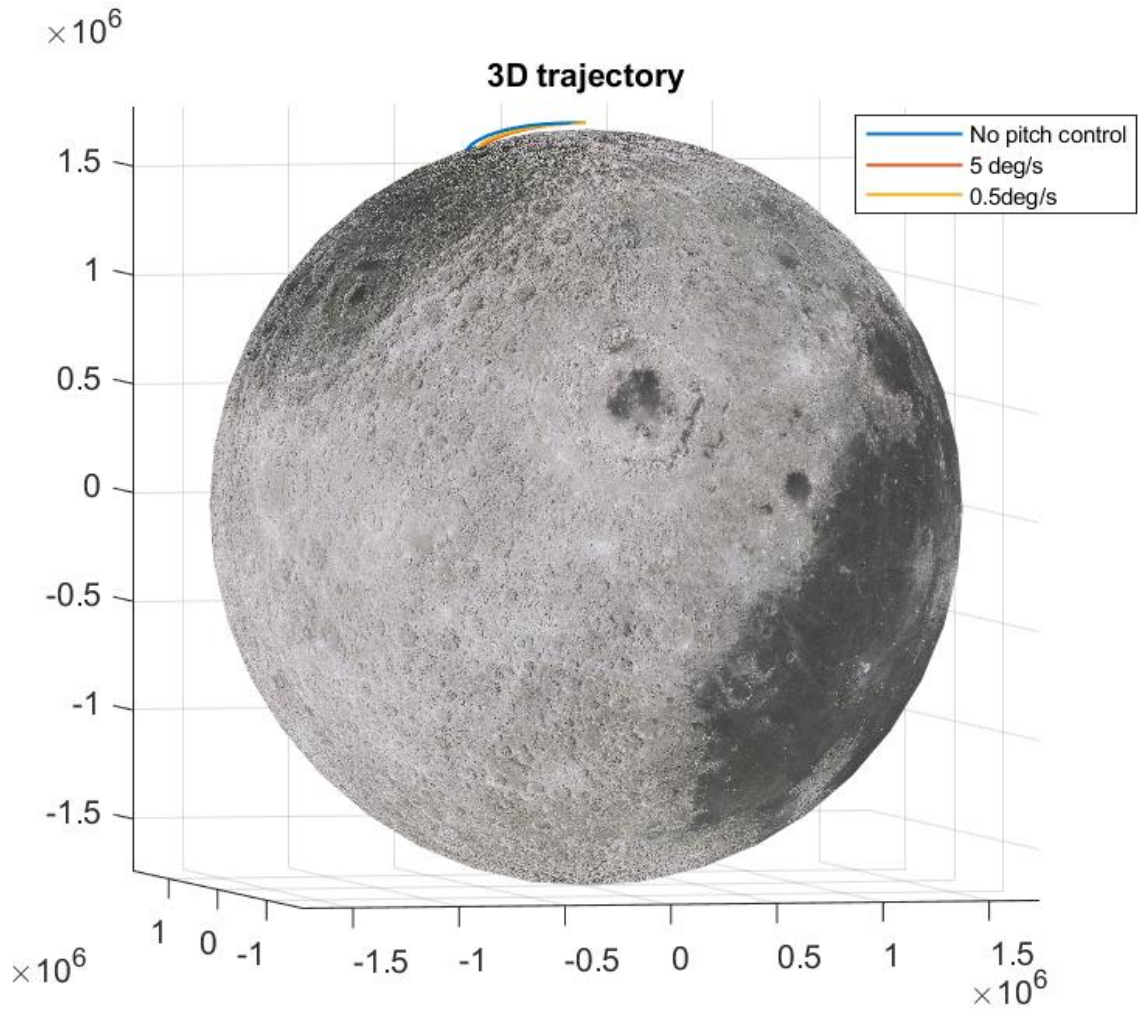


Figure 70: 3D trajectory for case 2.2

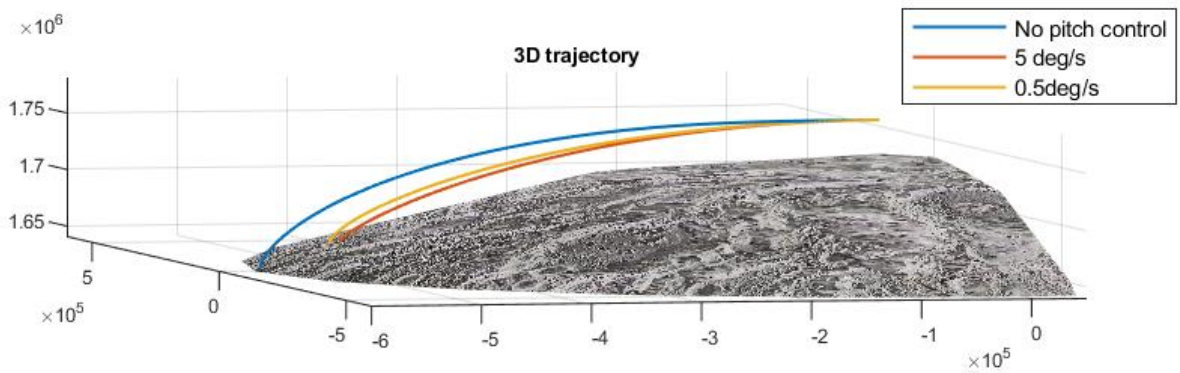


Figure 71: zoomed 3D trajectory for case 2.2

APPENDIX A3

Vertical and radial velocity for the best cases of the trade-off:

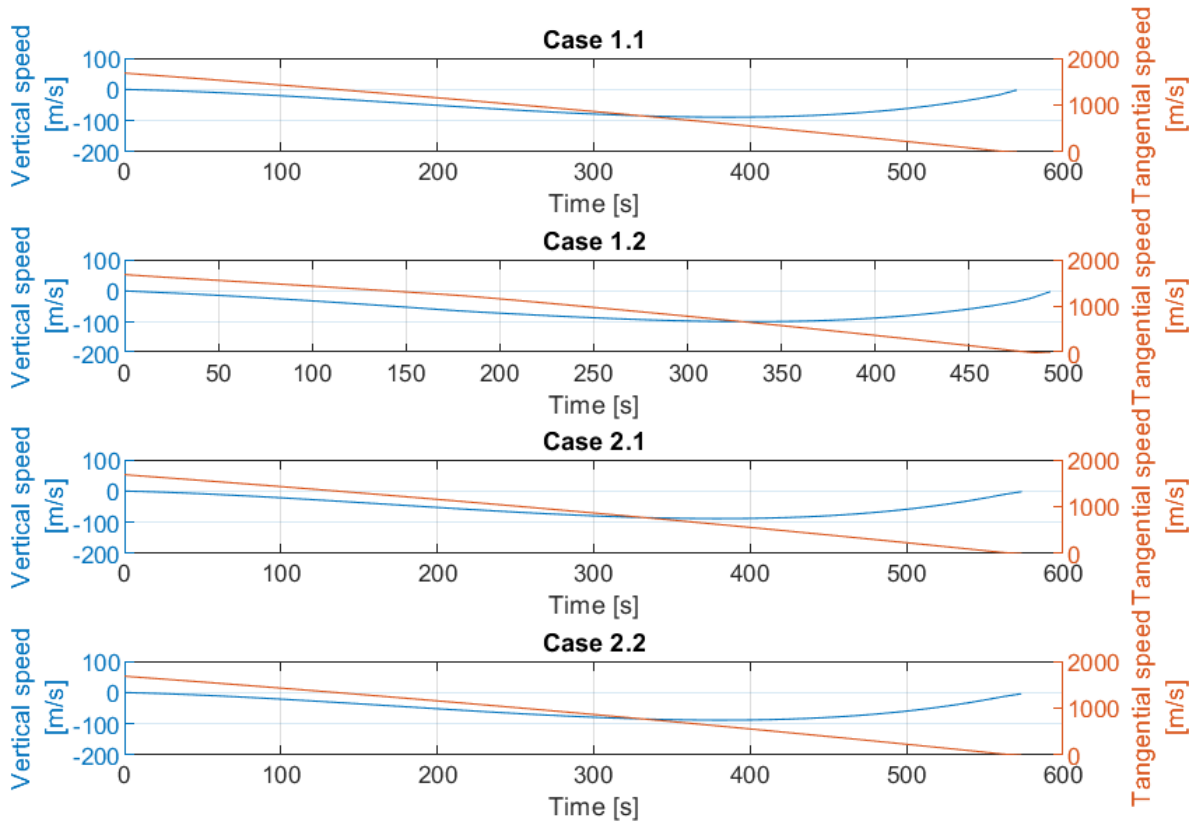


Figure 72: Vertical and Tangential velocity best cases comparison

BIBLIOGRAPHY

- [1] National Geographic, (2020), A brief history of moon exploration [Moon exploration, facts and information \(nationalgeographic.com\)](https://www.nationalgeographic.com/moon/exploration/)
- [2] NASA, (2022), Apollo 11 Mission Overview [Apollo 11 Mission Overview | NASA](https://www.nasa.gov/mission/apollo11/)
- [3] NASA, (2020), NASA's Lunar Exploration Program Overview https://www.nasa.gov/sites/default/files/atoms/files/artemis_plan-20200921.pdf
- [4] NASA, (2020), NASA Outlines Lunar Surface Sustainability Concept [NASA Outlines Lunar Surface Sustainability Concept](https://www.nasa.gov/feature/lunar-surface-sustainability-concept)
- [5] NASA, (2020), Lunar Living: NASA's Artemis Base Camp Concept <https://blogs.nasa.gov/artemis/2020/10/28/lunar-living-nasas-artemis-base-camp-concept/>
- [6] Herox, (2020), Introducing the Artemis Base Camp <https://www.herox.com/blog/960-what-is-the-artemis-base-camp-and-how-does-this-ch>
- [7] Joaquim R.R.A Martins, Andrew King, (2020), *Engineering Design Optimization*
- [8] Bruce A. Conway, (2010), The Problem of Spacecraft Trajectory Optimization, in *Spacecraft Trajectory Optimization*, Bruce A. Conway
- [9] Bruce A. Conway, (2010), Spacecraft Trajectory Optimization Using Direct Transcription and Nonlinear Programming, in *Spacecraft Trajectory Optimization*, Bruce A. Conway
- [10] E. Trélat, (2012), Optimal Control and Applications to Aerospace: Some Results and Challenges, in *Journal of Optimization Theory and Applications*, Tamás Terlaky
- [11] Marco Grammatico, (2020), Fuel-Optimal Lander Trajectory for Lunar Soft-Precision Landing
- [12] TechTarget, (2018), Evolutionary algorithm [What is evolutionary algorithm? - Definition from WhatIs.com \(techtarget.com\)](https://www.techtarget.com/whatis/definition/evolutionary-algorithm)
- [13] Victor M. Becerra, (2013) Practical Direct Collocation Methods for Computational Optimal Control, in *Modeling and Optimization in Space Engineering*, Giorgio Fasano, János D. Pintér
- [14] Ronald H.W. Hoppe, (2006), Sequential Quadratic Programming, in Optimization Theory Course at University of Huston
- [15] Northwestern University Open Text Book on Process Optimization, (2016), Sequential Quadratic Programming https://optimization.mccormick.northwestern.edu/index.php/Sequential_quadratic_programming
- [16] Ronald H.W. Hoppe, (2006), Optimization Theory Course at University of Huston https://www.math.uh.edu/~rohop/fall_06/
- [17] David A. Vallado, (2013), Satellite-based systems in: *Fundamental of Astrodynamics and Applications, Fourth Edition*
- [18] MATLAB, Global Optimization Toolbox <https://it.mathworks.com/products/global-optimization.html>

- [19] MATLAB, Optimization Toolbox
<https://it.mathworks.com/products/optimization.html>
- [20] MATLAB, ODE45
<https://it.mathworks.com/help/matlab/ref/ode45.html>
- [21] MATLAB, ODE113
<https://it.mathworks.com/help/matlab/ref/ode113.html>
- [22] MATLAB, MultiStart
<https://it.mathworks.com/help/gads/multistart.html>
- [23] Dong-Hyun Cho, Donghoon Kim and Henzeh Leeghim, (2015), Optimal Lunar Landing Trajectory Design for Hybrid Engine <https://www.hindawi.com/journals/mpe/2015/462072/>
- [24] NAIF, (2022), The SPICE toolkit
<https://naif.jpl.nasa.gov/naif/toolkit.html>
- [25] Giulio Avanzini, (2009), Entry, Descent, Landing and Ascent
http://www.ingaero.uniroma1.it/attachments/1978_AvanziniEDLA.pdf

ACKNOWLEDGEMENTS

Vorrei dedicare questo piccolo spazio a tutti coloro che mi hanno accompagnato in questa avventura senza i quali nulla di tutto questo sarebbe stato possibile.

Ringrazio il mio relatore Prof. Lorenzo Casalino per il supporto e tempo dedicatomi e per i preziosi consigli senza i quali non sarei stato in grado completare la mia tesi.

Ringrazio L'Ing. Andrea D'Ottavio, per l'infinità disponibilità e pazienza dimostratemi in questi mesi e per avermi trattato fin dal primo giorno non solo come un tesista, ma come un suo pari, facendomi subito sentire parte del gruppo e permettendomi di fare del mio meglio durante questo percorso.

Ringrazio il Dott. Giorgio Fasano, senza il quale l'ottimizzazione sarebbe stata una montagna ben più difficile da scalare e per avermi trasmesso tutta la passione per questo vastissimo argomento, permettendomi di afferrare anche solo una piccola parte.

Ringrazio i miei amici tutti, nuovi e vecchi, a chi mi conosce e sopporta da anni e chi da poco tempo. Grazie per aver condiviso con me gioie, dolori, risate, pianti e soprattutto per aver costruito tanti ricordi indelebili, insieme.

Ringrazio la mia ragazza Alessia, che mi è stata vicina durante ogni piccolo passo fatto in questi anni, soprattutto nei momenti di maggior difficoltà. Senza il tuo supporto tanti piccoli e grandi traguardi che ho tagliato sarebbero stati irraggiungibili.

Infine, voglio fare una menzione particolare alla mia famiglia, mio punto di riferimento. Senza i vostri sacrifici e insegnamenti non sarei nemmeno la metà dalla persona che oggi posso dire di essere e senza di voi veramente nulla di tutto questo sarebbe stato possibile.

A tutti voi, sinceramente e dal profondo del mio cuore, grazie.

Davide